

Separation of Similar Elements and Isotopes Separation in Non-Stationary conditions

A.A. Kopyrin^{*}, M.A. Afonin^{*}, K. Moody[†]

^{*}Saint-Petersburg Institute of Technology, 26 Moskovsky av., 190013, Saint-Petersburg, Russia

[†]Lawrence Livermore National Laboratory, Livermore CA 94552 USA

INTRODUCTION

Extraction methods based on the achievement of a chemical equilibrium traditionally have received the greatest attention. If the separation factor of two elements approaches the value one, then the required number of extractors in the separation cascade increases infinitely. The problem of separation of elements with similar properties is still vital. Separation of similar elements and isotopes in a non-steady state condition is a prospective method to increase the separation factor. Liquid-liquid extraction driven by an oscillatory oxidation-reduction reaction in the aqueous phase could provide an opportunity for the separation of similar elements using the repetition of extraction/stripping in a single extractor. The multiple extraction scenarios should improve the separation by exaggerating the small kinetic differences between similar metal ions. The same effect is possible to apply to the separation of isotopes.

EXPERIMENTAL

To induce the oscillatory extraction-stripping process, the cyclic Belousov-Zhabotinsky (BZ) reaction (a cyclic electrochemical oxidation-reduction reaction) was used. The experimental set up consisted of two extractors coupled by a bulk liquid membrane (extractant – 0.5 M TBP in tetradecane). The aqueous phase of both extractors consisted of a solution of cerium, praseodymium and neodymium nitrates in sodium nitrate media in the presence of potassium bromate and malonic acid. The experimental set up is described elsewhere¹.

RESULTS AND DISCUSSION

A new separation-extraction method was created based on an oscillatory extraction/stripping process in two extractors coupled by a bulk liquid membrane. The experimental setup, designed to investigate the kinetics of non-stationary processes, was constructed at the Saint Petersburg State Institute of Technology in the Rare Earth department. This setup can be used to separate macro-concentrations of similar elements or to enrich isotopes.

To induce the oscillatory extraction-stripping process, the cyclic Belousov-Zhabotinsky (BZ) reaction (a cyclic electrochemical oxidation-reduction reaction) was used. It is shown that it is possible to use an oscillatory extraction approach to separate similar elements by using the differences in their kinetic properties. We have obtained experimental evidence of the separation of uranium, cerium and neodymium isotopes. It is shown that the separation of Rare Earth Elements using the oscillatory extraction method is more complete than is the separation of these elements in classical extraction systems. A mathematical model of non-stationary oscillatory extraction systems has been created. The model results are in good agreement with the experimental results. The possibility of applying this new technique to separate similar elements and isotopes from aqueous phases is discussed.

In this work we present data on the possibility of isotope enrichment by means of the oscillatory extraction. The experimental set up consisted of two extractors coupled by a bulk liquid membrane (extractant – 0.5 M TBP in tetradecane). The oscillatory extraction method is based on exaggerating the small kinetic differences between isotopes during competitive extraction driven by the BZ reaction. Oscillations between Ce(III) and Ce(IV) concentrations driven by the BZ reaction are the cause of oscillations in the equilibrium concentration of the extractant. This leads to a difference in the partition of isotopes between aqueous phases and an organic phase. The organic phase of bulk liquid membrane is enriched by “light” isotopes, and stripping to the second aqueous phase causes a further enrichment in these isotopes as well. A possible explanation of our results is based on the fact that due to the difference in the kinetic properties of the isotopes toward extraction and complexation, differences in the average concentrations of the isotopes appear in the organic phase. Therefore the difference in the isotopic concentrations in different extractors appears.

The separation of ^{142}Ce and ^{140}Ce isotopes between aqueous phases of two extractors coupled by bulk liquid membrane in the experiments with cyclic chemical oxidation/reduction was observed, with an enrichment factor of about 2.5%. In the same conditions the separation of the Nd isotopes (heavy isotopes of Nd – ^{144}Nd , ^{145}Nd , ^{146}Nd , ^{148}Nd and ^{150}Nd from the light isotope – ^{143}Nd) in the same experiment with an enrichment factor about 0.7-1.4% was observed

Acknowledgements. This work was supported by the U.S. Department of Energy, Office of Basic Energy Sciences, under grant RC0-20000-SC14 and RUC2-20011-ST-04 administered by the Civilian Research and Development Foundation.

Leach Resistance of Murataite-Based Ceramics

Stefanovsky*, S.V., Yudinsev⁺, S.V., Perevalov^{*+}, S.A., Startseva*, I.V.,
Varlakova*, G.A..

*SIA Radon, 7th Rostovskii lane 2/14, Moscow 119121 RUSSIA

⁺Institute of Geology of Ore Deposits RAS, Starominetnii lane 35, Moscow 109017
RUSSIA

^{*+} V.I. Vernadsky Institute of Geochemistry and Analytical Chemistry RAS, Kosygin st.,
19, Moscow RUSSIA

Introduction

Pyrochlore, murataite and related phases with fluorite-derived structure are considered as host phases for actinide (An) and rare earth elements (REE)¹. Producing combined structures consisting of pyrochlore (two-fold elementary fluorite unit cell) and murataite (three-fold) modules² we can adjust ceramic formulations for immobilization of An/REE-bearing waste with variable chemical composition. In our previous work³ we have proposed a baseline composition (wt.%): 5 Al₂O₃, 10 CaO, 55 TiO₂, 10 MnO, 5 Fe₂O₃, 5 ZrO₂, and 10 (An,REE)O₂ or (An,REE)₂O₃ yielding >90% of the phases containing murataite modules in their structure. Preliminary studies have demonstrated high leach resistance of the murataite-based ceramics³. Zoned structure of the murataite grains with depletion of the rim with An and REEs protects core with the highest An/REE content from leachate attack and reduces leach rates to levels which are lower than those for zirconolite and pyrochlore by 1 to 3 orders of magnitude. In the given paper we present new data on leaching of ²³⁹Pu and ²⁴¹Am from the murataite-based ceramic and preliminary results of a SPFT test for the Th- and U-bearing murataite-based ceramics with above-mentioned formulation.⁴

Results

Major results of MCC-1 test⁵ for the ²³⁹Pu/²⁴¹Am-bearing (Am was present in the PuO₂ used for specimen preparation as an impurity in amount of 0.1 wt.%) murataite-based ceramic are given in Table I. Leach rate of both Pu and Am reduced gradually with time and achieved after 49-56 days of leaching values of $\sim 1 \times 10^{-5}$ g m⁻² d and $\sim 2 \times 10^{-4}$ g m⁻² d, respectively. Am existing in a trivalent form is more leachable element than Pu, which is tetravalent in this ceramic,⁶ due to higher electronegativity.

SPFT test was performed using an apparatus delivered by Pacific Northwest National Laboratory, USA under contract between US DOE and SIA Radon. Particle size of the U- and Th-bearing powdered ceramics were 87.5 μ m and 112.5 μ m, respectively. Measured density of both the ceramics was 4.52 g/cm³.

Main results of SPFT leach testing show that the ceramic specimens exhibit extremely low leachability of U and Th in deionized water at 90 °C and pH=7. Average leach rates for these elements were found to be 2.40×10^{-5} and 1.14×10^{-6} g/(m² d), respectively.

Discussion

Pu leach rate (MCC-1 test at 90°C in deionized water) from the murataite ceramic ($\sim 10^{-5}$ g m⁻² d) is similar to that of Pu-bearing Synroc-C⁷ and zirconolite-rich Synroc⁸.

For the pyrochlore-based ceramics designed for excess weapons plutonium immobilization 7-day Pu leach rate ranged between 4×10^{-5} and $\sim 10^{-3}$ g m⁻² d⁻¹ (depending on type and amount of impurities) reducing to $\sim 1 \times 10^{-4}$ after 50 to 100 days and to $(0.8-3) \times 10^{-5}$ g m⁻² d⁻¹ after more than 300 days of leaching⁹. Thus, Pu leach rate from the

Table I. Leach data for the Pu/Am bearing murataite ceramic (MCC-1 test in Teflon container with deionized water at 90 °C).

Leach time, days	Concentration in leachate, g/L		Mass of the nuclide leached, g		Leach rate, g m ⁻² d)	
	Pu	Am	Pu	Am	Pu	Am
3	2.22×10 ⁻⁵	3.39×10 ⁻⁸	3.02×10 ⁻⁷	4.62×10 ⁻¹⁰	8.37×10 ⁻³	5.48×10 ⁻³
7	4.25×10 ⁻⁶	3.23×10 ⁻⁸	5.79×10 ⁻⁸	4.41×10 ⁻¹⁰	6.88×10 ⁻⁴	5.23×10 ⁻³
14	7.19×10 ⁻⁶	3.12×10 ⁻⁸	9.79×10 ⁻⁸	4.26×10 ⁻¹⁰	5.82×10 ⁻⁴	2.39×10 ⁻³
21	2.40×10 ⁻⁶	2.88×10 ⁻⁸	3.27×10 ⁻⁸	3.93×10 ⁻¹⁰	1.30×10 ⁻⁴	1.55×10 ⁻³
28	4.73×10 ⁻⁷	4.25×10 ⁻⁹	6.44×10 ⁻⁹	5.78×10 ⁻¹¹	1.91×10 ⁻⁵	2.34×10 ⁻⁴
35	6.51×10 ⁻⁷	6.53×10 ⁻⁹	8.87×10 ⁻⁹	8.90×10 ⁻¹¹	2.11×10 ⁻⁵	2.88×10 ⁻⁴
42	6.05×10 ⁻⁷	7.28×10 ⁻⁹	8.24×10 ⁻⁹	9.92×10 ⁻¹¹	1.63×10 ⁻⁵	2.68×10 ⁻⁴
49	7.76×10 ⁻⁷	6.60×10 ⁻⁹	1.06×10 ⁻⁸	8.99×10 ⁻¹¹	1.79×10 ⁻⁵	2.08×10 ⁻⁴
56	4.99×10 ⁻⁷	9.42×10 ⁻⁹	6.80×10 ⁻⁹	1.28×10 ⁻¹⁰	1.01×10 ⁻⁵	1.90×10 ⁻⁴
63	6.64×10 ⁻⁷	1.19×10 ⁻⁸	9.04×10 ⁻⁹	1.62×10 ⁻¹⁰	1.19×10 ⁻⁵	2.14×10 ⁻⁴

murataite-based ceramic under steady-state conditions is by about one order of magnitude lower than from the pyrochlore-based ceramics. Higher leach rates at initial period (3 to 7 days) of leaching are probably due to dissolution of defect surface layer.

Ti release rate from the pyrochlore-based ceramics measured by SPFT test at 90 °C was found to be about 1×10⁻⁶ g m⁻² d⁻¹ at pH=7 and it increased to ~2×10⁻⁴ g m⁻² d⁻¹ at pH=2.¹⁰ U and Th leach rates measured in our tests were 2.40×10⁻⁵ and 1.14×10⁻⁶ g m⁻² d, respectively. Therefore, it can be expected that their release rates at pH=2 should be about ~10⁻⁴-10⁻⁵ and ~10⁻⁵-10⁻⁶ g m⁻² d⁻¹, respectively. Steady-state U and Pu release rates from the pyrochlore-based ceramics at 85 °C and pH=2 were found to be about ~10⁻⁴ g m⁻² d⁻¹.¹¹ Therefore, actinide release rates from the murataite-based ceramics are suggested to be by 1 to 2 orders of magnitude lower than those from the pyrochlore-based ceramics. Actual SPFT measurements of U and Th release from the murataite-based ceramics at pH=2 are in progress.

Acknowledgement

The work was supported from US DOE (Project RUC2-20009-MO-04).

References

1. Stefanovsky, S.V., Yudintsev, S.V., Gieré, R., Lumpkin, G.R., In Energy, Waste, and the Environment: a Geological Perspective, Geological Society, London, 236, 37-63 (2004).
2. Urusov, V.S., Organova N.I., Karimova, O.V., et. al., Transactions (Doklady) of the Russian Academy of Sciences/Earth Science Section, 401, 319-325 (2005).
3. Yudintsev, S.V., Stefanovsky, S.V., Omelianenko, B.I., Nikonov, B.S., Mat. Res. Soc. Symp. Proc. 663, 357-366 (2001).
4. Stefanovsky, S., Stefanovsky, O., Yudintsev, S., Nikonov, B. In: Proc. 35^{èmes} Journées des Actinides, Baden, Austria, April 23-26, 2005. Abstract E-19, CD-ROM.
5. Nuclear Waste Materials Handbook (Test methods), Rep. DOE/TIC-11400, Washington, DC (1981).
6. Yudintsev, S.V., Stefanovsky, S.V., Nikonov, B.S., et al/ In: Plutonium Future - The Science (2006), this volume.
7. Smith, K.L., Lumpkin, G.R., Blackford, M.G., et al/ Mat. Res. Soc. Symp. Proc. 465, 1267-1272 (1997).
8. Hart, K.P., Vance, E.R., Stewart, M.W.A., et al. Mat. Res. Soc. Symp. Proc. 506, 161-168 (1998).
9. Hart, K.P., Zhang, Y., Loi, E., et al. Mat. Res. Soc. Symp. Proc. 608, 353-358 (2000).
10. Icenhower, J.P., Strachan, D.M., McGrail, et al. Amer. Miner. 91, 39-53 (2006).
11. Strachan, D.M., Scheele, R.D., Buck, et al. Journ. Nucl. Mater. 345, 109-135 (2005).

XRD, SEM, TEM, and XPS Study of Pu-Bearing Murataite Ceramic

Yudintsev^{*}, S.V., Stefanovsky⁺, S.V., Nikonov^{*}, B.S., Teterin^{*+}, Yu.A. Ptashkin⁺, A.G.

^{*}Institute of Geology of Ore Deposits RAS, Staromonetnyi 35, Moscow 109017 RUSSIA

⁺SIA Radon, 7th Rostovskii lane 2/14, Moscow 119121 RUSSIA

^{*+}RRC "Kurchatov Institute", Kurchatov sq. 1, Moscow RUSSIA

Introduction

Murataite is considered as a promising host phase for actinides and rare earths as well as corrosion products and process contaminants in high level waste (HLW)¹. Murataite as well as pyrochlore has a fluorite-derived structure²⁻⁴. In general, pyrochlore, $A^{VIII}_2B^{VI}_2O_{7-x}$ ($A = REE^{3+}, An^{3+/4+}, Ca^{2+}$; $B = Ti^{4+}, Zr^{4+}, Hf^{4+}$) and murataite, $A^{VIII}_3B^{VI}_6C^V_2O_{20-x}$ ($A = REE^{3+/4+}, An^{3+/4+}, Zr^{4+}, Ca^{2+}, Na^{+}$; $B = Ti^{4+}, Fe^{3+}, Mn^{3+/4+}, Al^{3+}$; $C = Mn^{2+}, Fe^{2+}$) being structure-related form a polysomatic series of the phases with modular structure and two- (2C - pyrochlore), three- (3C – murataite), five- (5C), seven- (7C), and eight-fold (8C) elementary fluorite unit cell⁴. All the phases with three-fold elementary fluorite unit cell and higher multiplicity, i.e. containing murataite modules in their structure are considered as murataite polytypes. Previously we synthesized and examined Pu-bearing murataite-based ceramics.⁵ In the present work the Pu-bearing murataite ceramic is characterized in more details in particular using X-ray photoelectron spectroscopy (XPS).

Results

The murataite ceramic with specified composition (wt.%): 5 Al₂O₃, 10 CaO, 55 TiO₂, 10 MnO, 5 Fe₂O₃, 5 ZrO₂, 10 PuO₂ was prepared by melting of oxide mixtures in a platinum ampoule at 1500 °C for 3 hours followed by quenching. The sample was characterized with X-ray diffraction (XRD), scanning electron microscopy – energy dispersive system (SEM/EDS), and transmission electron microscopy (TEM) – selected area electron diffraction (SAED). XPS spectra were measured with an electrostatic spectrometer MK II VG Scientific using AlK_α and MgK_α radiation under 1.3×10⁻⁷ Pa at a room temperature.

The ceramic is composed of predominant murataite-type phases: 5C, 8C and 3C, and minor Fe-Mn-titanate. Core of the murataite grains is composed of the 5C phase (the lightest on SEM-image) with the highest Pu content. The 8C phase with intermediate Pu content composes major bulk of the grains (light-gray). Rim is formed by the 3C phase (gray) with the lowest Pu content. Fe-Mn-titanate (dark-gray) is almost free of Pu.⁵

The low binding energy XPS from murataite exhibits the OVMO structure attributed to the outer Ca 4s, Pu 5f, 7s, Zr 4d, 5s, Fe 3d, 4s, Ti 3d, 4s, Mn 3d, 4s, Al 3s, 3p, and O 2p electrons, as well as the IVMO structure due to the Ca 3s, 3p, Pu 6s, 6p, Zr 4p, Ti 3p, Mn 3p, and O 2s electrons (Table I). This binding energy range exhibits only the lines typical of the compounds studied. The Pu 4f spectrum of the sample exhibits the fine structure typical of the Pu⁴⁺ ions (Figure 1) with the doublet split at $\Delta E_{sl}=12.5$ eV. On the higher binding energy side from the basic peaks at $\Delta E_{sat}=7.4$ eV the typical shake up satellite of about 19% intensity was observed. The oxidation states of the elements were determined to correspond to the following ions: Ca²⁺, Ti⁴⁺, Mn²⁺, Fe³⁺, Zr⁴⁺, Al³⁺, Pu⁴⁺. The O1s spectrum consists of the two peaks at 530.0 and 532.1 eV. Taking into account equation $R_{M-O} = 2.27 (E_b - 519.4)^{-1}$, derived in⁶, on the basis of the O1s binding energy the interatomic distances R_{M-O} (nm) calculated are 0.214 nm and 0.173 nm. Probably the value 0.173 nm can be attributed to the hydroxide groups on the surface of the sample. The value $R_{M-O} = 0.214$ nm corresponds to average M-O distance in the murataite structure².

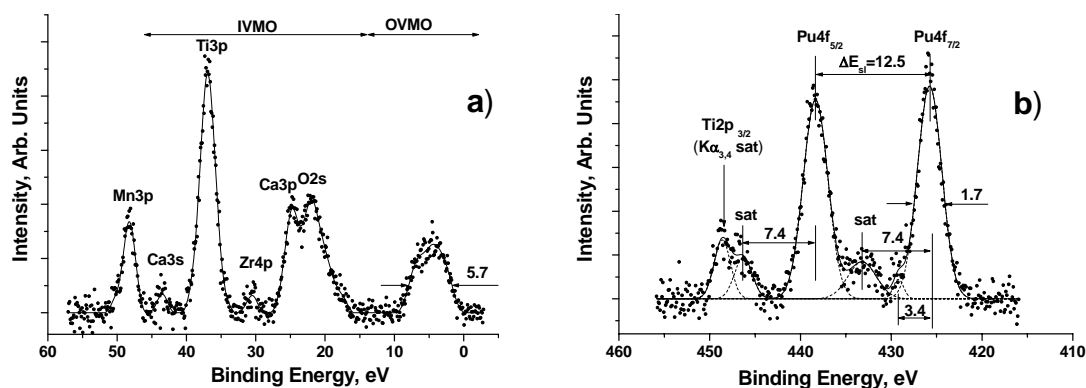


Figure 1. Low binding energy (a) and Pu 4f (b) XPS from the murataite ceramic.

Table. Binding energies E_b (eV) and FWHMs^{a)} (eV) of the outer (MO) and core electrons for the the actinide-doped murataite ceramics.

Ceramic	MO	Pu(Np) 4f _{7/2}	Ca2p _{3/2}	Ti2p _{3/2}	Mn2p _{3/2}	Fe2p _{3/2}	Zr3d _{5/2}	Al2p	O1s
Murataite	4.4; 22.0;	426.1 7.4 sat	346.7 (1.6)	458.5 (1.2)	641.0 (2.4)	710.3 (2.9)	182.2 (1.2)	74.0 (1.4)	530.0
	24.7; 30.5;								532.1
	36.9; 43.5; 48.3								(1.3)

^{a)}FWHMs are given in parentheses relative to the FWHM of the C1s-peak accepted to be 1.3 eV. Initial C 1s FWHM for Pu-bearing murataite is 2.1 eV.

Discussion

The phase composition and texture of the Pu-bearing murataite ceramic are typical of those for the murataite ceramics produced by melting and crystallization^{1,3-5}. Such ceramics are composed of zoned murataite grains with increasing of the number of the murataite modules in the structure of the murataite polytypes from core to rim. Because actinide content reduces in a series: 2C (pyrochlore) < 7C < 5C < 8C < 3C^{1,4,5} actinide depletion of the rim with respect to the core creates an additional barrier against their leaching into environment. As follows from XPS data such elements as Ca, Al, Ti, and Zr have their typical oxidation states (are present as Ca²⁺, Al³⁺, Ti⁴⁺, and Zr⁴⁺ ions). Transition elements - Mn and Fe were found to be mainly di- and trivalent, respectively. Occurrence of trivalent iron (Fe³⁺ ions) is consistent well with Mössbauer spectroscopy data⁷.

The work was performed under financial support from US DOE (Project RUC2-20009-MO-04).

References

1. Stefanovsky, S.V., Yudintsev, S.V., Gieré, R., Lumpkin, G.R., in Energy, Waste, and the Environment: a Geological Perspective, Gieré, R. and Stille, P. (eds) Geological Society, London, 236, 37-63 (2004).
2. Ercit, T.S., Hawthorne, F.C., Canad. Miner. 33, 1223-1229 (1995).
3. Ewing, R.C., Weber, W.J., Lian, J., Journ. Appl. Phys. 95, 5949-5971 (2004).
4. Urusov, V.S., Organova N.I., Karimova, O.V., Yudintsev, S.V., Stefanovsky, S.V., Trans. (Doklady) Russ. Acad. Sci./Earth Sci. Sec., 401, 319-325 (2005).
5. Stefanovsky, S., Stefanovsky, O., Yudintsev, S., Nikonov, B. In Proc. 35^{èmes} Journées des Actinides, Baden, Austria, April 23-26, 2005. Abstract E-19, CD-ROM.
6. Sosulnikov, M.I., Teterin, Yu.A., Rep. Acad. Sci. USSR (Russ.) 317, 418-421 (1991).
7. Urusov, V.S., Rusakov, V.S., Yudintsev, S.V., Stefanovsky, S.V. Mat. Res. Soc. Symp. Proc. 807, 243-248 (2004).

OPEN POSTER #4 Wednesday 3:30 PM

Elucidation of reactions yielding uranyl phosphate layers connected by organic amine cations.

T. Bray*, T. Albrecht-Schmitt*

*Department of Chemistry and Biochemistry, Auburn University, 179 Chemistry Building,
Auburn, AL 36849, USA

ABSTRACT

Three two-dimensional uranyl phosphates, synthesized from the reaction of uranyl nitrate hexahydrate, phosphoric acid, and different organic amines, are presented in this poster. Two compounds, synthesized with 2,2'-bipyridine and 4,4'-bipyridine, are arranged in a pseudotectouranophosphate fashion in which the uranyl unit exists in an octahedral environment, bridged by four tetrahedral phosphate groups. The resulting layers are connected by self-assembled bipyridinium cations, directed by π -stacking. The final compound, produced in the presence of ethylene diamine, has a different structure in which the uranyl units are in pentagonal bipyramid geometry with three equatorial oxygens bridged to phosphate groups, and two equatorial oxygens allowing for dimerization between uranyl centers. This system of dimers and bridging phosphate groups allows for two-dimensional propagation. In all three, the negatively charged framework is charge-balanced by the presence of the amine cations.

Spectroscopic Studies of Intra-5*f* Fluorescence from $\text{Cs}_2\text{Np(VI)O}_2\text{Cl}_4$

M. P. Wilkerson and J. M. Berg

Los Alamos National Laboratory, Los Alamos NM 87545 USA

We have recently measured fluorescence from an excited 5*f* state of crystalline $\text{Cs}_2\text{Np(VI)O}_2\text{Cl}_4$ at room temperature following visible excitation. To date, the most successful efforts at rigorously describing the electronic structures of actinyl ions have focused on uranyl (U(VI)O_2^{2+}), which is a specific case that has no valence electrons in the 5*f* shell of the ground state.¹ The lowest-energy electronic transitions to occur in this system are ligand-to-metal charge-transfer (LMCT), in which an electron is promoted from a state of primarily ligand orbital character to a state of principally metal orbital character. These transitions are associated with an extensive series of vibronic bands with an energy spacing corresponding to the symmetric stretch, ν_1 , of the excited uranyl ion. Fluorescence-based methods have been applied quite successfully to work ranging from field surveys of uranyl dispersal in the environment to fundamental studies of electronic structure. In contrast to uranyl ions, all other chemically stable oxidation states of actinide species contain at least one electron in the 5*f* valence shell of the ground state. There are two types of transitions in the spectra of 5*fⁿ* (*n*>0) molecules; LMCT's and transitions that correspond to promotion of an electron from one state of predominantly 5*f* orbital character to another state of primarily 5*f* orbital character. These transitions lie in both the near-infrared and higher ultraviolet/visible region. Investigations of lower energy 5*f*-5*f* transitions of actinyl compounds are not well explored, and an insight into the nature of compounds with a single electron in the 5*f* shell could provide a unique opportunity to probe 5*f* electronic properties without introducing some of the typical complicating factors resulting from more than one electron in a valence shell.²

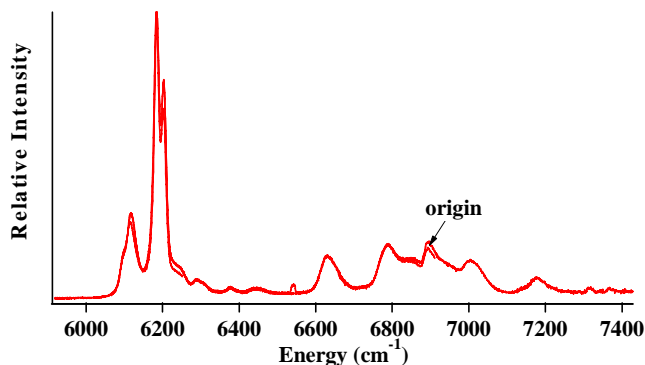


Fig 1: Fluorescence spectrum of $\text{Cs}_2\text{Np(VI)O}_2\text{Cl}_4$ at room temperature using an array detector following excitation at 633 nm (continuous wave).

Our prior work has shown that trans-dioxo forms of other actinides with partially filled 5*f* shells may also produce detectable fluorescence upon photo-excitation.³ In particular, we have demonstrated that a simple 5*f¹* system, the neptunyl ion, luminesces with relatively high resolution and vibronic structure in the near-infrared at 77K, and more notably, it luminesces strongly at room temperature. Dilution of the luminescent analyte into host crystals was employed in order to study neptunyl fluorescence in the absence of potential self-quenching while offering some degree of control over the

local environment. In particular, neptunyl tetrachloride ($\text{Np(VI)O}_2\text{Cl}_4^{2-}$) was doped into the slightly larger isostructural uranyl tetrachloride ($\text{U(VI)O}_2\text{Cl}_4^{2-}$) matrix, which offers a large window throughout the near-infrared and most of the visible region and apparently lacks vibrational modes that could allow radiationless deactivation.

We will discuss here a more recent observation of near-infrared fluorescence from neat single crystals of $\text{Cs}_2\text{NpO}_2\text{Cl}_4$ following excitation at 633 nm. These characteristically broad spectra show that the relaxation pathway from the excited state of this material is competitive with radiationless deactivation at room temperature (Figure 1). Initial assignments of the vibronic bands, based upon energies of ground state vibrational modes of $\text{Cs}_2\text{NpO}_2\text{Cl}_4$, reveal the presence of hot bands. We will also compare time-resolved measurements of this compound with lifetimes of doped $\text{Cs}_2\text{U(Np)O}_2\text{Cl}_4$.

This research at Los Alamos National Laboratory was supported by NA-22, Office of Nonproliferation Research and Engineering, U. S. Department of Energy, National Nuclear Security Administration, and Division of Chemical Science, Office of Basic Energy Research, U. S. Department of Energy.

1. a) Denning, R. G. *Struct. Bonding (Berlin)* **1992**, 79, 215. b) Hopkins, T. A.; Berg, J. M.; Costa, D. A.; Smith, W. H.; Dewey, H. J. *Inorg. Chem.* **2001**, 40, 1820. c) Metcalf, D. H.; Dai, S.; Del Cul, G. D.; Toth, L. M. *Inorg. Chem.* **1995**, 34, 5573.
2. a) Denning, R. G.; Norris, J. O. W.; Brown, D. *Mol. Physics* **1982**, 46, 287. b) Denning, R. G.; Norris, J. O. W.; Brown, D. *Mol. Physics* **1982**, 46, 325.
3. Wilkerson, M. P.; Berg, J. M.; Hopkins, T. A.; Dewey, H. J. *J. Solid State Chem.*, **2005**, 178(2), 584.

Computational Modelling of Actinide Complexes

M. Benson, R. S. Herbst, D. Peterman

Idaho National Laboratory, Idaho Falls ID 83402 USA

The chemistry and separation of key radionuclides, primarily the actinides, lanthanides, and select fission products, figures predominately into the Global Nuclear Energy Partnership, notably in the area of advanced nuclear fuel cycles. Computational chemistry can play a role in that research by providing much needed information to the experimental scientists, information that may be extremely difficult or impossible to determine experimentally. At this time, computational efforts have been focused on one of the two most challenging and important areas in the development of an advanced fuel cycle: trivalent actinide/lanthanide (An(III)/Ln(III)) separation, with the second area being Cs/Sr separation.¹⁻³ In the concept of a closed fuel cycle, the minor actinides (Am, Cm, Np) are recycled to reactor fuels or transmuted, so efficient separation from the trivalent lanthanides is mandatory. This is due to the lanthanides high thermal neutron absorption cross-sections (they are neutron poisons), which substantially interferes with reactor efficiency.

The separation system of interest is the TALSPEAK process (Trivalent Actinide Lanthanide Separations by Phosphorus reagent Extraction from Aqueous Complexes). Separation of actinides and lanthanides is extremely difficult, though, due to their similarities. The softer donor atoms, specifically nitrogen and sulfur, coordinate preferentially to actinides.² This fact has been exploited in several separation methods, such as the nitrogen based TALSPEAK process, and the sulfur based Cyanex 301 extractants.

Modelling the actinides presents several problems, such as strong relativistic and correlation effects, that need to be addressed to obtain reliable and useful results. These problems arise from high charge, a large number of electrons, and the complexities of modelling the f orbitals. At this point, modelling has been focused on known extractants, with the goal of gaining insight into the coordination chemistry of these systems. Complexes of the minor actinides (Am, Cm, Np) and of Europium have been modelled using a variety of methods (UHF, MP2, uB3LYP, uPW91, uBLYP, and CAS, CAS-MP2 for the smaller systems). The results of these calculations will be presented.

This research was supported by The United States Department of Energy under Contract DE-AC07-05ID14517.

1. C. Madic, M. J. Hudson, J. O. Liljenzin, J. P. Glatz, R. Nannicini, A. Facchini, Z. Kolarik, R. Odoj, *New Partitioning Techniques for Minor Actinides*, Final Report, EUR 19149, Nuclear Science and Technology (2000).
2. M. Miguiditchian, D. Guillauneux, D. Guillaumont, P. Moisy, C. Madic, M. P. Jensen, K. L. Nash, *Inorg. Chem.*, **44**, 1404 (2005).
3. W. W. Schultz, L. A. Bray, *Sep. Sci. Technol.*, **22(2&3)**, 191 (1987).

Raman Studies Of Solid Plutonium Compounds

P. Rance and K. Webb

Nexia Solutions, Sellafield, Seascale, Cumbria CA20 1PG

RAMAN MICROSCOPE

A Raman Microscope has recently been installed in the active laboratories of Nexia Solutions at Sellafield in the UK and will be used as a tool in wide ranging studies covering both clean-up and decommissioning activities as well as forward looking fundamental studies investigating phenomena relevant to advanced reprocessing and waste management. This abstract describes the installation of the equipment, gives preliminary results and describes some future studies.

The Raman microscope (InVia, Renishaw) consists of Leica microscope (x5, x20 and x50 objectives) and Raman spectrometer with a peltier cooled CCD detector. Three lasers, argon ion (50 mW, 514 nm), helium-neon (17 mW, 633 nm) and near infrared diode (300 mW, 785 nm) are available.

PLUTONIUM SOLID STUDIES

Fumehood limits for active powders (3.7×10^6 Bq α) restrict plutonium dioxide holdings to somewhat less than 1 mg without resort is made to more exotic, long-lived isotopes (Pu-242,244). However, the focussing ability of the microscope optics is such that high quality spectra can be recorded from very small sample masses.

Figure 2, shows a Raman spectrum recorded from an approximately 10 ng sample of PuO₂ secured to an aluminium foil-backed glass microscope slide secured with adhesive cellulose tape. Spectrometer settings were 633 nm laser irradiation, 5% power, single capture. The

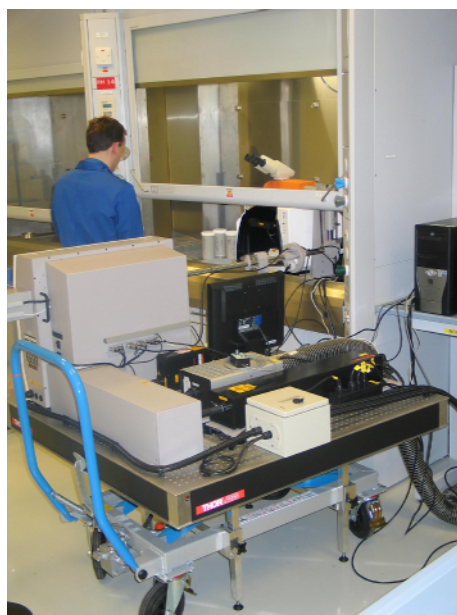


Figure 1. Raman microscope

spectrum clearly shows the single peak of PuO₂ at 476 cm⁻¹ (cf. 478 cm⁻¹ reported previously¹). The smaller peaks at just below 400 cm⁻¹ and above 800 cm⁻¹ are artefacts resulting from the mounting arrangement. Other preliminary results recorded from different samples have shown a slight variation in the peak position, down to 473 cm⁻¹, perhaps due to variation in sample stoichiometry although this is far from certain.

A range of plutonium bearing residues are to be characterised in future programmes with plutonium nitrate, chloride and oxalate samples to be analysed imminently.

Also purchased is a glovebox unit and associated fibre-optics. This is to be installed and commissioned during 2006 and will enhance significantly the utility of the spectrometer in analysing powder samples as the amount of material that can be handled will be increased substantially. This unit will be used in combination with infrared spectroscopy to study a number of aspects of plutonium chemistry relevant to its storage and encapsulation in ceramic wasteforms.

For example the interaction of water with the PuO₂ surface from monolayer coverage to ‘damp powder’ is being investigated in a number of ways including radiolysis of water/PuO₂ mixtures and desorption of water from PuO₂ within closed environments. Raman and infrared spectroscopy will form part of these studies in which samples are to be characterised prior to and following exposure to water vapour for varying lengths of time. Other potential applications include characterisation of non-stoichiometric oxides and analysis of amorphisation by radiation damage.

The authors would like to thank British Nuclear Fuels for financial support in purchasing the Raman Spectrometer used in this work and the [UK] Nuclear Decommissioning Authority for funding these studies as part of their commitment to supporting key skills.

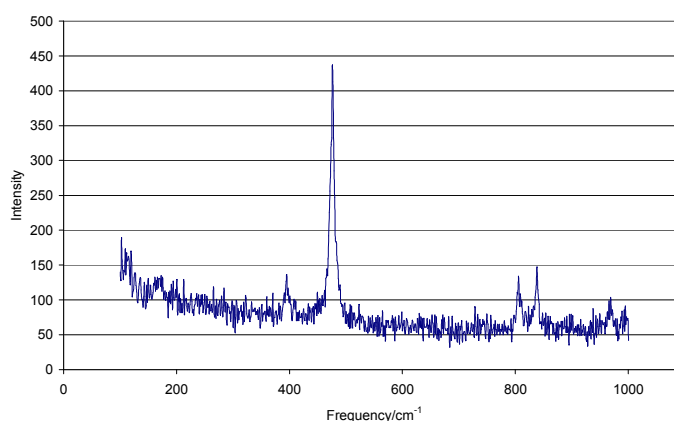


Figure 2. Raman spectrum of PuO₂

1 G.M. Begun *et al.*, *J. Less-common Met.* **162**, 129 (1990)

Calculation of Low-Lying Excited States of PaO^+ and PuO^+

M. Mrozik,* R. Pitzer,* B. Bursten[†]

*The Ohio State University, Columbus OH 43209 USA

[†]The University of Tennessee, Knoxville TN 37996 USA

ABSTRACT

Recent experimental investigations into the reactivity of several actinide-oxide cations have identified a need for high accuracy calculations of some low-lying excited states. Questions that are still unanswered in the actinide systems regard the increased reactivity of some actinide oxide cations over their actinyl counterparts. Predictions of low energy transitions of actinide complexes have helped elucidate some of the more complicated bonding pictures that would be extremely difficult to assign without theory. The understanding of the nature of the bonding in actinide oxide cations will help explain their reactivity. Implementation of multiple-reference configuration interaction with single and double excitations (MR-CISD) including spin-orbit coupling within the *Columbus Suite* of programs allows for accurate determination of electronic configuration contributions to the overall wave function. Inclusion of medium size (68 electrons) effective core potentials (ECP) allow for determination of spin-orbit coupling effects present within the actinide species. Application of MR-CISD with ECP's has proven indispensable for actinyl ions and is used in this study to identify the ground and low-lying excited states in PaO^+ and PuO^+ .

Acknowledgments:

This work was supported by Department of Energy Grant # DE-FG02-01ER15135.

Raman and Infra-Red Analysis of Plutonium Compounds

C. Puxley

Atomic Weapons Establishment, Aldermaston, Berkshire RG7 4PR, United Kingdom

INTRODUCTION

The unambiguous identification and characterisation of plutonium compounds rapidly by non-destructive means is a desirable goal in the area of plutonium chemistry. One of the fields that has the potential to achieve this is that of vibrational spectroscopy. The accumulation of both the Raman spectrum and the infra-red spectrum of a sample gives an unique fingerprint for the plutonium compound under study.

The hazards inherent with the manipulation of plutonium and its compounds necessitate strict containment of these materials and this has a negative effect on the ease of analysis. The options available are to either to site the analytical equipment inside the containment region or to have a link from the analytical equipment outside the containment area to a probe within the containment area. Results achieved using these two approaches will be presented.

FIBRE-OPTIC AND NON FIBRE-OPTIC SPECTROMETERS

The difficulties associated with working with plutonium make it preferable to conduct analyses of samples remotely, e.g. through fibre-optic cables interfaced to the glovebox containment. Whereas Raman spectroscopy lends itself easily to the employment of optical fibres to carry the laser radiation to the sample and the scattered laser radiation back to the detector, infra-red spectroscopy is not as pliant. Significant losses in the infra-red signal can occur through fibre-optic media and this results in a reduced sensitivity and efficiency for the analysis.



Figure 1: Miniature Infra-Red Spectrometer.

Advances in infra-red spectrometer technology have resulted in the production of spectrometers that are sufficiently small to be wholly accommodated within a glovebox (Figure 1).

The sample can be analysed using the technique of attenuated total reflectance (ATR). For this, the infra-red beam is reflected at a diamond/sample interface and directed to the detector where the infra-red spectrum is generated. Results obtained with a miniature infra-red spectrometer will be displayed.

ANALYSIS UNDER INERT ATMOSPHERES

Since certain plutonium compounds, such as plutonium tetranitrate, are oxygen and/or moisture sensitive, and other compounds of plutonium may be pyrophoric, it is necessary to obtain the vibrational spectra of these materials whilst they are under an inert atmosphere. In the case of the infra-red analysis, the siting of the entire infra-red spectrometer inside the glovebox means that the glovebox atmosphere must be inert.

In the case of the fibre-optic Raman spectrometer, cells may be constructed within which the sample is contained under an inert atmosphere. These cells may then be analysed in a glovebox with an air atmosphere without degradation of the sample. Examples of these cells and the Raman spectra obtained will be provided.

RESULTS

The Raman and infra-red spectra of a number of simple inorganic plutonium compounds will be presented. These spectra will be assigned according to the structure of the compound and the nature of the ligands attached to the plutonium.

The Use of Glovebox-Mounted High Resolution Inductively-Coupled Plasma Mass Spectrometry for the Analysis of Trace Metals in Actinide Materials

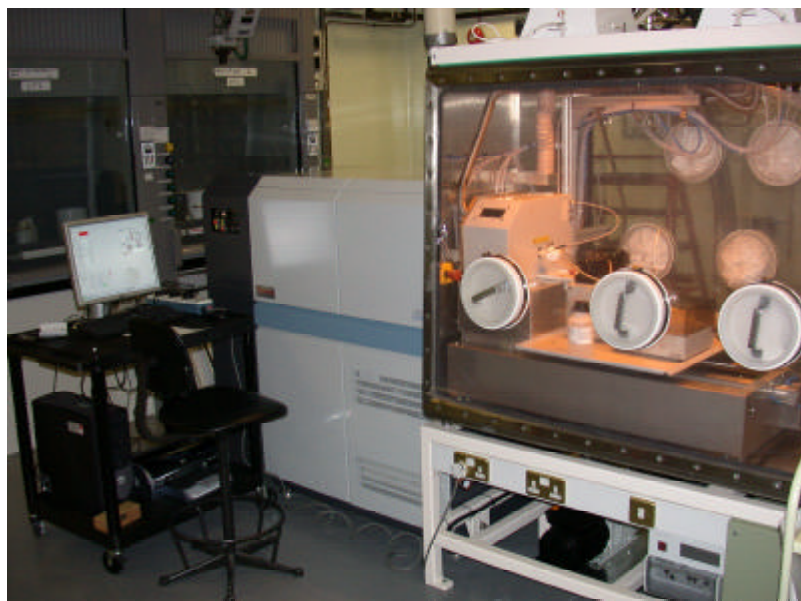
P. I. Kaye and O. J. Marsden

Atomic Weapons Establishment, Aldermaston, Berkshire, RG7 4PR, United Kingdom

INTRODUCTION

The presence of trace elements in plutonium and uranium materials can affect the mechanical, metallurgical and chemical properties of the materials. In addition, they may yield information on the source and age of the material. For these reasons, the identification and characterisation of the trace elemental content of actinide materials is of interest to AWE.

This poster will describe a glovebox mounted High Resolution Inductively Coupled Plasma Mass Spectrometer (HR-ICP-MS) recently installed at AWE (Figure 1). The performance and engineering aspects of the spectrometer will be discussed, as will the merits of double pass and cyclonic spray chambers for sample introduction.



The benefits of using ICP-MS in comparison to ICP-OES for trace metals analysis of actinide materials will also be considered¹. For example, at AWE, uranium samples are prepared for ICP-OES analysis by dissolution, followed by the extraction of uranium by tributyl phosphate (TBP). The use of ICP-MS allows the omission of the separation stage, affording significant reductions in sample preparation time and the volume of aqueous wastes generated

Figure 1: Glovebox-Mounted HR-ICP-MS

1 C. Mahan, S. Bonchin, D. Figg, D. Gerth and C. Collier. J. Anal. At. Spectrom., **15**, (2000) p 929-935.

A high efficiency cavity ion source using TIMS for nuclear forensic analysis

S. Bürger^{*}, L. R. Riciputi^{*}, S. Turgeon^{*}, D. Bostick^{*}, E. McBay^{*}, M. Lavelle^{*}

^{*} Oak Ridge National Laboratory, Chemical & Isotope Mass Spectrometry Group, Transuranic Research Institute, Oak Ridge, TN 37831, USA

INTRODUCTION

The investigation of illicit trafficking of nuclear materials and non-proliferation control requires sensitive and isotope-selective detection methods to gain crucial nuclear forensic information like isotope ‘fingerprints’, allowing the origin and age of the sample of concern to be determined. One of the standard types of samples analyzed by IAEA’s Safeguards Environmental Sampling Program are environmental samples collected on cotton swipes by IAEA inspectors, which can contain picogram or even sub-picograms of plutonium. The analysis of plutonium for bioassay, or low-level environmental monitoring in the surrounding of a nuclear waste repository or nuclear facility might require the identification of even lower concentrations. Thus, sub-femtogram detection and characterization capabilities for plutonium are desirable.

Alpha-spectrometry, conventionally used for ultra trace detection of plutonium, is not well-suited for isotope resolved analysis due to the very similar alpha-energies of certain isotopes and the fact that the detection limit depends on the half-life of the isotope. In contrast, mass spectrometric methods provide detection limits independent of the half-life. Inductively coupled plasma mass spectrometry (ICP-MS), multi-collector inductively coupled plasma mass spectrometry (MC-ICP-MS), thermal ionization mass spectrometry (TIMS), and secondary ion mass spectrometry (SIMS) are routinely used for bulk or particle analysis of plutonium, with detection limits at the picogram to femtogram level [1,2]. Resonance ionization mass spectrometry (RIMS) demonstrates detection limits on sub-femtogram levels for isotope resolved analysis of plutonium [3,4], but no RIMS system is yet commercially available. Accelerator mass spectrometry (AMS) has a detection limit of low attograms of plutonium [5,6], with extremely high isotopic selectivity, but the experimental equipment of an AMS is rather complicated and costly, and sample utilization is generally inefficient.

HIGH EFFICIENCY CAVITY TIMS

The efficiency and thus the detection limit of a TIMS system can be enhanced by replacing the conventional ribbon filament with a high efficiency cavity (HEC) ion source [7]. Previous studies for uranium and plutonium at Oak Ridge National Laboratory and the IAEA’s Safeguard Analytical Laboratory showed promise for high efficiency [8] when utilizing this source. For a HEC, a rhenium, tungsten or tantalum rod with a narrow cavity bored into the end is used and the sample is loaded in the base of the cavity. The cavity is heated via electron bombardment, and the sample inside the cavity is thus evaporated and ionized. With higher operating temperatures, larger ratio of surface area to volume, and confined geometry, higher ionization efficiencies are potentially feasible.

We present here results using a HEC interfaced with a ThermoFinnigan Triton MC-TIMS to explore the accuracy, precision, efficiency and detection limit for several elements including strontium, neodymium and plutonium.

RESULTS AND CONCLUSION

For the HEC-TIMS instrument at ORNL, initial plutonium isotope ratio measurements focused on liquid samples loaded and dried in the cavity, as liquid loads allow for relatively straightforward sample handling. Isotope ratio measurements have been performed on loads down to femtogram levels of plutonium for certified reference material performed using a discrete dynode secondary electron multiplier (SEM) detector. With a total efficiency of about 0.2% (amounts of atoms loaded to ions detected), a detection limit of (0.1 - 1) fg of plutonium ($^{239-242}\text{Pu}$, ^{244}Pu) can be reported. These results were surprising, as the efficiencies were far higher in tests on previous HEC systems; similar or better efficiencies can be obtained using a normal ribbon filament. However, these earlier tests did not use liquid loads. Instead of introducing the analyte into the cavity as a solution, sub-millimeter resin beads containing adsorbed plutonium were loaded into the cavity.

To further investigate the HEC-Triton system, isotope ratio measurement experiments were performed on strontium and neodymium samples loaded using both liquid and resin bead methods. An efficiency of about 0.2% for Sr and about 1% for Nd has been achieved using liquid loads. Variable but much higher efficiencies (1 - 20%, average around 10%) are achieved when the samples are loaded on resin beads, significantly improving the sensitivity and detection limit for isotope ratio analysis of Sr and Nd. These results suggest that the use of bead loading should similarly enhance efficiency towards (5 - 25%) for plutonium and uranium [8].

The cause of the dramatic difference in efficiencies using bead and liquid loading is not currently understood. Further studies with different cavity materials (Re, W, Ta), cavity sizes, elements, and loading techniques will be performed to better understand the significant increase in efficiency using bead loading instead of solution loading.

Research sponsored by the Office of Non-Proliferation Research and Engineering (NA-22), National Nuclear Security Administration (NNSA), U.S. Department of Energy, under contract DE-AC05-00OR22725 with Oak Ridge National Laboratory, managed and operated by UT-Battelle, LLC.

- 1 R. N. Taylor et al., Journal of Analytical Atomic Spectrometry. **18**, (2003).
- 2 M. Betti et al., Analytical Chemistry. **71**, (1999).
- 3 C. Grüning et al., International Journal of Mass Spectrometry. **235**, (2004).
- 4 S. Bürger et al., Journal of Environmental Radioactivity. **in press**.
- 5 J. E. McAninch et al., Nuclear Instruments and Methods in Physics Research B. **172**, (2000).
- 6 L. K. Fifield et al., Nuclear Instruments and Methods in Physics Research B. **117**, (1996).
- 7 P. G. Johnson et al., Nuclear Instruments and Methods. **106**, (1973).
- 8 L. R. Riciputi et al., International Geological Conference Abstract. **32**, (2004).

Determination of $^{241}\text{Pu}/^{239}\text{Pu}$ Amount Ratio in PHWR-Pu Samples Using Isotope Correlations

S.K. Aggarwal and D. Alamelu

Fuel Chemistry Division, Bhabha Atomic Research Centre, Trombay, Mumbai 400 085, INDIA

INTRODUCTION

Data on the isotopic composition of Pu produced in power reactors are required to know the fissile content of Pu when used as a fuel in fast reactors. Also, this information is useful to determine the α -specific activity of Pu, which is required to calculate the weight percentage of ^{241}Am in any Pu sample as well as for the determination of Pu concentration by radiometric methods. Usually the amount ratios of different Pu isotopes in a Pu sample are obtained by thermal ionisation mass spectrometry (TIMS) which requires a detailed chemical separation procedure. This increases the amount of analytical effort, in addition to the cost per analysis. There are many instances when such data, if available with a reasonable accuracy by an alternative fast and cost-effective method, suffice for the purpose e.g. in assay of waste solutions by radiometric method. Isotope correlations can be used to generate the data, in such cases, without resorting to mass spectrometric analysis procedure.

We have developed and reported isotope correlations¹⁻³ for the determination of amount ratios of Pu isotopes, using the data obtained by alpha spectrometry and by thermal ionisation mass spectrometry. With these correlations, the amount ratios of different Pu isotopes, except for the one involving ^{241}Pu , could be obtained with reasonable accuracy (2 to 5%). The uncertainty on the correlation involving ^{241}Pu was large due to its relatively short half-life (14.4 yr) which necessitates the availability of Pu samples with known irradiation and cooling history. Thus an attempt was made to develop a simple and independent method for determining $^{241}\text{Pu}/^{239}\text{Pu}$ amount ratio. This method is based on the determination of total α and total β activity of Pu isotopes using a suitable liquid scintillation counter.

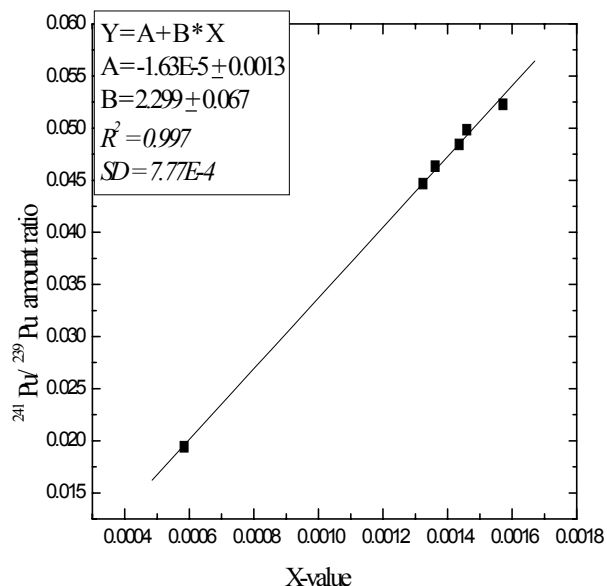


Fig 1. Correlation for the determination of $^{241}\text{Pu}/^{239}\text{Pu}$ amount ratio

The details of the experimental work carried out and the methodology developed for determining $^{241}\text{Pu}/^{239}\text{Pu}$ amount ratio are presented here. The decrease in the uncertainty of $^{241}\text{Pu}/^{239}\text{Pu}$ amount ratio along with the data on amount ratios of other Pu isotopes, obtained by isotope correlations, would improve the accuracy in the data on the percentage amounts of different Pu isotopes in the Pu sample.

EXPERIMENTAL

Five PHWR Pu samples, with varying amounts of different Pu isotopes, were used for the present study. The Pu samples were purified from ^{241}Am by anion exchange resin in 1:1 (v/v) HNO_3 using anion exchange separation and purification procedure. From each of the purified Pu samples, weighed amount (about 100 mg) of the solution was taken in a glass scintillation vial. The solution was dried under an infrared lamp. 5 mL of Ultima Gold AB scintillator (DIN based) was then added to the vial which was subjected to ultra-sonication for redissolving the Pu in the scintillation cocktail. The vials were then counted in a low back ground Liquid Scintillation Spectrometer for sufficient time in order to reduce the uncertainties due to counting. The total counts in the alpha region (100 to 400 keV) from ^{238}Pu , ^{239}Pu , ^{240}Pu and ^{242}Pu and in beta region (0 to 20 keV) from ^{241}Pu were recorded. The overall counts in the beta channel were much higher due to the high β specific activity of ^{241}Pu (half-life = 14.4 yr). In order to improve the statistics of measurements, the counts in the alpha region were recorded for 5 minutes.

Aliquots containing about 10 μg of Pu were taken for mass spectrometric analysis. The solutions were concentrated under an IR lamp and were loaded on to the vaporization filament of a double filament assembly of high purity rhenium. The TIMS used was equipped with a multi-Faraday cup detector system. $^{240}\text{Pu}/^{239}\text{Pu}$, $^{241}\text{Pu}/^{239}\text{Pu}$ and $^{242}\text{Pu}/^{239}\text{Pu}$ amount ratios were obtained by acquiring the data in static mode of multi-collection. $^{238}\text{Pu}/^{239}\text{Pu}$ amount ratios were determined by using electrodeposited sources of Pu samples and recording the alpha spectra using a 100 mm^2 PIPS semiconductor detector. The alpha spectra were acquired using a PC based multi-channel analyser. The $^{238}\text{Pu}/^{239}\text{Pu}$ amount ratios in the samples were calculated by using the $^{238}\text{Pu}/(^{239}\text{Pu} + ^{240}\text{Pu})$ alpha activity ratios determined by alpha spectrometry and $^{240}\text{Pu}/^{239}\text{Pu}$ atom ratio determined by TIMS, taking the half-life values of 87.74 yr, 24110 yr and 6553 yr, respectively for ^{238}Pu , ^{239}Pu and ^{240}Pu isotopes.

RESULTS & DISCUSSION

Using ratio of the total counts in the β region i.e. (0 - 20 keV) to total counts in the α region i.e. (100 to 400 keV) and knowing the pre-determined $^{238}\text{Pu}/^{239}\text{Pu}$, $^{240}\text{Pu}/^{239}\text{Pu}$ and $^{242}\text{Pu}/^{239}\text{Pu}$ amount ratios, a relation was established to determine the $^{241}\text{Pu}/^{239}\text{Pu}$ amount ratio ($R_{1/9}$) as given below:

$$R_{1/9} \propto (\text{Total } \beta / \text{Total } \alpha) \times [R_{8/9} \lambda_{238} + R_{0/9} \lambda_{240} + R_{2/9} \lambda_{242} + 1/\lambda_{239}] / \lambda_{241} \text{ -----(1)}$$

$$R_{1/9} \propto X \text{ -----(2)}$$

Figure 1 shows the correlation developed for the determination of $^{241}\text{Pu}/^{239}\text{Pu}$ amount ratio using the X value calculated as given in Eqs. (1) and (2), from ratio of total beta counts to the total alpha counts obtained by LSC and the amount ratios obtained from TIMS. It can be seen

that this relation is linear over the entire region of $^{241}\text{Pu}/^{239}\text{Pu}$ amount ratios expected for Pu from PHWR reactors. Table 1 gives a comparison of $^{241}\text{Pu}/^{239}\text{Pu}$ amount ratio obtained by TIMS as well as that calculated using the developed correlation for an unknown Pu sample. The two values agree well within 5 % showing the usefulness of the present methodology.

Table 1. A comparison on $^{241}\text{Pu}/^{239}\text{Pu}$ amount ratio determination by LSC and by TIMS

Atom % abundances by TIMS					β/α by LSC	$^{241}\text{Pu}/^{239}\text{Pu}$ by correlation	LSC / TIMS
^{238}Pu	^{239}Pu	^{240}Pu	^{241}Pu	^{242}Pu			
0.181	68.156	26.60	3.124	1.940	10.36	0.0452	0.987

It may be noted that since the amount ratio $^{241}\text{Pu}/^{239}\text{Pu}$ would reduce as a function of time due to radioactive decay of ^{241}Pu , the determination of the same will be possible by adopting the methodology discussed in this work. It may, however, be noted that the correlation presented here might be biased if there is a large difference in the cooling history (5 years or more), since the total alpha activity would also decrease due to the radioactive decay of ^{238}Pu (half-life 87.74 yr) in the sample.

The authors are thankful to Dr. V.Venugopal, Director of the Radiochemistry and Isotope Group of BARC, for his keen interest in this work.

1. S.K.Aggarwal and D.Alamelu, International Journal of Nuclear Energy and Science Technology **1**, 215 (2005).
2. D.Alamelu and S.K.Aggarwal, Radiochim. Acta **89**, 131 (2001).
3. S.K.Aggarwal, D.Alamelu and P.M.Shah, Radiochim. Acta **81**, 129 (1998).

High Resolution Alpha Spectrometry for the Determination of $^{240}\text{Pu}/^{239}\text{Pu}$ Amount Ratio in Pu Samples from PHWR

S.K. Aggarwal and D. Alamelu

Fuel Chemistry Division, Bhabha Atomic Research Centre, Trombay, Mumbai 400 085, INDIA

INTRODUCTION

Alpha Spectrometry is a useful analytical technique for the determination of alpha emitting isotopes in environmental, biological and nuclear fuel samples. Using the commercially available passivated and ion implanted planar silicon (PIPS/IPE) detectors, the best possible resolution that can be achieved is about 10 keV (FWHM) at 5.50 MeV using electrodeposited sources. But this resolution is not sufficient to allow complete resolution of the close-lying alpha energy groups in some of the important actinide isotopes. These include ^{240}Pu (5.168 MeV), ^{239}Pu (5.155 MeV); ^{238}Pu (5.499 MeV), ^{241}Am (5.486 MeV); ^{233}U (4.824 MeV), ^{234}U (4.784 MeV); ^{243}Cm (5.780 MeV), ^{244}Cm (5.804 MeV); ^{232}U (5.320 MeV), ^{228}Th (5.342 MeV) etc. It is nevertheless possible to employ sophisticated computer algorithms to resolve these close lying alpha energies and obtain information on $^{240}\text{Pu}/^{239}\text{Pu}$ amount ratios etc. However, most of these algorithms available previously were highly complex and could not be adopted by all the interested laboratories world-wide. Recently, under an International Atomic Energy Agency (IAEA) Coordinated Research Program (CRP) on the development of alpha spectrometry, a more generalized and user friendly version of the software (WinALPHA) for high resolution alpha spectrometry (HRAS) has been developed¹ and is now available to different users. The analytical function used in this program is a combination of an asymmetrical gaussian for the main part of the peak and a low energy exponential tail function. It was, therefore, considered interesting to employ this software for evaluating the precision and accuracy in the determination of $^{240}\text{Pu}/^{239}\text{Pu}$ amount ratios in NIST SRM-947 Pu as well as in Pu samples generated from Pressurized Heavy Water Reactors (PHWRs) using sources prepared in our laboratory and the alpha spectrometry system available with us. The values obtained from HRAS were compared with those determined experimentally by thermal ionization mass spectrometry (TIMS).

EXPERIMENTAL

For the determination of $^{240}\text{Pu}/^{239}\text{Pu}$ alpha activity ratio by HRAS, a few Pu samples obtained from PHWR reactors (burn-up about 10,000 MWD/TU) were taken up. These Pu samples were obtained after purifying the aliquots taken from irradiated fuel dissolver solutions, by using suitable anion exchange procedure in HNO_3 medium. Electro-deposited sources were prepared using electro-polished stainless steel disks as the backing material and a Pt stirrer as the anode. The sources were used as such, without heating in a flame or furnace. The alpha spectra were recorded using a 25 mm² PIPS detector, mounted in a vacuum chamber. The multiplets of $^{240}\text{Pu} + ^{239}\text{Pu}$ were resolved into individual components using the WinALPHA program, giving the abundances of all the alpha energy peaks of ^{240}Pu and ^{239}Pu as input in the software. For spectrum fitting, a region of 4.930 MeV to 5.200 MeV was used in all the spectra. Further, for the energy calibration, a value of 5.161 MeV, which corresponds to the average of the energies

of main peaks of ^{239}Pu (5.155 MeV) and ^{240}Pu (5.168 MeV) was used for the unresolved peak of $^{239}\text{Pu} + ^{240}\text{Pu}$ in addition to a value of 5.499 MeV for ^{238}Pu peak. This was found to be critical since otherwise the $^{240}\text{Pu}/^{239}\text{Pu}$ atom ratios were found to be positively or negatively biased w.r.t. mass spectrometric value when using the energy of ^{240}Pu or of ^{239}Pu peak alone, respectively for energy calibration.

RESULTS & DISCUSSION

Tables 1 and 2 give the typical results obtained after spectrum fitting on independent sources prepared from NIST-SRM-947 Pu and Pu samples from PHWR, respectively. $^{240}\text{Pu}/^{239}\text{Pu}$ atom ratios given in Tables 1 and 2 were obtained from the $^{240}\text{Pu}/^{239}\text{Pu}$ alpha activity ratios obtained by HRAS and using the half-life values of 24110 yr and 6553 yr, respectively for ^{239}Pu and ^{240}Pu . It is seen that the results obtained by HRAS for $^{240}\text{Pu}/^{239}\text{Pu}$ atom ratios in PHWR Pu samples as well as those in NIST-SRM-947 Pu² sample agree within 2 to 5% with TIMS values. These studies demonstrate the applicability of the new software developed under IAEA CRP for the determination of $^{240}\text{Pu}/^{239}\text{Pu}$ atom ratio by HRAS. Rigorous evaluation of the software by varying different parameters e.g. source quality, counting statistics etc. is planned in future.

The authors are thankful to Dr. V.Venugopal, Director of the Radiochemistry and Isotope Group of BARC, Mumbai for his keen interest in this work.

1. R.Capote Noy, E.Garcia-Torano, E.Maineira, E. Lopez, Nucl. Instr. Methods in Phys. Res. **A 525**, 522 (2004).
2. D.Alamelu, P.M.Shah and S.K.Aggarwal, Nuclear and Radiochemistry Symposium, March 15-18, 2005, Guru Nanak Dev University, Amritsar (NUCAR 2005), (Eds. Keshav Chander, R.Acharya, B.S.Tomar and V.Venugopal), p.493 (2005).

Table 1. Typical data after spectral fitting using WinALPHA on replicate spectra for NIST-SRM-947 Pu

Source number	Area under the peak		Fitted parameters			$^{240}\text{Pu}/^{239}\text{Pu}$ atom ratio
	^{240}Pu	^{239}Pu	χ^2	Tail parameter	FWHM (keV)	
1	105761	120493	15.4	0.94	16.7	0.23856
2	212640	238013	39.2	1.06	17.8	0.24282
3	145356	157580	16.2	1.05	17.9	0.25071
4	106330	123130	11.9	1.03	17.1	0.23471

Certified $^{240}\text{Pu}/^{239}\text{Pu}$ atom ratio (corrected for decay) : 0.24099

Table 2. Typical data after spectral fitting using WinALPHA on replicate spectra for PHWR Pu samples

Sample no.	Source no.	Area under the peak		Fitted parameters			²⁴⁰ Pu/ ²³⁹ Pu atom ratio by HRAS	Mean value from HRAS/TIMS value
		²⁴⁰ Pu	²³⁹ Pu	χ^2	Tail parameter	FWHM (keV)		
1.	A	9479	5643	3.0	1.02	17.7	0.4566	1.029
	B	18843	11957	2.7	1.01	16.2	0.4283	
2.	A	20783	13031	3.5	1.02	16.9	0.4335	1.036
	B	18828	12553	2.6	0.96	15.8	0.4077	
3.	A	103041	72063	11.9	1.00	16.2	0.3886	0.986
	B	136125	97132	16.7	1.01	16.9	0.3809	
4.	A	141488	109582	11.9	1.05	17.6	0.3509	1.008
	B	150385	125655	15.9	1.04	17.7	0.3253	

A Novel Methodology for Determining Traces of Uranium in Plutonium by Thermal Ionisation Mass Spectrometry

D.Alamelu and S.K.Aggarwal

Fuel Chemistry Division, Bhabha Atomic Research Centre,
Trombay, Mumbai - 400 085, INDIA

INTRODUCTION

Determination of trace amounts of uranium (U) in plutonium (Pu) is required for variety of purposes. These include chemical quality assurance of Pu bearing fuel materials, characterisation of certified reference material for Pu amount and for determining the chemical purity of Pu obtained after reprocessing of the irradiated fuel. Most of the analytical methodologies involve prior separation of U from bulk of Pu. Isotope dilution - thermal ionisation mass spectrometry (ID-TIMS) using atomic ions (U^+) for measurements also depends upon the separation of U from Pu, prior to mass spectrometric determination of U amount ratios in the spiked sample. This becomes essential to minimise the isobaric interference of $^{238}Pu^+$ at $^{238}U^+$ peak during measurements by mass spectrometry.

Previously, studies have been reported¹⁻³ from our laboratory on the formation of atomic and molecular ions (M^+ and MO^+) using synthetic mixtures of U and Pu with different amount ratios. During these studies, it was possible to identify the filament heating conditions, using a multiple filament assembly, when only UO^+ ions are produced and no PuO^+ ions are formed. These studies prompted us to investigate the possibility of determining trace levels of U using UO^+ ions in TIMS, without involving the separation from bulk of Pu in the sample. In this work, this methodology has been adopted to the determination of U in a chemical assay standard of Pu as well as in the synthetic dissolver solutions of Indian PHWR fuels.

EXPERIMENTAL

Two synthetic samples, representing the PHWR irradiated fuel dissolver solution samples, with U/Pu amount ratios of 100 and 300, were prepared by mixing weighed aliquots of purified NIST-SRM -947 Pu and NIST- SRM - U chemical assay standard.. The synthetic mixtures were subjected to purification by anion exchange separation procedure using DOWEX 1 X 8 resin in

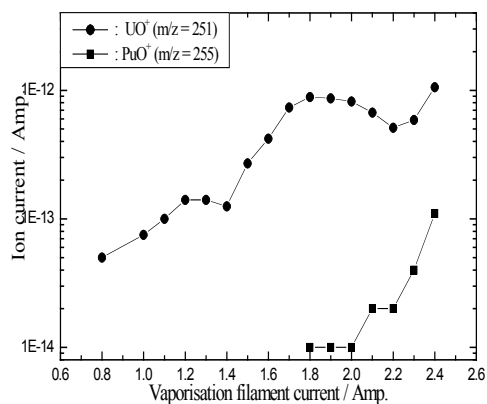


Fig 1 : Production of UO^+ and PuO^+ ions as a function of vaporisation filament heating current. The heating current of ionisation filament is kept constant.

1:1 (v/v) HNO₃. Uranium present on the column was washed with 1:5 HNO₃ and Pu was eluted with 1:50 HNO₃. The eluted Pu solutions, containing traces of U, were taken up in pre-weighed volumetric flasks. The concentration of Pu in these solutions was determined using liquid scintillation counting (LSC) and the specific activity calculated from the isotopic composition data determined by TIMS. Weighed aliquot from each of these solutions, containing 5 to 10 µg of Pu was taken and was mixed with pre-calibrated NIST-SRM- 930 U solution (²³⁵U > 93 atom%) to obtain an Pu/U amount ratio of 5 in the mixture. 2 µL solution from the mixture was loaded on to a high purity rhenium filament of a double filament assembly. The ionisation and vaporization filaments were heated to about 6 A and 2 to 2.4 A, respectively to obtain sufficient ion current of UO⁺ without PuO⁺. A thermal ionization mass spectrometer equipped with multi-Faraday cups was employed for acquiring the data in static mode of multi-collection. The amount ratios of U isotopes in the samples were obtained using UO⁺ ions at m/q values of 251 and 254 corresponding to ²³⁵UO⁺ and ²³⁸UO⁺, respectively. The concentration of U in the purified solution was then evaluated by usual equation used in ID-TIMS. Experiments were also conducted to determine the amount of uranium in the proposed chemical assay standard of plutonium viz. K₄Pu(SO₄)₄ without resorting to any ion exchange separation and using the same methodology as discussed above.

RESULTS

Tables 1 and 2 show the results of the ID-TIMS experiments on the determination of uranium at ppm levels in plutonium. The synthetic samples used to simulate U/Pu amount ratios as those expected in PHWR irradiated fuel samples (Table 1) also provide data on the decontamination factor achieved for U w.r.t. Pu in the anion exchange separation procedure employed in the present work for purification of Pu. The results given in Table 2 clearly demonstrate the applicability of the present ID-TIMS approach using enriched ²³⁵U (> 93 atom%) for the determination of trace amounts of U in Pu samples, without resorting to any separation and purification procedure.

The authors are thankful to Dr V.Venugopal, Director of Radiochemistry and Isotope Group at BARC for his keen interest in the work and constant support and encouragement.

1. S.K.Aggarwal, M.K.Saxena, P.M.Shah, S.Kumar, U.Jairaman and H.C.Jain, Int. J. Mass Spectrom. Ion Process. **139**, 111 (1994).
2. D.Alamelu, P.S.Khodade, P.M.Shah and S.K.Aggarwal, Int. J. Mass Spectrom. **239**, 51 (2004).
3. S.K.Aggarwal and D.Alamelu, Int. J. Mass Spectrom. **241**, 83 (2005).

Table 1. Determination of U in synthetic samples with U/Pu amount ratios as seen in PHWR irradiated fuel dissolver solution samples, after subjecting them to purification by anion exchange method

Initial U/Pu amount ratio in the synthetic mixture	Weight of solution (in gm)		$^{235}\text{UO}^+ / ^{238}\text{UO}^+$ amount ratio determined by TIMS in the mixture	Concentration (μg of element/gm of solution)		% of U in Pu	Decontamination factor (DF) of Pu w.r.t. U
	Sample (purified Pu solution)	Spike (NIST-SRM-930-U)		U	Pu		
100	5.97	0.1053	9.6318 (0.23 %)	0.00894	0.87	1.028	9730
300	5.96	0.0766	6.6549 (0.4 %)	0.01307	0.89	1.469	20422
300	13.46	0.0971	5.6959 (0.07 %)	0.00934	0.42	2.225	13483

Table 2. Determination of U in $\text{K}_4(\text{PuSO}_4)_4$ chemical assay standard of Pu

Weights of the solution (gms)		$^{235}\text{UO}^+ / ^{238}\text{UO}^+$ amount ratio determined in the mixture	Concentration (μg of element/gm of solution)		U/Pu amount ratio / 10^{-6}
Pu standard sample	NIST-U-930 spike		U	Pu	
1.06225	1.00905	17.1849 (0.14 %)	0.0057	71.171	80.23
1.3127	1.0123	17.1483 (0.12 %)	0.0071	87.951	80.82

Effect of Radioactive Decay of Pu Isotopes for Determination of Pu Concentration with High Accuracy by Isotope Dilution Mass Spectrometry (IDMS) and Isotope Dilution Alpha Spectrometry (IDAS)

D.Alamelu and S.K.Aggarwal

Fuel Chemistry Division, Bhabha Atomic Research Centre, Trombay, Mumbai 400 085, INDIA

INTRODUCTION

Determination of the total amount of Pu at the input point of a fuel reprocessing plant is one of the very important requirements of nuclear material accounting. This determination usually involves two measurements: (i) the total volume or weight of the solution in the tank and (ii) the concentration of Pu in the solution. The latter is generally achieved by following isotope dilution methodology due to complex nature of the irradiated fuel dissolver solution and also due to high radiation dose associated with the solution. The use of isotope dilution involves the addition of a known amount of tracer solution to an accurately known amount of the sample solution followed by the determination of change in the atom ratio by thermal ionisation mass spectrometry (TIMS) or change in the alpha activity ratio by alpha spectrometry (AS). The two methodologies are popularly known as isotope dilution mass spectrometry (IDMS) and isotope dilution alpha spectrometry (IDAS). In our laboratory, we have developed and demonstrated the use of ^{239}Pu and ^{238}Pu as spikes (tracers), respectively, for IDMS^{1,2} and IDAS³ experiments on Pu. In the IDMS experiments, we have used Pu containing about 65 atom% of ^{239}Pu as a spike for Pu from low burnt fuels with ^{239}Pu abundance of 90 atom% or higher.

The uncertainty in Pu concentration measurements by IDMS or IDAS depends upon many components including the uncertainty in the atom ratio or the alpha activity ratio determination in the spiked mixture. It is well recognised by the scientific community that any uncertainty in the data of Pu spike will contribute a systematic error in the concentration value of Pu in the sample. Thus it is essential that the isotopic composition of Pu in the spike, average atomic weight of Pu in the spike and the amount of Pu in the spike aliquot used must be known with the smallest possible uncertainty. These measurements again involve the use of thermal ionisation mass spectrometry and calibration of the spike by IDMS or IDAS by using a primary reference material of Pu. It is generally assumed that once the spike calibration is done, the aliquots of the spike distributed in different vials and stored properly may be employed for several years in future. However, due to the radioactive decay of Pu isotopes present in the spike, there would be changes in these parameters (i.e. isotopic composition, total amount of Pu in the aliquot etc.) which could contribute additional uncertainties in the Pu concentration measurements. This paper presents our experience in using two such spikes viz. ^{239}Pu about 65 atom% and ^{238}Pu about 93 atom% for IDMS and IDAS experiments. It is shown that the radioactive decay of Pu isotopes, if not considered properly, can contribute appreciable uncertainty in the Pu concentration values, particularly, when using ^{238}Pu as a spike in IDAS or in IDMS. This

assumes great importance in the present global scenario when tonnes of Pu are available and the concentration measurements are expected to have overall uncertainties of less than 0.1% .

RESULTS & DISCUSSION

Table 1 gives the isotopic composition data of ^{239}Pu and ^{238}Pu spikes used in our laboratory for IDMS and IDAS work on Pu. In the ^{239}Pu spike, the amount of ^{238}Pu was determined by alpha spectrometry whereas the amounts of all other isotopes in the two spikes were obtained by thermal ionisation mass spectrometry. Table 2 shows the changes in the atom % abundance, average atomic weight of Pu and the amount of Pu in the spike aliquot due to radioactive decay of Pu isotopes over a period of 1,2,5 and 10 years after fresh calibration of the spike (assumed as zero time). Figures 1 and 2 present the effects of these changes in ^{239}Pu and ^{238}Pu spikes respectively. It is evident that there is a combined effect to the extent of 0.25% and nearly 7%, respectively, when using pre-calibrated ^{239}Pu and ^{238}Pu spikes with amount% of different isotopes given in Table 1. These changes must be included in the isotope dilution equation used for calculation of concentration after measuring the atom ratio of alpha activity ratio in the spiked mixtures. When these measurements are carried out on a routine basis by an operator and all the calculations are made by using an excel sheet, there is a possibility of overlooking the changes in the parameters given here and the concentration values will, therefore, have uncertainties due to the radioactive decay of Pu isotopes in the spikes used. The investigation presented in this paper are extremely important when aiming at an overall uncertainty of better than 0.1% in the Pu concentration or in the total amount of Pu at a reprocessing plant.

The authors are thankful to Dr. V.Venugopal, Director of the Radiochemistry and Isotope Group of BARC, Mumbai for his keen interest in this work.

1. S.K.Aggarwal, G.Chourasiya, R.K.Duggal, R.Rao and H.C.Jain, Int. J. Mass Spectrom. Ion Processes, **69**, 137 (1986)
2. S.K.Aggarwal, R.K.Duggal, R.Rao and H.C.Jain, Ibid, **71**, 221 (1986).
3. M.V.Ramaniah, H.C.Jain, S.K.Aggarwal, S.A.Chitambar, V.D.Kavimandan, A.I.Alamula, P.M.Shah, A.R.Parab and V.L.Sant, Nucl. Technol. **49**, 121 (1980).

Table 1. Data on the amounts of different Pu isotopes in ^{239}Pu and ^{238}Pu spikes

S.No.	Amounts (atom%) of different isotopes in spike		
	Nuclide (<i>Half-life in yr</i>)	^{239}Pu spike	^{238}Pu spike
1.	238 (87.74)	0.225	92.254
2.	239 (24110)	65.14	7.3017
3.	240 (6553)	28.62	0.4143
4.	241 (14.4)	3.604	0.0277
5.	242 (3.76×10^5)	2.406	0.00212

Table 2. Change in atom % abundance, average atomic weight of Pu and the amount of Pu in the spike aliquot due to radioactive decay of Pu isotopes

Spike (methodology)	Decay period (Yrs)	Spike isotope	Correction factor due to radioactive decay			
			Atom fraction (a)	Average atomic weight (b)	Pu amount (c)	Combined effect of (a), (b) and (c)
^{239}Pu (IDMS)	0	^{240}Pu	1.00	1.00	1.00	1.00
	1		1.001658	0.999989	0.99824	0.999905
	2		1.003241	0.999978	0.996559	0.99981
	5		1.007574	0.999949	0.991958	0.999522
	10		1.013571	0.999909	0.985568	0.999034
^{238}Pu (IDAS)	0	^{238}Pu	1.00	1.00	1.00	1.00
	1		0.999401	1.000003	0.992727	0.99213
	2		0.998799	1.000005	0.985511	0.984322
	5		0.996964	1.000012	0.964205	0.961266
	10		0.993814	1.000025	0.929807	0.924032

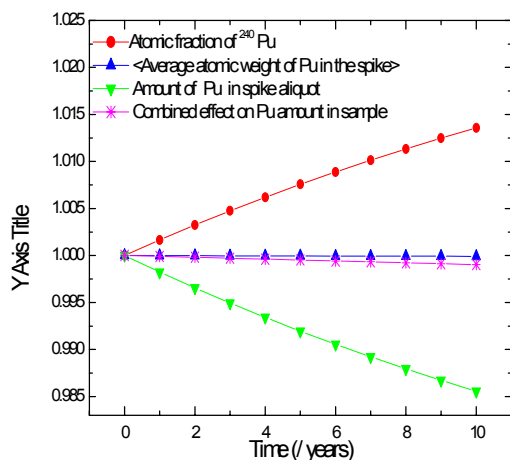


Fig1 : Fractional changes in different parameters as a function of time due to radioactive decay of Pu isotopes in ^{239}Pu spike

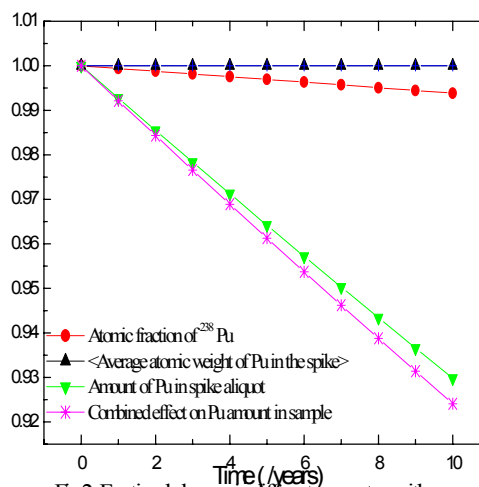


Fig2 : Fractional changes in different parameters with time due to radioactive decay of Pu isotopes in ^{238}Pu spike

Gamma Spectroscopy Applications in D&D Process Development, Inventory Reduction Planning & Shipping, Safety Analysis & Facility Management During the Heavy Element Facility Risk Reduction Program

Mark Mitchell*, Brian Anderson, Leonard Gray, Robert Vellinger, Michael West, Lennox Harris, Reginald Gaylord, Jennifer Larson, Greg Jones, Norris Harward, John Shingleton
*Lawrence Livermore National Laboratory, Livermore CA 94552 USA
UCRL-ABS-218325

This presentation discusses the development of new applications for gamma ray spectroscopy for D&D process development, inventory reduction planning and shipping, safety analysis, and facility management. These applications of gamma spectroscopy were developed and implemented during the Risk Reduction Program (RRP). The RPP successfully downgraded the Heavy Element Facility (B251) from a Category II Nuclear Facility to a Radiological Facility. Gamma spectroscopy is concluded to be an important tool in project management, work planning, and work control (“*expect the unexpected and confirm the expected*”), minimizing worker dose, and resulted in significant safety improvements and operational efficiencies.

Inventory reduction activities utilize gamma spectroscopy to identify and confirm isotopes of legacy inventory, in-growth of daughter products and the presence of process impurities; quantify inventory; prioritize work activities for project management; and supply documentation satisfying shipper/receiver requirements. D&D activities utilize *in-situ* gamma spectroscopy to identify and confirm isotopes of legacy contamination; quantify contamination levels and monitor the progress of decontamination; and determine the point of diminishing returns in decontaminating enclosures and glove boxes containing high specific activity isotopes such as ^{244}Cm and ^{238}Pu . *In-situ* gamma spectroscopy provided quantitative comparisons of several decontamination techniques (e.g. TLC-free Stripcoat, Radiac wash, acid wash, scrubbing) and is used as a part of an iterative process to determine the appropriate level of decontamination and optimal cost to benefit ratio. Radioactive contaminants included: $^{166\text{m}}\text{Ho}$, ^{232}U , ^{233}U , ^{235}U , ^{237}Np , ^{238}Pu , ^{239}Pu , ^{240}Pu , ^{241}Pu , ^{242}Pu , ^{241}Am , $^{242\text{m}}\text{Am}$, ^{243}Am , ^{243}Cm , ^{244}Cm , ^{246}Cm , ^{248}Cm , and ^{249}Cf .

Facility management utilizes gamma spectroscopy, in conjunction with other characterization techniques, process knowledge, and historical records, to provide information for work planning, work prioritization, work control, and safety analyses (e.g. development of stop work points). This approach resulted in B251 successfully achieving Radiological status on schedule. Gamma spectroscopy helps define operational approaches to achieve ALARA, e.g. hold points, appropriate engineering controls, PPE, workstations, and time/distance/shielding. Applications of gamma spectroscopy can improve upon similar activities at other facilities.

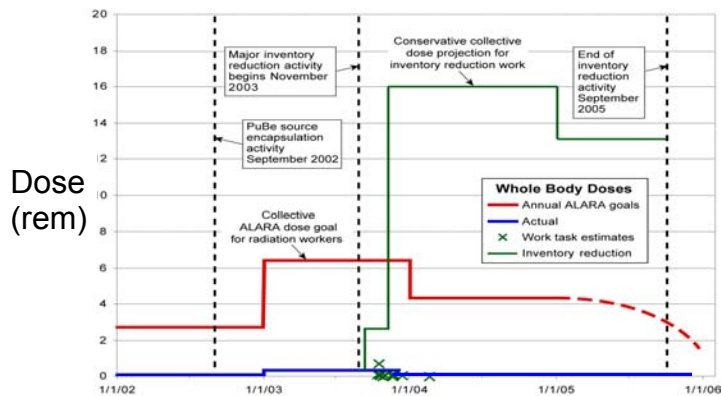


Figure 1. ALARA Comparison of Actual vs. Predicted Dose Demonstrates Success of Work Control Practices

***IN-SITU* GAMMA SPECTROSCOPY SUPPORTED D&D PROCESS DEVELOPMENT**

The D&D Project utilized gamma spectroscopy both as a D&D process development tool and as characterization tool in support of D&D. The RRP monitored the progress of decontamination and compared the effectiveness of several decontamination techniques by using *in-situ* gamma spectroscopy. Gamma spectroscopy resulted in a ground breaking success - no one had decontaminated facilities with this level and variety of high specific activity isotopes (e.g. ^{244}Cm , ^{238}Pu , ^{228}Pa , aged ^{232}U). D&D processes developed using applications of *in-situ* gamma spectroscopy were pivotal to the success of the RRP. The RRP completed D&D of 40 of 49 Enclosures in 1 year; characterized all enclosures (gamma spectroscopy, alpha-swipe tab sampling); processed 37 lower-contaminated gloveboxes through D&D and shipped to RHWM as LLW; and emptied 2 highly-contaminated Blue Cave enclosures with little or no contamination to the room. Special packaging of contaminated equipment included a glovebox transferred as TRU Waste in a Standard Waste Box (SWB) and 2 glove boxes transferred as TRU Waste in a Type A Box. This work generated over 800 waste parcels, 84 TRU drums, and numerous LLW drums.



Figure 2. *In-situ* gamma spectroscopy of contaminated glove boxes and equipment

Reference: Mark Mitchell et al, *New Applications of Gamma Spectroscopy: Characterization Tools for D&D Process Development, Inventory Reduction Planning & Shipping, Safety Analysis & Facility Management During the Heavy Element Facility Risk Reduction Program*, submitted to: 2006 MARC VII Conference

Calculated Neutron Source and Spectra in Plutonium Metal and Compounds

G.Vlaskin

A.A.Bochvar VNIINM (All-Russian Research Institute of Inorganic Materials), Moscow, Russia

METHOD OF EVALUATION

An accurate knowledge of the specific neutron yields and spectra are very important values for plutonium metal and compounds. It appeared evident that the best way of obtaining the yield and spectrum is by calculation, using the differential (α, n) cross sections and decay constants.

NEDIS[1] is a computer code that determines neutron production rates and spectra from (α, n) reactions and spontaneous fission. The code is capable of calculating (α, n) source rates and spectra in four types of problems: homogeneous media (i.e. mixture of α -emitting source material and low-Z target material), where the radius of α -emitting source material particles (as sphere) may be account for, two-region interface problems (i.e. a thin/thick slab of α -emitting source material in contact with a thick slab of low-Z target material), three-region interface problems (i.e. thin or thick slab of α -emitting source material between of different low-Z target material), and (α, n) reactions induced by a monoenergetic beam of (α, n) particles incident on a thick slab of target material. Spontaneous fission spectra are calculated with evaluated half-life, spontaneous fission branching, and Watt spectrum parameters for 51 actinides. The (α, n) spectra are calculated using experimental anisotropic angular distribution in the center-of mass system with a library of 23 sets of measured and/or evaluated total cross sections and for each product nuclide level states, and functional α -particle stopping cross sections for $Z \leq 98$. The code outputs the magnitude and spectra of the resultant neutron source. It also provides an analysis of the contributions to that source by each light element in the problem. Fig.1 show comparisons of calculated (α, n) neutron source spectra for the $^{238}\text{PuBe}_{13}$ (1 gr. ^{238}Pu) compound determined by 1-NEDIS, 2-NEDIS using isotropic library JENDL[2], 3-SCALE5 (isotropic library LANL[3]).

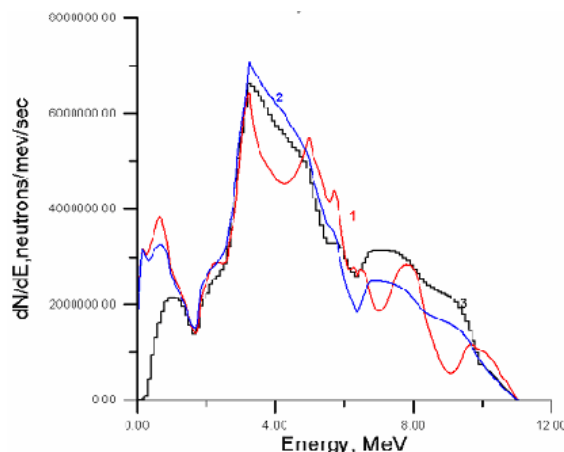


Fig.1 Energy-dependent neutron sources strength in $^{238}\text{PuBe}_{13}$ as calculated by 1)NEDIS, 2)NEDIS library JENDL, 3)SCALE5

When light element impurities $\leq 1\%$ in plutonium metal the simple formula 1 may be used to calculate neutron yield due to (α, n) reactions.

$$Y = \sum a_{il} C_l M_{Pu} \alpha_i \quad (1)$$

Where

C_l – mass content of light element l (weight percent);

α_i – mass content of isotope i in plutonium (weight percent);

M_{Pu} - mass of plutonium (gram)

a_{il} - coefficients in Table 1 calculated using the NEDIS computer program (per 1 gram Pu).

$$a_{il} = Y_{NEDIS} / (C_l M_{Pu} \alpha_i) \quad (2)$$

Table 1

element	a_{il}			
	²³⁸ Pu	²³⁹ Pu	²⁴⁰ Pu	²⁴² Pu
Li	5.32e+02	1.04e+00	3.91e+00	2.68e-02
Be	1.70e+04	4.96e+01	1.83e+02	2.66e+00
B	4.37e+03	1.34e+01	4.95e+01	7.40e-01
C	2.52e+01	6.54e-02	2.42e-01	3.29e-03
O	1.52e+01	4.28e-02	1.58e-01	2.29e-03
F	1.87e+03	4.78e+00	1.77e+01	2.33e-01
Mg	2.43e+02	5.55e-01	2.06e+00	2.55e-02
Al	1.28e+02	2.38e-01	8.88e-01	9.28e-03
Si	2.20e+01	4.79e-02	1.78e-01	1.87e-03

- 1 G.N.Vlaskin, E.V.Chvankin. Atomnaya energiya.(Rus), v.74, n.2, 1993, p.134-139.
- 2 T. Murata, K. Shibata. Evaluation of The (α ,n) Reaction Nuclear Data for Light Nuclei, J.of Nucl.Sci. &Tech.,Supl,2, Aug.,2002, Proc. Of Int. Conf. Nucl. Data for Sci. &Tech. Tsukuba, Japan, 2001,v.1 p. 76-79.
- 3 ORIGEN-ARP 2.00 Isotope Generation and Depletion Code System - Matrix Exponential Method with GUI and Graphics Capability, RSICC code package C00702PC58600. - May 2002

Determination of long-lived Plutonium isotopes in environmental samples

E. Hrnccek^{*}, R. Jakopič[†], P. Steier[‡], A. Wallner[‡]

^{*} ARC Seibersdorf research GmbH, 2444 Seibersdorf Austria

[†] Jožef Stefan Institute, Ljubljana Slovenia

[‡] Institut für Isotopenforschung und Kernphysik der Universität Wien, VERA Laboratory, Währinger Str. 17, 1090 Wien Austria

A combination of Alpha Spectrometry and Accelerator Mass Spectrometry (AMS) was used for the determination of the isotopic ratios of Plutonium isotopes in environmental reference samples and samples contaminated from nuclear reprocessing.

After adding Pu-236 tracer, Plutonium was separated by ion exchange with AG1-X8 resin from 7.2 M HNO₃. Samples for Alpha Spectrometry were prepared by microprecipitation with NdF₃ using cellulose nitrate membrane filters. The Pu-236 tracer was used to determine the absolute specific activity of Pu-239 and Pu-239+Pu-240 by Alpha Spectrometry.

Sequentially, a part of the filter was used for determination of the isotope ratios of Pu-239, Pu-240, Pu-242 and Pu-244 by AMS at the Vienna Environmental Research Accelerator (VERA) facility. To this end the filter material was reprocessed. Fe was added, Pu was co-precipitated with Fe(OH)₃ and finally solid samples were prepared. The various Pu isotopes were extracted from a sputter ion source and separated by their masses. AMS - being independent on the half-life of a radionuclide - provides isotope ratios directly by counting the radionuclides with a particle detector.

Results for the isotopic ratios of the samples will be shown and the capabilities and detection limits achievable for determination of Pu-242 and Pu-244 will be discussed.

Pu, Np and U Valence States and Type of Molecules Determination by Chemiluminescence Effects and Pulse Laser Spectroscopy Methods

I.N.Izosimov¹, N.G.Gorshkov¹, L.G.Mashirov¹, N.G.Firsin¹

¹ Khlopin Radium Institute, 2nd Murinski ave 28, St. Petersburg 194021, Russia
e-mail: izosimov@atom.nw.ru

Selective and sensitive direct actinide elements trace amounts detection in the different samples presents today major importance for ecology, radwaste handling and control, rehabilitation of contaminated areas and risk assessment. The behavior of actinides in environment is determined by actinides valence states and type of molecules. Information about actinide valence states in trace analysis is essential to fix the actinides emission source and the propagation history. The most sensitive (for example – TRLIF) laser spectroscopy methods with time resolution (TR) use photoluminescence for detection, don't give information about valence states and for some actinides and lanthanides detection in solutions [1,2] have limit of detection (LOD) up to 10^{-13} mol/l(M) (Table 1).

Table 1. LOD by Time Resolved Laser Induced Fluorescence (TRLIF) method.

Element	UO ²⁺	Cm ³⁺	Am ³⁺	Eu ³⁺	Tb ³⁺	Gd ³⁺	Dy ³⁺	Sm ³⁺	Ce ³⁺
LOD(M)	10^{-13}	10^{-13}	10^{-9}	10^{-13}	10^{-9}	10^{-8}	10^{-10}	10^{-10}	10^{-9}

Pu, Np and some valence form of U does not give the photoluminescence in solutions and for it's detection not most sensitive (LOD – 10^{-5} - 10^{-7} M) laser spectroscopy methods are used.

Today the chemiluminescence effects using in biology and medicine [3] for trace amount detection of different substances with LOD up to 10^{-9} - 10^{-13} M and it is possible to determine the elements valence states and type of molecules. In our experiments [4,5] we observed the chemiluminescence of solutions induced by Pu, Np and U after excitation by pulse laser radiation. High sensitive TR methods may be used for this chemiluminescence detection (fig.1).

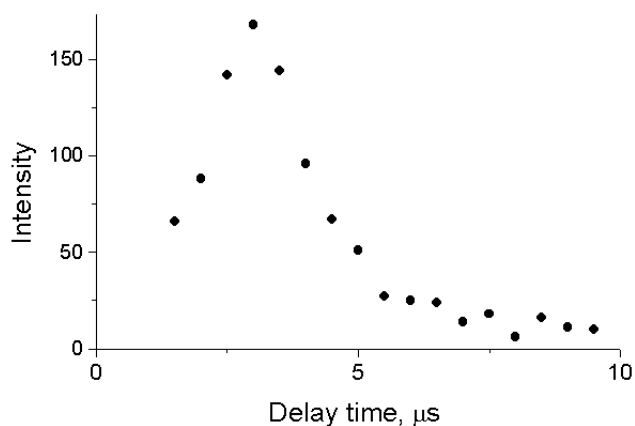


Fig.1: Kinetic curve of luminol chemiluminescence induced by excited plutonyl complexes.

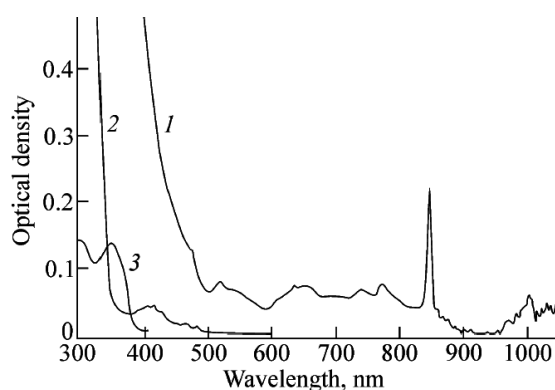


Fig.2: Absorption spectra of (1)-PuO₂²⁺, (2)- UO₂²⁺ and (3)-luminol.

Chemiluminescence is widely used as a base for detection methods in many fields, such as flow injection analysis, chromatography, biology, medicine, etc. [3]. We have observed and study the chemiluminescence effects

in solutions containing U, Pu and Np [4,5]. It's open possibility for chemiluminescence application in *Nuclear Chemistry*.

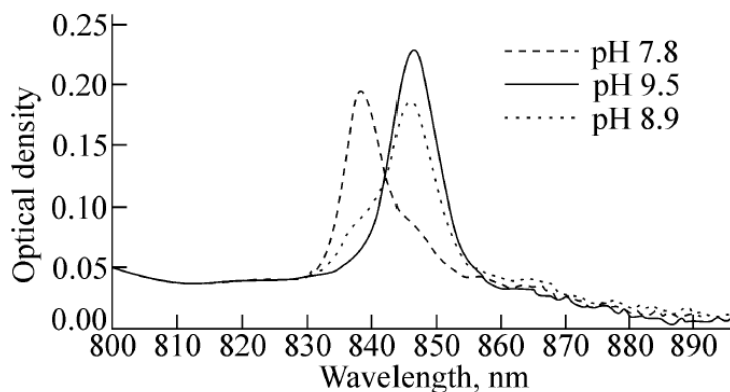


Fig.3: Absorption spectra of plutonyl complexes in 42 % CsF + H₂O solutions at different pH values. Two complexes are in solution: PuO₂F₅³⁻ (band 839nm) and PuO₂F₄OH³⁻ (band 846.5nm).

By proper selection of lasers radiation wavelengths (fig.2, fig.3), one or multi-step actinides complexes excitation scheme and chemiluminogenic label it is possible to induced chemiluminescence only by selective excitation of detectable actinide complexes .

The chemiluminescence effects using allows to essentially spread scope for trace amount detection of actinide in solutions, determination of the actinide valence states in solutions and determination of the molecule type containing actinide. Especially perspective is to use the chemiluminescence effects for detection of actinides and complexes containing actinides in solution in the cases when in such systems actinide does not give direct luminescence but can induce chemiluminescence. Multi step chemiluminescence excitation scheme may be efficiently used for detection selectivity increasing [5].

The sensitivity of the chemiluminescence methods is higher than sensitivity of other methods (LIPAS for example) which are used for non-luminescent actinides and molecules detection now. The combinations of the chemiluminescence effects with high sensitivity and high selectivity laser spectroscopy methods make it possible to carry out an effective detection both of luminescent and *non-luminescent* actinides and molecules containing actinides (especially U, Pu and Np) in different solutions.

- 1 C.Moulin, P.Decambox and P.Mauchien, *Anal.Chem.* **68**,(1996) 3204.
- 2 I.N.Izosimov, *Proc. 4th International Workshop "Laser spectroscopy on beams of radioactive nuclei"*, May 24-27, 1999, Poznan, Poland. . Ed. JINR, Dubna, E15-2000-75, p.169.
- 3 C.Dodeigne, L.Thunus and R.Lejeune, *Talanta* **51**, (2000) 415.
- 4 I.N.Izosimov, N.G.Gorshkov, L.G.Mashirov, N.G.Firsin, A.A.Kazimov, S.V.Kolichiev, N.A.Kudryshev and A.A.Rimski-Korsakov, *Proc. 5th International Workshop "Application of lasers in atomic nuclei research"*, Poznan, Poland, 2001. Ed. JINR, Dubna, E15-2002-84, p.153.
- 5 N.G.Gorshkov, I.N.Izosimov, A.A.Kazimov, S.V.Kolichiev, N.A.Kudryshev, L.G.Mashirov, A.V.Osokin and N.G.Firsin, *Radiochemistry* **45**, (2003) 28.

Plutonium in Higher Oxidation States in Alkaline Media

I.G. Tananaev, M.V. Nikonov, B.F. Myasoedov

Vernadsky Institute of Geochemistry and Analytical Chemistry Russian Academy of Science,
Moscow 199991 Russia

INTRODUCTION

The discovery and studies of *5f* elements in unknown oxidation states are of a noticeable interest for theoretical inorganic chemistry and enrich the chemistry of transuranium elements. Before our experiments it was well known that the highest oxidation state for Pu was (VII). Hence the electron structure of Pu(VII) as $5f^7$ permits to suppose that this actinide may exists in the oxidation state +8 with the electron configuration of an inert gas. During 40+ years a several attempts to prepare Pu(VIII) have been made. The main aim on these experiments was to oxidize Pu(VII) by different agents in the various media, but all of these attempts were not successful. Seemingly, there is no way to prepare Pu(VIII), indeed. However the discovery of unexpected Pu(VIII) species has a great interest, and we started the experiments in this field.

EXPERIMENTS

The blue-black solution of Pu with the characteristic absorption spectrum (AS) having the main maximums at 607, and 635 nm is prepared by interaction of fine pure 2,9 mM Pu(VI) in 1,5M NaOH with 3,5% vol. O₃/O₂ mixture (gas flow 5-7 dm³/h, 20°C) during 30 min. It was detected that addition of a small (0,05 ml) drops of a non ozonized 1.3 mM Pu(VI) in 1,5M NaOH step by step to the 3 ml portion of ozonized (colored) solution goes to instantly decrease of optical density of the blue-black solution proportionally to the growth of amount of the added initial solution of Pu(VI). It was supposed that the ozonizing of Pu(VI) in 1-3M NaOH leads to formation of a mixture of Pu(VII), and assumed Pu(VIII), who directly in the experiments above interacted with the initial non ozonized Pu(VI) solution by the following scheme: Pu(VI) + Pu(VIII) → 2Pu(VII) (1). Knowing the amount of Pu(VI) in the first aliquote, interacted with Pu, treated with ozone (0,05 ml × 1,3 mM = 6,5•10⁻⁵ mmol) and decrease of an optical density of the mixture at 635 nm (~ 0,18), the probably value of molar extinction coefficient (ϵ) of Pu(VIII) was estimated as ~2600 ± 400 M⁻¹cm⁻¹. The value of $\epsilon^{\text{Pu(VII)}}$ at the 500-550 nm was found as ~100 M⁻¹cm⁻¹. From data above the yield of assumed Pu(VIII) in the experimental solution was estimated to be ~(15±5)%.

Alternative way, the unknown oxidant could produced during Pu(VI) ozonizing in alkaline solution (Pu ozonide, peroxy compound of Pu^{VII}, and so on), which can interacted with initial Pu(VI) in alkaline solution. For specification of the data obtained the complementary experiments have been carried out:

1. The spectrophotometric titration of the product of reaction (1) by H₂O₂ was provided. The addition of H₂O₂ causes well seen changes in the spectra of the testing solution. The stoichiometric ratio of [Pu]:[H₂O₂], determined after the completing of the titration was ~2.2:1. The data obtained can confirm that Pu in the tested solution was in +7 oxidation state.

2. The interaction of 0.2 ml aliquots of the just ozonized 1.8 mM Pu(VI) in 2M LiOH with 1 ml of 5mM Np(VI) in 2M LiOH had been carried out. The considerable changes in the AS of the mixture solution had been observed in the result of titration. Addition of ozonized Pu(VI)

solution to Np(VI) cause the appearance of the band with 620 nm in the spectrum, typical for Np(VII) solutions. Knowing the amount of Pu in the added aliquote and the amount of the formed Np(VII), it was possible to design that the ratio of Np:Pu $\sim 1.2 \pm 0.1$. This fact confirms the initial supposition that ozonization of Pu(VI) in alkaline media leads to the formation of the mixture of Pu(VII) and unknown oxidant, probably Pu(VIII) in the experimental solutions.

3. Two redox-reactions had been studied: (a) interaction of Pu(VI) with Fe(VI) in 1M NaOH solution; and (b) contact of ozonizing Pu(VI) alkaline solution with Fe(III). As a results of these experiments it was found that Pu(VI) solutions are found to be oxidized by ferrate-ions in 1,5M NaOH. On the other hand, the preliminary ozonized Pu solutions oxidize Fe(III) to Fe(VI). These data contradict to the known literature ones about the behavior of Pu ions in the highest oxidation states in alkaline solutions. As ferrate-ions oxidize Pu(VI) ions we conclude that the value of the redox potential of pair Pu(VII)/Pu(VI) is $<0,72$ V (vs NHE).

4. Reducing of assumed Pu(VIII) by different kind reducing agents to direct Pu(VII) were carried out. As the work was based on spectrophotometry, AS of the chosen reductant and the products of their oxidation should not have intensive absorbance bands in visible range at least in the interval of absorbance of Pu(VIII), and (VII). The Cl^- , Br^- , I^- , IO_3^- and $\text{C}_2\text{H}_5\text{OH}$ were tested. Unfortunately, it was found that even small excess of these reagents, added to assumed Pu(VIII) led to fast and irreversible formation of Pu(VI). Contrary, the AS of the product of interaction of a mixture of Pu(VII) and assumed Pu(VIII) with $[\text{NO}_2^-] = 0.1\text{M}$ at $[\text{NaOH}] < 1\text{M}$ had not neither intensive absorbance band at 607, and 635 nm, supposed for the spectrum of Pu(VIII), nor maximums of absorbance at 655, 871 and 1021 nm, known for alkaline solutions of Pu(VI) (fig.1). The similarity of AS of solutions after interaction of a mixture of Pu(VII) and assumed Pu(VIII) with nitrite-ions, and with Pu(VI) are detected.

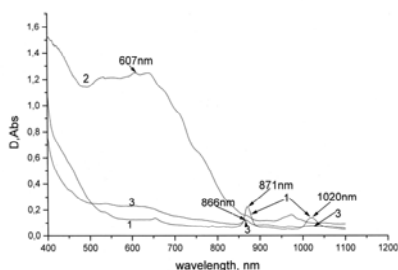


Fig.1. (1) AS of the initial 1,8 mM Pu(VI) in 0,45 M NaOH; (2) AS of the same solution after 1 h ozonization; (3) AS of the ozonized solution (2) after 0.05ml of 2M NaNO_2 was introduced there.

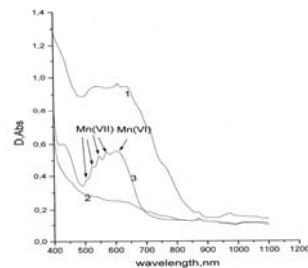


Fig.2. AS of 1 mM Pu(VI) in 0,5M NaOH, after 1 h ozonizing before (1) and after (2) addition of 0,005 mmole NaNO_2 , and with the consequent introduction of 0,001mmole of K_2MnO_4 .

5. The interaction of the just described solution with manganate ions at $[\text{NaOH}] = 0.5\text{M}$ causes the crimson coloration of the reaction product, and the bands of absorbance of Mn(VII) appeared in the AS (fig. 2). It was shown also in the separate experiment that Mn(VI) did not interact with Pu(VI) stock solution under the same conditions. Thus, it is possible to conclude that Pu in +7 oxidation state is really the product of reducing of an ozonizing colored solution by nitrite-ion in alkaline media. All of the data obtained confirmed that the Pu(VIII) formed during ozonizind of Pu(VI) in the alkaline solution, which has a characteristic AS with the main maximums at 607, 635 nm, that earlier is attributed to absorption of Pu(VII).

The work was supported by the U.S.DOE-OBES, Project RC0-20004-SC14, and RUC2-20012-MO-04.

Optical absorbance spectroscopy of Pu ions in aqueous solution

E. Bauer, S. D. Reilly, M. P. Neu

Los Alamos National Laboratory, Los Alamos NM 87545 USA

INTRODUCTION

There is frequent need to determine the oxidation state and concentration of plutonium ions in aqueous solution for research and development applications. Optical absorbance spectroscopy of plutonium ions in acidic solutions is an efficient and effective way to determine the combination of oxidation states present. The characteristic optical absorbance spectrum for each oxidation state, as seen in Figure 1, together with Beer's Law, is used to determine the concentration of each ion present.

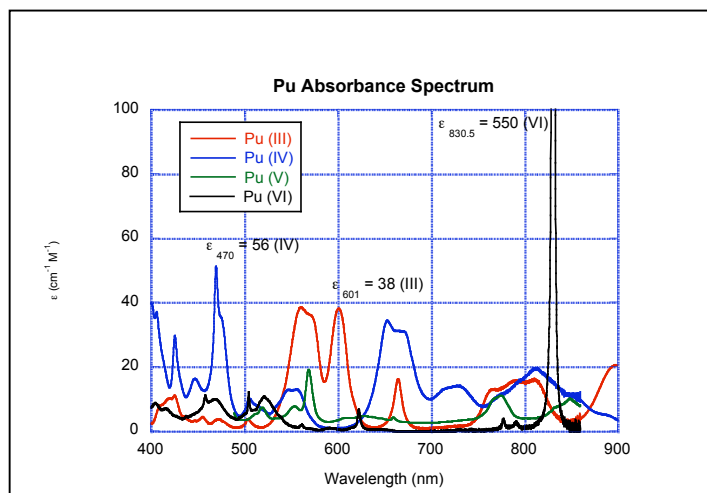


Fig 1: Characteristic optical absorbance spectra of Pu oxidation states in 1 M HClO_4 solution.

The frequently-cited Pu spectra reported by Cohen in 1961¹ were recorded using a Cary Model 14, the first commercial recording spectrophotometer. With the widespread use of optical absorbance spectrophotometers with greater resolution and sensitivity, it would be beneficial to reinvestigate the characteristic spectra and absorptivities of each plutonium ion in commonly used media. For instance, the Cary 6000i UV-vis-NIR spectrometer utilizes an InGaAs detector in the NIR region, which provides better resolving power and is approximately 100 times more sensitive than the traditional PbS detector in older models.² This NIR

region encompasses the narrow, characteristic PuO_2^{2+} 830.5 nm absorbance band.

We will use a Cary 6000i to analyze well-characterized solutions of plutonium in different oxidation states. We will determine and report the characteristic spectra of each oxidation state in common mineral acids, as well as solutions of sodium chloride (0.5, 2 and 5M) and sodium nitrate (1 and 3M).

EXPERIMENTAL

A ^{239}Pu solution of known concentration and isotopic composition in 1 M HClO_4 was prepared and then analyzed using the Cary 6000i. The spectra for this solution is shown in Figure 2. The solution was oxidized to a pure Pu (VI) solution by saturation with ozone for several days. We varied the spectral band width (SBW) to determine the minimum SBW necessary to resolve the

narrow PuO_2^{2+} 830.5 nm peak (Fig. 3). The optimum SBW will be used to analyze duplicate samples of Pu (VI) solutions and results will be compared to counted samples to determine Pu (VI) concentration in the analyzed solution. From this information epsilon for this peak will be determined using the Beer-Lambert law:

$$A = \epsilon bc \quad (1)$$

In the above equation 1, A is a proportionality constant called the absorptivity and refers to the amount of light absorbed at a given wavelength. The path length (length of the path of light traveling through the sample) is signified by b and is expressed in cm. Concentration is expressed in molarity. Epsilon is a constant that is calculated by comparing absorptivity vs. concentration and is expressed as $\text{cm}^{-1} \text{M}^{-1}$.

A similar analysis will be done for pure oxidation states of III, IV and V in mineral acids as well as sodium chloride and sodium nitrate solutions. Characteristic peaks for each oxidation state will be examined and epsilons calculated and reported.

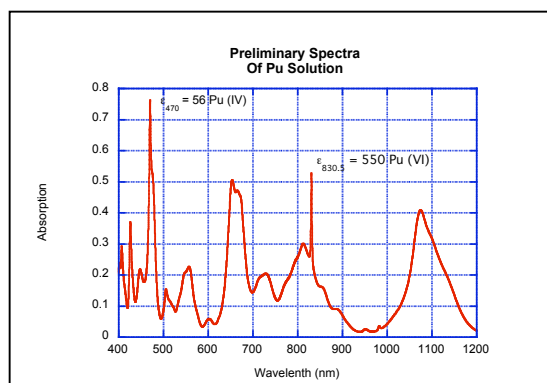


Fig 2: UV-vis/NIR spectrum of Pu in 1 M HClO_4 before oxidation with ozone.

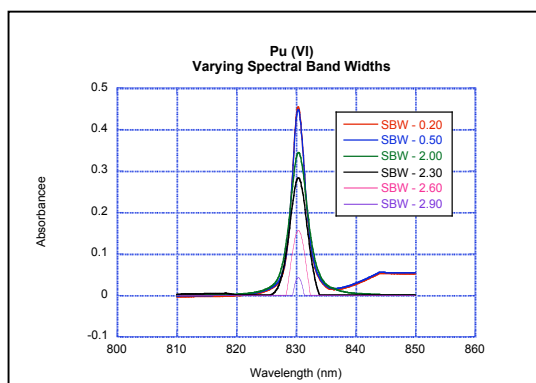


Fig 3: Characteristic 830.5 nm PuO_2^{2+} peak recorded using different spectral band widths.

RESULTS AND DISCUSSION

The preliminary spectrum of the Pu solution to be used in the experiments (Fig 2) indicated that the solution was a mixture of Pu (III, IV and VI). Saturating the solution with ozone resulted in complete oxidation to Pu(VI). The spectrophotometer spectral band width must be set small enough to resolve the narrow Pu absorbance bands such as the one at 830.5 nm (full width half height is approximately 2 nm). The spectrum of the pure Pu(VI) solution recorded using different SBW values is shown in Fig. 3. SBW values larger than 0.20 do not fully resolve the narrow peak.

- 1 D. Cohen, J. Inorg. Nucl. Chem. **18**, 211 (1961).
- 2 J. J. Comerford, Varian Instruments UV-Vis-NIR Application Note No. 88, 2003.

Study on Valence of Pu, Np and Tc in Nitric Acid after Electrolytic Reduction

H. Hoshi^{*}, Y.-Z. Wei^{*}, M. Kumagai^{*}, T. Asakura[†], Y. Morita[†]

^{*}Institute of Research and Innovation, Kashiwa, Chiba 277-0861 Japan

[†]Research Group for Aqueous Separation Process Chemistry, Nuclear Science and Engineering Directorate, Japan Atomic Energy Agency, Tokai-mura, Ibaraki 319-1195 Japan

INTRODUCTION

For the development of nuclear fuel cycle, it is one of the most important tasks to improve reprocessing process more economically and efficiently¹. Especially, to establish the Fast Breeder Reactor (FBR) cycle system for the future, it is strongly desirable to develop a new reprocessing process which uses more compact equipments and produces less radioactive wastes compared to the present PUREX process. For this purpose, we have proposed a novel aqueous reprocessing system named ERIX Process (The Electrolytic Reduction and Ion Exchange Process for Reprocessing Spent FBR-MOX Fuel) to treat spent FBR-MOX fuels. As shown in Fig. 1, this process consists of (1) Pd removal by selective adsorption using a specific anion exchanger; (2) electrolytic reduction for the valence adjustment of the major actinides including

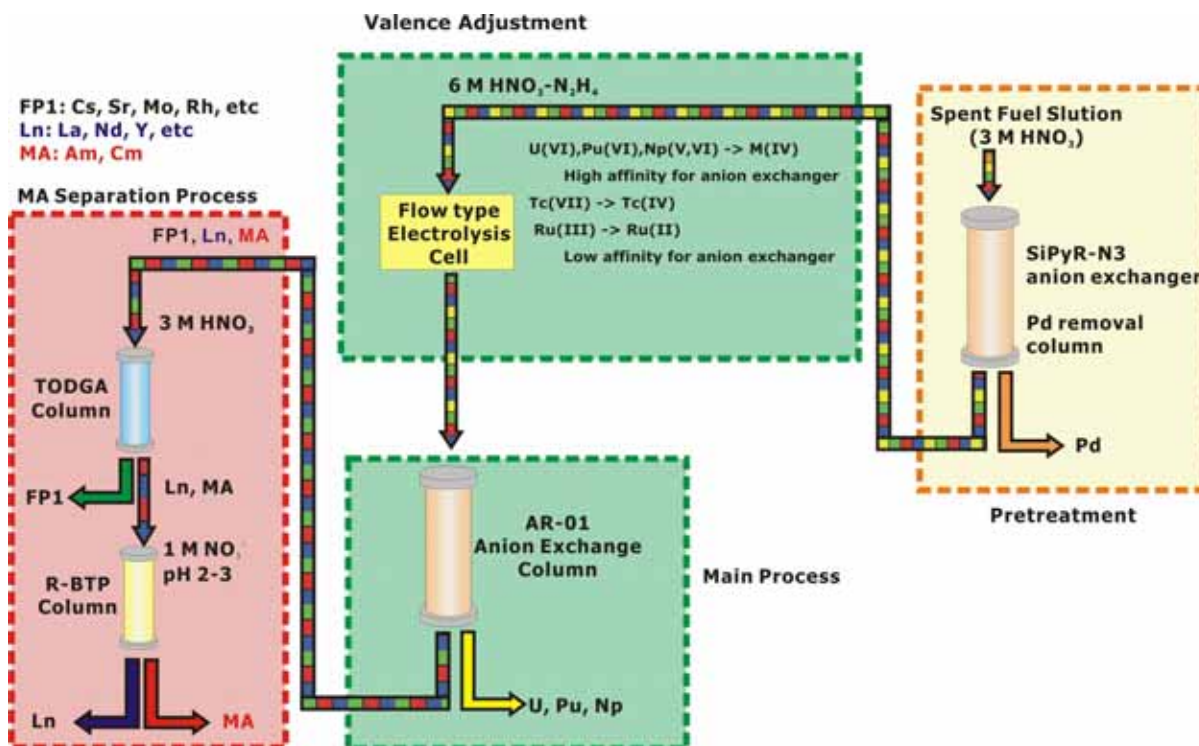


Fig 1: ERIX Process

U, Pu, Np and some fission products (FP) such as Tc and Ru; (3) anion exchange separation for the recovery of U, Pu and Np using a new type of anion exchanger, AR-01; and (4) selective separation of long-lived minor actinides (MA = Am and Cm) by extraction chromatography^{2,3}.

The adjustment of valence of actinides, e.g. U(VI) to U(IV), is one of the most important subject to increase affinity onto anion exchanger for quantitative recovery of U, Pu and Np in this process. For this purpose, nitric acid concentration of spent fuel solution is adjusted to 6 M and it is reduced at -300 mV (vs. Ag/AgCl) through a novel flow-type electrolysis cell. In this work, valence of Pu, Np and Tc in concentrated nitric acid solution after the electroreduction was studied.

ELECTRO REDUCTION

It is well known that Pu and Np take several oxidation states in nitric acid solution. Usually, Pu(IV) is most stable in nitric acid solution. Pu(III) is quickly oxidized to Pu(IV) by nitrous acid, however, Pu(III) exists in nitric acid solution with some reductant, e.g. hydrazine. In this ERIX Process, U(VI) is reduced to U(IV) in 6 M HNO₃ solution at -300 mV (vs. Ag/AgCl) and hydrazine is used as a HNO₂ scavenger.

Electroreduction of 6 M HNO₃ solution containing Pu, Np and Tc through flow-type electrolysis cell was examined. According to the UV-Vis spectra, Pu and Np were reduced to Pu(III) and Np(IV), respectively. Under the modification of hydrazine, Pu stably existed as Pu(III) in 6 M HNO₃ solution after electroreduction. However, Pu(III) was liable to be oxidized to Pu(IV) in case of coexisting with Tc or Ru by their catalytic reaction. Especially, oxidation ratio of Pu(III) to Pu(IV) with Ru was faster than that with Tc. Anion exchanger column separation of the reduced solution was also performed. As the results, it was found that all of the Np was reduced to Np(IV) which was quantitatively recovered from the column by dilute nitric acid solution. Since Pu was eluted together with the Np(IV), it is presumed that the Pu(III) was oxidized to Pu(IV) inside the anion exchanger column.

Tc(VII) is the most stable oxidation state of Tc in spent fuel solution and it is strongly adsorbed onto an anion exchange resin in nitric acid as the form of pertechnetate anion (TcO₄⁻). Therefore, quantitative recovery of Tc from anion exchanger column is one of the important subjects in this process. Owing to the difficulty of evaluation of Tc oxidation state by UV-Vis spectra, above reduced solution was analyzed by anion exchanger column. After electro reduction, because Tc indicated no adsorption onto anion exchanger column, Tc(VII) was considered to be reduced to Tc(IV) or Tc(II)⁴. Tc was separated from U, Pu, and Np, through anion exchanger column after electro reduction.

This paper is the results from “Development of the ERIX Process for Reprocessing Spent FBR-MOX Fuel” entrusted by the Ministry of Education, Culture, Sports, Science and Technology of Japan (MEXT).

- 1 Y.-Z. Wei, et al., , *Proc. of PBNC-2002*, Shenzhen, China, October 21 - 25, 2002.
- 2 H. Hoshi, et al., *J. Alloy. Compd.*, **374**, 451 (2004).
- 3 Y.-Z. Wei, et al., *J. Alloy. Compd.*, **374**, 447 (2004).
- 4 H. Hoshi, et al., *J. Radioanal. Nucl. Chem.*, **262**, 601-605(2004)

Condensation and Fragmentation Reactions of Cationic Uranium Complexes in the Gas Phase

Gary Groenewold^{1*}, Michael Van Stipdonk², Garold Gresham¹, Winnie Chien², Anita Gianotto¹, and Kevin Cossell¹

¹Department of Chemical Sciences, Idaho National Laboratory, Idaho Falls ID, USA

²Department of Chemistry, Wichita State University, Wichita KS, USA

INTRODUCTION

The ultimate disposition of uranium in the environment or in processes related to separations is dependent on aspects of its chemical speciation, including oxidation state, organic complexing ligands, and attached solvent molecules. Ligand preferences and exchange reactions play a key role in dictating how uranium will be partitioned in heterogeneous systems, and hence knowledge of these factors is important for predicting behavior. Useful insight can be gained by examining solvent addition and exchange reactions of gas-phase uranium ions occurring in the gas phase of a trapped-ion mass spectrometer. The appeal of working in this environment is that explicitly-defined species can be isolated and examined for reactivity trends and relative ligand binding preferences.

EXPERIMENTAL METHODS

Examination of reactions uranium cations requires their formation, isolation, which then enables either condensation or fragmentation reactions to be carried out. Ion formation was accomplished using either electrospray, or by primary ion bombardment. Electrospray of uranyl-solvent solutions was performed using a Finnigan LCQ-DECA instrument, which has a quadrupole ion trap for its mass analyzer. Primary ion bombardment of U-containing solid targets was conducted using an ion trap-secondary ion mass spectrometer, that was designed and conducted in-house at the INL. In all experiments, ions of interest were isolated by ejecting competing ions that have different masses from the ion trap. In the condensation experiments, ions were then allowed to react with gaseous neutral molecules, which enables evaluation of reaction pathways and kinetics. In the fragmentation experiments, ionic complexes were excited by application of an external resonant frequency to the end caps of the ion trap, which increased the kinetic energy and produced hyperthermal collisions with the He bath gas.

RESULTS

Initial studies of U(IV), U(V) and U(VI) dioxo cations examined addition of H₂O.¹ The extent of ligation increased with the oxidation state. [UOOH]⁺ (U(IV)) eventually formed [UOOH(H₂O)₃]⁺ (total of 5 ligands), whereas [UO₂OH]⁺ (U(VI)) formed [UO₂(OH)(H₂O)₃]⁺ (6 ligands). The U(V) cation [UO₂]⁺ displayed intermediate behavior.

Acetone (A) is a stronger gas-phase nucleophile than water, and formed complexes in an analogous manner: for example, the U(VI) ion [UO₂OH]⁺ formed [UO₂OH(A)₃]⁺, indicating that A and out-competed water in ligation on the U center. The [UOOH]⁺ cation was the exception to this pattern, ultimately preferring to form the mixed complex [UOOH(A)₃(H₂O)]⁺. Increasing the charge state from +1 to +2 increased the extent of ligation in the U(VI) species: starting from

$[\text{UO}_2]^{2+}$, the penta-ligated $[\text{UO}_2(\text{A})_5]^{2+}$ uranyl complex was formed.² This showed that the extent of ligation in the gas phase was similar if not identical to that in solution.

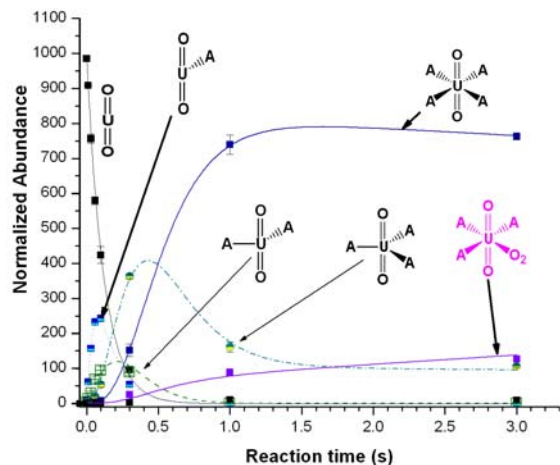


Figure 1. Kinetic profile showing addition of consecutive addition of acetone (A) and O_2 to $[\text{UO}_2]^+$.

The dioxoxygen complex was best described as a ligated $[\text{UO}_2^{2+}\text{O}_2^-]$ ion pair.

New horizons were also revealed by examining fragmentation reactions of uranyl complexes. Fragmentation of undercoordinated $[\text{UO}_2\text{NO}_3(\text{ROH})_n]^+$ showed elimination of HNO_3 , indicating that in the local environment of the U center, the alcohol was functioning as a stronger acid than was HNO_3 .⁴ In the case where R = isopropyl, the isopropoxy ligands present on the intermediates that were formed by the HNO_3 elimination then underwent U-mediated oxidation, forming both acetone and acetaldehyde and eliminating H_2 at the same time.⁵ Other evidence for U insertion into C-H and C-C bonds has since been observed in amide and phosphoryl complexes.

This research was supported by the U. S. Department of Energy, and by the National Science Foundation.

¹ Gresham, G. L., et al. *J. Phys. Chem. A*, **2003**, 107, 8530.

² M. J. Van Stipdonk et al., *J. Phys. Chem. A*, **2004**, 108, 10448.

³ G. S. Groenewold et al.; *J. Am. Chem. Soc.*, **2006**, Web Release: 2/11/2006; DOI: 10.1021/ja0573209.

⁴ Van Stipdonk, M. J., et al. *J. Am. Soc. Mass Spectrom.*, **2003**, 14, 1205.

⁵ Van Stipdonk, M. J., et al., *Int. J. Mass Spectrom.*, **2004**, 237, 175.

Soft X-ray Synchrotron Radiation Investigations of Actinide Materials

D. K. Shuh^{*}, H. J. Nilsson^{*†}, T. Tyliszczak^{*}, R. E. Wilson^{*}, S. M. Butorin[‡], K. Kvashina[‡], J.-H. Guo^{*}, L. Werme^{†‡}, and J. A. Nordgren[‡]

^{*}Lawrence Berkeley National Laboratory, Berkeley, CA 94720 USA

[†]SKB, Box 5864, S-102 40, Stockholm, Sweden

[‡]Dept. of Physics, Uppsala University, Box 530, S-751 21, Uppsala, Sweden

INTRODUCTION

Microspectroscopic and fluorescence-based techniques have been exploited for investigations of actinide materials at sources of soft X-ray synchrotron radiation (SR) because of the capability to perform experiments with small amounts of actinide materials. Soft x-ray SR methods are able to elucidate the roles of the 5f electrons in the chemical bonding of the actinides, characterize the electronic structures of actinide materials, and probe the surface chemistry of actinide materials. Soft x-ray SR techniques generally require optimization and modification of experimental hardware for use with radioactive materials. Results from soft x-ray SR investigations have had and will impact in areas of actinide science related to f-electron bonding, aging, corrosion, gas-solid interactions, actinide transport, and the development of nanoscale actinide materials characterization techniques.

At the Advanced Light Source of Lawrence Berkeley National Laboratory (LBNL), we have been utilizing and developing soft x-ray methods for use with actinide materials. Currently, we have been regularly employing near-edge x-ray absorption fine structure (NEXAFS), x-ray emission spectroscopy (XES), resonant inelastic x-ray scattering (RIXS), and scanning transmission x-ray microscopy (STXM) to investigate a range of fundamental properties in actinide and actinide-relevant materials.

ACTINIDE SCANNING TRANSMISSION X-RAY MICROSCOPY

The ALS Molecular Environmental Science (ALS-MES) STXM has been developed into a characterization tool for actinide particulates and for general soft x-ray actinide science. The ALS-MES STXM permits NEXAFS and imaging with 30 nm spatial resolution. The results from studies of U, Np, and Pu oxides will be presented, demonstrating the capabilities and limitations of soft x-ray STXM spectromicroscopy for investigations of actinide systems^{1,2}. The actinide 4d edges are employed for both imaging and for oxidation state determination. Of particular importance is the capability to directly probe the edges of light elements by NEXAFS, such as the oxygen K-edge, that are integral constituents of many actinide materials. A plutonium elemental map from a particle obtained during precipitation of colloids containing Pu is shown in Figure 1. Representative oxygen K-edge spectra from the AnO₂ were collected, and for UO₂, the spectrum resembles the oxygen K-edge from the bulk material. Actinide sample preparation methods, as well as sample radiation damage considerations, will be described.

ACTINIDE X-RAY EMISSION/RESONANT INELASTIC X-RAY SCATTERING

Soft x-ray XES and RIXS investigations of actinide materials have been performed at the actinide 5d and light element 1s edges at ALS Beamline 7.0.1. Reference spectra have been collected from the dioxides of uranium through plutonium. The chemical reactions of aqueous transuranic species with Fe surfaces have been characterized under the same conditions as in previous studies of U interactions with Fe surfaces³. For Np, the oxidation state of the surface species was Np(V) since the RIXS loss features differed from those of NpO₂. The first Np measurements have been followed by recent studies of PuO₂ and Pu interactions with Fe. The initial XES/RIXS measurements of curium have also been recently performed. Complementing the spectroscopy at the actinide 5d edge have been the measurements of several actinide oxide reference materials at the oxygen K-edge.

In addition to the bonding information gained on fundamental actinide reference materials, the application of NEXAFS/XES/RIXS at both the actinide and light element edges has the potential to fully characterize the nature of bonding in a larger range of actinide materials and complexes.

This work was supported by the Director, Office of Science, Office of Basic Energy Sciences, Division of Chemical Sciences, Geosciences, and Biosciences of the U.S. Department of Energy at the Lawrence Berkeley National Laboratory under Contract No. DE-AC02-05CH11231.

- 1 H. J. Nilsson, T. Tylliszczak, R. E. Wilson, L. Werme, D. K. Shuh, J. Anal. Bioanal. Chem. **383**, 41 (2005).
- 2 H. J. Nilsson, T. Tylliszczak, R. E. Wilson, L. Werme, D. K. Shuh, Proc. Royal Soc. Chem., in press, (2006).
- 3 S. M. Butorin, D. K. Shuh, K. Kvashnina, I. Soroka, K. Ollila, J.-H. Guo, K. E. Roberts, L. Werme, J. Nordgren, Mater. Res. Soc. Symp. Proc. **807**, 166 (2004).

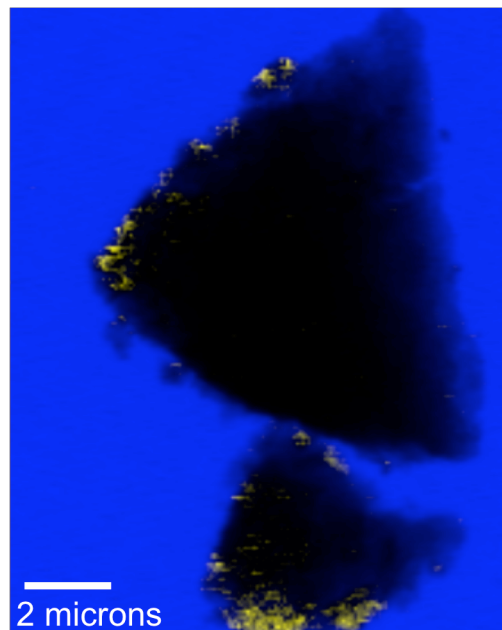


Fig. 1: Elemental map of plutonium (yellow) on silicon dioxide particles collected with the ALS-MES Beamline 11.0.2 STXM.

Electrochemical Studies of Actinide Species in Room Temperature Ionic Liquids

M. E. Stoll^{*}, W. J. Oldham[†], D. A. Costa^{*}

Los Alamos National Laboratory, Los Alamos NM 87545 USA

^{*}Nuclear Materials Technology Division (NMT-15) and [†]Chemistry Division (C-INC)

The use of room temperature ionic liquids (RTIL's) for electrochemical methods is currently receiving a great deal of attention¹. The properties of RTIL's that make them advantageous for electrochemistry include a large electrochemical window (~5 V), relatively high conductivity, negligible vapor pressure, and high thermal stability. Our research efforts have focused on exploring the electrochemical behavior of actinide ions and complexes in RTIL's comprised mainly of the bis(trifluoromethylsulfonyl)imide anion, $\text{N}(\text{SO}_2\text{CF}_3)_2$, paired with 1,3-dialkylimidazolium, quaternary ammonium, and pyrrolidinium cations. The electrochemical behavior of actinide complexes in non-aqueous media is an area of research that deserves further attention due to the potential for new processing methods. The inherent properties of RTIL's compared to conventional organic solvent/supporting electrolyte systems and molten salts may make them ideally suited for the processing of nuclear materials. In this regard knowledge concerning the fundamental redox behavior of actinide complexes in RTIL's is needed. Our presentation will focus on our recent results with coordination and organometallic complexes of uranium including some novel imido analogs of the uranyl ion prepared recently by our colleagues at LANL². Another related aspect of our research that will be covered concerns the electrodeposition of electropositive metal ions from RTIL solutions. Pyroprocessing in molten salt media is a powerful method of purification and separation for actinide metals. The ability to perform similar processes at ambient temperature in RTIL's could enable more efficient processes with increased safety. Results on the cathodic electrodeposition of Na, K, Li, and Al ions will be presented along with our efforts to date on the electrodeposition of uranium.

1 P. He, H. Liu, Z. Li, J. Li, *J. Electrochem. Soc.* **152**, E146, (2005) and references therein.

2 T.W. Hayton, J.M. Boncella, B.L. Scott, P.D. Palmer, E.R. Batista, and P.J. Hay, *Science* **310**, 1941 (2005).

Hydrolysis of Plutonium(IV) in 0.5 M HCl/NaCl

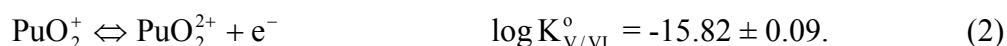
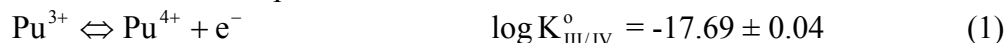
J.-I. Yun^{*}, H.R. Cho^{*}, M. Altmaier^{*}, V. Neck^{*}, A. Seibert[†], C.M. Marquardt^{*}, C. Walther^{*}, Th. Fanghänel^{*}

^{*}Institut für Nukleare Entsorgung, Forschungszentrum Karlsruhe, D-76021 Karlsruhe, Germany

[†]European Commission, JRC, Inst. for Transuranium Elements, D-76125 Karlsruhe, Germany

There have been a number of potentiometric, extraction, solubility, and spectrophotometric studies of the first hydrolysis constant of Pu(IV) as discussed in the NEA-TDB.^{1,2} The values scatter by about 1.5 orders of magnitude primarily because of redox reactions. Reliable hydrolysis constants can be found only when the electrochemical potentials are cautiously controlled, and when the total equilibrium Pu(IV) concentrations in solution are measured. None of the available studies provide reliable thermodynamic data for higher hydrolyzed species of Pu(IV). The extraction study of Metivier and Guillaumont³ was considered as the best available.^{2,4}

A spectrophotometric study of the hydrolysis of Pu(IV) in 0.5 M H/NaCl is performed in the concentration range from 10^{-5} to $3 \cdot 10^{-4}$ mol/l and at pH_c 0.3 – 2.1. The Pu(IV) stock solutions are prepared electrochemically by oxidation of Pu(III) and the oxidation state distribution is confirmed by spectrophotometry (UV/Vis for higher concentrations, 1-m capillary waveguide UV/Vis for lower concentrations). The redox potentials are both measured and calculated from the plutonium oxidation distributions by spectrophotometry using well-known equilibrium constants for the redox reactions of plutonium.^{1,2,4}



Our recent study⁵ demonstrates that the molar absorbance of Pu(IV) at 470 nm remains unaffected by mononuclear hydrolysis and the normalized absorption spectra of the first and the second hydrolyzed species ($\text{Pu}(\text{OH})_n^{4-n}$, $n = 1, 2$) do not differ from those of the Pu^{4+} ion. The decrease in the molar absorbance of Pu(IV) is merely ascribed to the formation of polymeric and/or colloidal species. Therefore, the total equilibrium concentration of $\text{Pu(IV)}_{\text{aq}}$ can be determined directly by spectrophotometry. By applying the hydrolysis constants of Pu(IV) selected in the NEA-TDB^{1,2} and using Eq. (3), the equilibrium concentration of the Pu^{4+} ion is calculated:

$$[\text{Pu}^{4+}] = [\text{Pu(IV)}_{\text{aq}}] / (1 + \sum_{y=1}^4 \beta'_{1y} [\text{OH}^{-}]^y). \quad (3)$$

In parallel, the poised Eh values of the plutonium oxidation distributions are measured with Pt and Ag/AgCl reference electrode and corrected versus the SHE ($\text{pe} = 16.9 \cdot \text{Eh(V)}$ at 25°C) for the purpose of comparison.

As shown in Fig 1 a), the pe values calculated from the plutonium redox couple, Pu(V)/Pu(VI) (○), are consistent with the measured pe values (+). However, the pe values calculated from Pu(III)/Pu(IV) couple (□) deviate. This implies that the formation constants of hydrolyzed Pu(IV) species² are overestimated. Combining Eq. (1) and (3) allows the independent determination of the hydrolysis constants of Pu(IV):

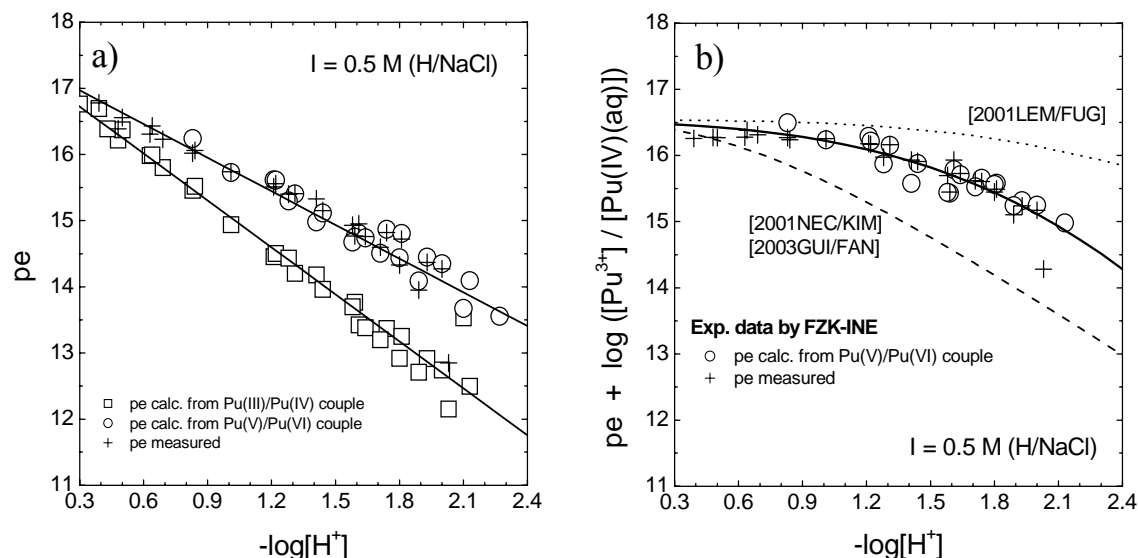


Fig 1: a) Redox potentials calculated from the different plutonium couples, Pu(III)/Pu(IV) (\square) and Pu(V)/Pu(VI) (\circ) by using Eq. (1) and (2) based on the spectrophotometry and measured pe values (+), b) Calculation with Pu(IV) hydrolysis constants of the present work (solid line) in comparison with calculation using previous selections (dotted line¹ and dashed line^{2,4}).

$$pe + \log([Pu^{3+}]/[Pu(IV)_{aq}]) = -\log K'_{III/IV} - \log(1 + \sum_{y=1}^4 \beta'_{ly} [OH^-]^y). \quad (4)$$

The first, the second, and the third hydrolysis constants for Pu(IV) determined in our study and corrected to $I = 0$ with the SIT are systematically lower than those of Metivier and Guillaumont selected in recent reviews:^{2,4}

$$\begin{aligned} \log \beta_{11}^0 &= 14.0 \pm 0.2 \quad (\log \beta_{11}^0 = 14.6 \pm 0.2^{2,4}) \\ \log \beta_{12}^0 &= 26.8 \pm 0.6 \quad (\log \beta_{12}^0 = 28.6 \pm 0.3^{2,4}) \\ \log \beta_{13}^0 &= 38.9 \pm 0.9 \quad (\log \beta_{12}^0 = 39.7 \pm 0.4^{2,4}). \end{aligned}$$

- 1 R.J. Lemire, *et al.*, (OECD-NEA TDB) Chemical thermodynamics of neptunium and plutonium, Elsevier (2001).
- 2 R. Guillaumont, *et al.*, (OECD-NEA TDB) Update on the chemical thermodynamics of uranium, neptunium, plutonium, americium and technetium, Elsevier, (2003).
- 3 H. Metivier and R. Guillaumont, *Radiochim Acta* **10**, 27 (1972).
- 4 V. Neck and J.I. Kim, *Radiochim Acta* **86**, 1 (2001).
- 5 C. Walther *et al.*, *submitted to: Radiochim Acta* (2006).

Anhydrous Photochemical Reduction of Well-defined Uranyl(VI) Complexes

P. Duval*, S. Kannan

*University of Missouri-Columbia, Columbia MO 65211 USA

Abstract

Applications directed toward the remediation and reprocessing of nuclear waste have focused on various redox strategies to immobilize soluble UO_2^{2+} to insoluble U(IV), employing microorganisms (i.e., sulfate-reducing bacteria)¹ or chemical (i.e., citrate, TiO_2 , $\text{Fe}(0)$), electrochemical or photochemical reduction methods.² The photochemical reduction with substrates such as alcohols is considered to proceed through two steps, entailing a one-electron reduction to uranyl(V) followed by the disproportionation of the unstable UO_2^+ intermediate, although mechanistic details remain remarkably sparse.³ While the redox instability of the UO_2^+ ion hampers study of this elusive oxidation state, details are even murkier surrounding the transformation of the dioxo group and the identity of the final uranium(IV) species, as well as the complex interplay of the bimolecular disproportionation reaction. Although these reactions have been evaluated under a variety of experimental conditions, perhaps the most important factor that influences this redox chemistry, *the coordination sphere of the precursor uranyl species*, has largely been ignored.

It is in this context that the photochemical reactivity of *well-defined cationic* uranyl(VI) complexes under *non-aqueous* conditions employing systematic control over variable experimental conditions (i.e., light source, reductant, solvent, etc.) is presented, with a focus on structural and electronic characterization of the products. The results offer mechanistic insight into alternate pathways of dioxo activation during the photochemical reduction of uranyl(VI) that are operable only under anhydrous conditions.

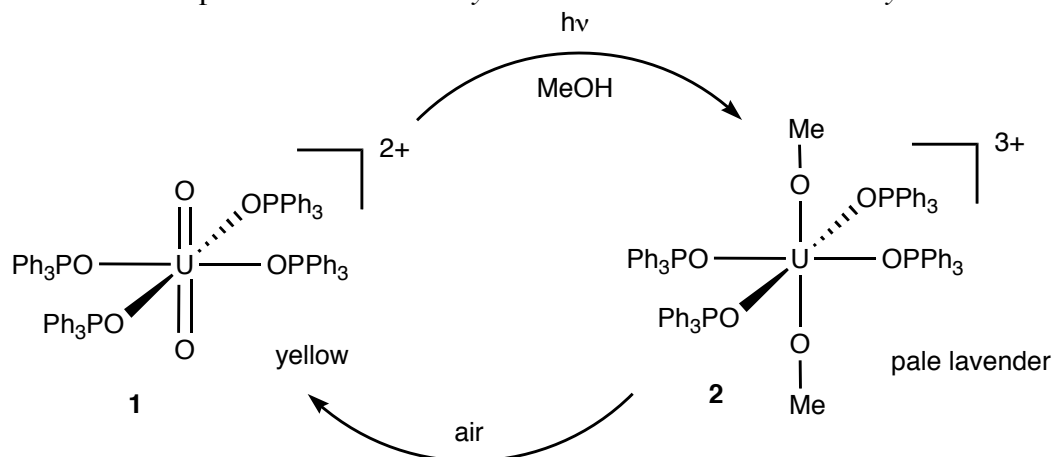


Fig 1: Reversal in the normal trend of uranyl(VI) reactivity: interchanging axial occupancy with an intact equatorial coordination sphere.

One example illustrated in Figure 1 includes an unprecedented reversal of the normal trend in uranyl ligand substitution reactivity, whereby the equatorial coordination sphere *remains intact* while the axial site occupancy cleanly and *reversibly* interchanges between oxo and methoxide ligands. Replacement of the dioxo unit with *trans* methoxide groups occurs during the photochemical reduction of a uranyl(VI) complex in *anhydrous* methanol, yielding a uranium(V) methoxide complex **2** instead of the expected tetravalent oxidation state. Complex **2** quantitatively reverts to the starting uranyl(VI) precursor upon exposure to air.

This work was supported by the American Chemical Society Petroleum Research Fund, the Missouri University Research Reactor, and the University of Missouri Research Board.

- 1 R B Payne, D M Gentry, B J Rapp-Giles et al., Appl. Environ. Microbiol. **68**, 3129 (2002).
- 2 T M McClesky, T M Foreman, E E Hallman et al., Environ. Sci. Technol. **35**, 547 (2001).
- 3 C P Baird and T J Kemp, Prog. React. Kinet. **22**, 87 (1997).

Spectrophotometric Determination of Iron in Plutonium Materials: Qualification and Trace Optimization

K. Garduno*, E. J. Lujan*, L. F. Walker*, and L. Tandon*

*Los Alamos National Laboratory, Los Alamos, NM 87545 USA

ABSTRACT

The Plutonium Assay Team within the Analytical Chemistry Group (C-AAC) at Los Alamos National Laboratory performs a broad range of analyses for the Pit Manufacturing Project including: “Controlled-Potential Coulometric Determination of Plutonium in Sulfuric Acid Electrolyte” (CPC) and “Spectrophotometric Determination of Iron in Plutonium Materials.” The standard spectrophotometric method that is presently used for iron analyses has been used for over fifty years and has not been superseded by any other instrumentation method. Inductively Coupled Plasma by Mass Spectrometry (ICP-MS), Inductively Coupled Plasma by Atomic Emission Spectrometry (ICP-AES), and X-Ray Fluorescence (XRF) are all methods that can be used to determine iron concentrations; however, these methods are quite limiting primarily because the instrumentation is expensive and the analytical results do not meet the accuracy and precision attained by using the spectrophotometric procedure. The iron determination must be performed prior to the CPC determination for total plutonium because iron is quantitatively oxidized during CPC measurement. Iron assay can have a significant impact on the final results of the plutonium assay where each 23 ppm of iron content will contribute to a 0.01% correction to the plutonium value by CPC. Significant experimental work has been performed on the methodology of “Spectrophotometric Determination of Iron in Plutonium Materials” to qualify the method for pit manufacturing. This method was initially developed for the assay of iron in various plutonium materials. The major steps in this procedure are reduction to iron(II) and plutonium(III) oxidation states with hydroxylamine hydrochloride; separation of plutonium by oxalate precipitation; formation of the iron-orthophanthroline complex; and spectrophotometric measurement. When the plutonium metals or oxides have been dissolved, it is recommended that the sample aliquot that will be analysed for iron is an aliquot taken from the same solution that has been dissolved and prepared for the coulometric determination of plutonium. Hydroxylamine is added to the supernate to ensure complete reduction of iron to Fe(II). The Fe(II) o-phenanthroline complex is formed in an acetate-buffered solution at pH 6. Iron is measured as the Fe(II) o-phenanthroline complex at 510 nm. The spectrum is characteristically broad and a spectrophotometer with a broad pass of up to 10 nm is acceptable.

Since the instruments used in many analyses range from the newest state-of-the-art to older, aging equipment, the pit manufacturing program requires that all analytical instruments be qualified before they are used to analyse materials that will eventually be used in the weapons program. To maintain this robust capability, certification of a backup instrument is required in case the currently qualified instrument fails. It is evident that there is value added to the pit manufacturing program because it avoids a single-point failure for plutonium as well as for iron

assay. Since the instrument for iron assay is relatively inexpensive, the qualification of a second instrument as backup is an economically sound investment. The analytical instrument currently used for the spectrophotometric determination of iron in plutonium materials is the Bausch and Lomb Spectronic 100. The experimental data that has been collected will demonstrate the accuracy and precision of the new Secomam Prim Light spectrophotometer against the qualified Spectronic 100.

Outside the qualification program, this basic procedure can be adjusted to meet varying needs. By slightly changing some of the parameters of the procedures, further experiments involving lower detection limits for electro refined plutonium metal have been completed using the same methods and instruments previously mentioned. Through dilution techniques the upper limits for iron determination may extend into the percent range. Using controls for lower detection limits, the iron content can be measured as low as <10 ppm. At the high end the relative precision is 2% and at the low end a precision of 5 ppm absolute can be obtained.

LA-UR-06-1132



Photo A: After reduction to the Pu(III) oxidation state, the oxalic acid is added and the oxalate precipitate appears immediately.



Photo B: After the reduction to Fe(II), the iron-orthophenanthroline complex forms.

Development of a Continuous Crystallization Process for Separating Uranium from Nitric Acid Solution

D. Ford, G. Jarvinen, D. Mullins, M. Mayne, H. Reichert, R. Gonzales

Los Alamos National Laboratory Los Alamos, NM 87545

Crystallization of uranyl nitrate at low temperatures from nitric acid solution has been considered as a potential head-end process for removing most of the uranium from spent light water reactor fuel after the fuel is dissolved in nitric acid. The crystallization process potentially could reduce the cost of LWR fuel partitioning because it provides a selective and compact process for removing most of the uranium. Subsequent separation processes would only need to handle the smaller volume of remaining actinides and the fission products. We have evaluated an approach that uses a continuous adiabatic crystallizer operating near room temperature. The crystallizer vessel chosen is a vertical circulating loop where the solution will be cooled and concentrated by the evaporation of a portion of the nitric acid and water at reduced pressure; uranyl nitrate hexahydrate crystallizes from this supersaturated solution. The distilled acid can be recycled for use in the fuel dissolver, for crystal washing, or for dissolving washed crystals. A detailed process flowsheet was defined and data on crystallization conditions and decontamination factors for various fission product elements has been obtained from small-scale batch tests. Prototype continuous crystallizer units have been built and tested first using non-radioactive solutions and then depleted uranyl nitrate solution. The progress to date on developing this crystallization process will be reviewed.

Self-Diffusion Coefficients and Structure of the Trivalent f-Element Ions, Eu, Gd and Am , Bk, Cf and Es in Aqueous Solution

H. Latrous

Faculté des Sciences de Tunis, 2092 El-Manar, Tunisia

This paper is dedicated to the memory of J. Oliver[†] TLR Oak Ridge, USA and M Chemla[†] Paris VI - France

INTRODUCTION

Self-diffusion coefficients D of the trivalent aquo ions of Eu, Am and Bk have been determined in dilute (pH =2.5) HClO_4 , $\text{Nd}(\text{ClO}_4)_3\text{-HClO}_4$ solutions at 25°C by an open end capillary method (O.E.C.M.). This method measures the transportation time of ions across a fixed distance. The variation of D versus the square root of the concentration of the solution was found to be non-linear in the studied concentration range. The limiting value D_0 for **f-Element trivalent ions, Eu, Gd and Am , Bk, Cf and Es in Aqueous Solution** at zero ionic strength are respectively 6.10 , 5.90 , 6.19 , 5.95 , 5.72 and $5.72 \times 10^{-6} \text{ cm}^2\text{s}^{-1}$. The plot of $D = f(\sqrt{C})$ for the **Am, Cf and Bk** trivalent ions can be compared to those for **Eu, Es and Gd** obtained under the same conditions, tacking into account of electronic configuration,

Moreover, it may be argued that the trivalent ions of **Eu, Gd , Am , Bk, Cf and Es** in aqueous solutions, have the same hydration number, as the $5f$ and $4f$ trivalent ions in the absence of hydrolysis, complexing or ion pairing at pH 2.5 should be the same.

EXPERIMENTAL METHOD

The O.E.C.M has been run at a constant temperature ($T = 25 \pm 0.01^\circ\text{C}$) ^[1]. The quartz capillaries of length 1 were filled with an electrolyte solution of concentration C labelled with the radioactive tracer $^{152}\text{Eu}^{3+}$, $^{153}\text{Gd}^{3+}$ and $^{241}\text{Am}^{3+}$, $^{249}\text{Bk}^{3+}$, $^{249}\text{Cf}^{3+}$ and $^{254}\text{Es}^{3+}$ The radioactive solution was kept in contact with an inactive solution of the same composition. We denote by $C_0(x,0)$ the total activity in the capillary at time $t = 0$. After a diffusion time t , the final average activity will be $C(x,t)$. By solving Fick's equation with the proper limiting conditions, the ratio $= C(x,t)/C_0(x,0)$ can be related to the self-diffusion coefficient D by the equation:

$$D_i = D_i^0 - \frac{a\sqrt{C}}{(1 + b\sqrt{C})} \quad (1)$$

The radioactivity measurements have been carried out separately for each actinide. For Eu, Gd , Am, and Cf, which are gamma emitters, the measurements were obtained directly on quartz capillary using a hollow NaI crystal detector.

For the alpha emitter Es, the initial and final activities were measured as the specific activities of the inner solutions.
The beta counting of $^{249}\text{Bk}^{3+}$ has been confirmed by alpha radiometry.

RESULTS AND DISCUSSION

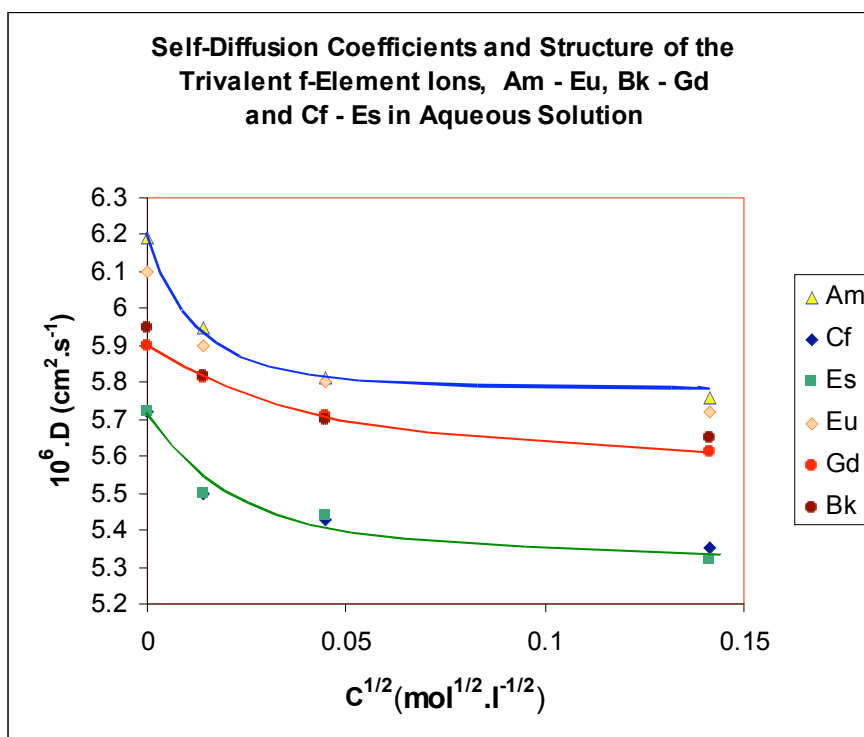
Experimental results of self diffusion coefficients ($10^6 \cdot D \text{ cm}^2 \cdot \text{s}^{-1}$) are shown in table 1^[2,3]

Table 1: Experimental Self Diffusion coefficients Values for 4f and 5f trivalent ions

C	$c^{1/2}$	Am	Cf	Es	Eu	Gd	Bk
0	0	6.19	5.72	5.72	6.1	5.9	5.95
0.0002	0.01414214	5.95	5.5	5.5	5.9	5.81	5.82
0.002	0.04472136	5.81	5.43	5.44	5.8	5.71	5.70
0.02	0.14142136	5.76	5.35	5.32	5.72	5.61	5.65

The plot of $D=f(C^{1/2})$: are shown in figure 1

Figure 1: Self Diffusion coefficients Values for trivalent ions of the selected f-Elements Shown.



The values of hydration numbers of trivalent ions are given in table 2.

Table 2: Hydration number for some 4f and 5f trivalent ions^[5]

Element	Am	Eu	Bk	Gd	Cf	Es
N	9	8.76	(8.8)	8.4	9	8.1

The plot of $D = f(\sqrt{C})$ (Figure 1) for these f-Elements trivalent ions shows the similarity as following :

- **Am** and **Eu** has similar electronic configuration the $4f^7$ et $5f^7$
- **Cf** and **Es** has similar sub shell 5f and successive elements , $5f^{10}7s^2$, $5f^{11}7s^2$
- **Bk** and **Gd** has 5f and 4f sub half-filled configuration $5f^9 7s^2$ and $4f^7 5d^1 6s^2$

The electronic configuration of 4f and 5f-Elements are given by G.T Seaborg

CONCLUSION

We have avoid hydrolysis, complexing and ion pairing by working at $pH = 2.5$.

- The results of diffusion of **Cf** and **Es** shows us that the **5f** elements whose has similar sub shell 5f half-filled configuration, has the same behavior .
- Results of diffusion of the two couples **Am** - **Eu** and **Bk** – **Gd** shows us that **4f and 5f**, similar electronic configuration and sub half-filled configuration ,trivalent ions element has the same behavior ^[4,6].

We can conclude that we can predict the transport properties of 4f elements from 5f elements and reverse.

The observations on plot of $D = f(\sqrt{C})$ for these f-elements trivalent ions make a diagnostic on the other 4f and 5f-Elements .

The variation of D is the same for 4f and 5f-Elements having the same configuration and in the case of filling the second half of shell 4f or 5f. Theses results are confirmed by the same hydration number ~ 8 (water molecules) ^[5].

Acknowledgements: We thank Prof. L.G. Haire(TRL., Oak-Ridge USA) , P.Turq (PARIS VI P.M. Curie), R.Guillaumont, (PARIS XI) J.Barthel (Regensburg) for helpful discussions and suggestions. We thanks Dr M. Fluss for the invitation to attend **Pu Futures-2006**.

References

1. H. Latrous, Rev. Fac. Sci. Tunis, 1 (1981) 75.
2. H. Latrous, M. Ammar, J. M'Halla, Radiochem. Radioanal.Lett., 53 (1982) 33.
3. H. Latrous, J. Oliver, M. Chemla, Zeitschrift, fur Physikalische Chemie, Neue Folge, 159(1988)195..
4. H. Latrous & J Oliver Radioanal.Nucl, Chem. Act, 156: 291-296 (1992)
5. F. H. David and B. Fourest, New J. Chem., 1997, 21, n°2, 167-176
6. H. Latrous & J.Oliver J.Mol .Liq, 81 (1999) 115-121

Solubility and Solubility Product of Tetravalent Metal Hydrous Oxides

T. Sasaki^{*}, T. Kobayashi^{*}, K. Fujiwara[†], I. Takagi^{*}, H. Moriyama^{*}

^{*}Department of Nuclear Engineering, Kyoto University, Kyoto 606-8501 Japan

[†]Japan Atomic Energy Agency, Muramatsu, Tokai, Naka-Gun, Ibaraki 319-1194 Japan

INTRODUCTION

The solubility products of actinides and fission products are one of the most important factors to be considered for the safety assessment of radioactive waste disposal since it directly controls their solubility. However, the reported values especially for tetravalent actinides often scatter and there are very large differences of several orders of magnitude between the lowest and the highest values. It has been recognized that such large differences are possibly due to the chemical property of samples, the solubility as low as the detection limit, the long equilibration period, the separation technique, and so on.^{1,2} Careful measurements and analysis are thus needed for the solubility of tetravalent actinides. For comparison, we have measured the solubility of a similar tetravalent metal, zirconium, in our recent study.³ Zirconium was observed to form not only mononuclear species but also polynuclear or colloidal species even in the lower pH region by hydrolysis reaction. In the present study, the results of zirconium are discussed by comparing with those of tetravalent actinides.

SOLUBILITY CURVES

The solubility of Zr at 25°C and a given ionic strength with NaClO₄ was measured by ICP-MS after separating the aqueous phase from the solid phase by the ultrafiltration method (3k Da NMWL membrane). The solid phases used were the amorphous hydrous oxide, Zr(OH)₄(am), and crystal oxide, ZrO₂(cr), for over- and undersaturation methods, respectively. Obtained results are shown in Fig.1. The solubility for Zr(OH)₄(am) decreases with an increase of pH in the acidic condition, and it is not significantly dependent on the ionic strength. On the other hand, much lower solubility for ZrO₂(cr) was obtained from

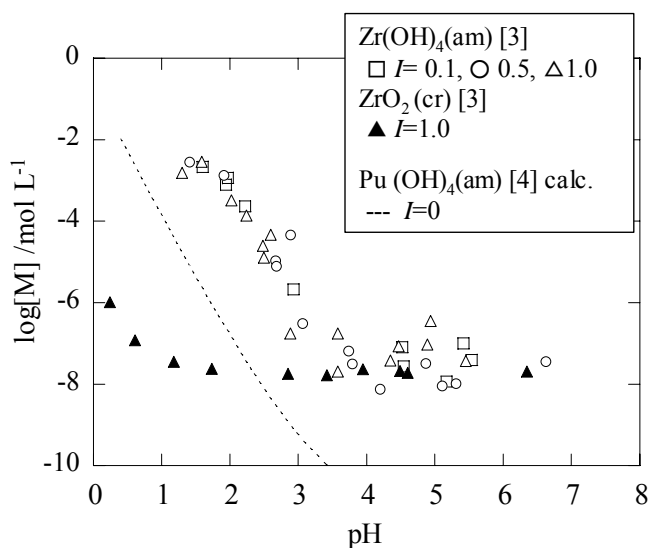


Fig 1: Solubility of tetravalent metal oxides as a function of pH.

undersaturation. It is interesting to note that, in spite of different conditions of the initial solid phase, the two solubility curves agreed with each other at higher pH than 4 as low as 10^{-7} to 10^{-8} mol L⁻¹.

For comparison, the solubility curve for Pu(OH)₄(am), predicted by the improved hard sphere model, is also shown in Fig.1⁴. It is noticed that the predicted curve is almost composed of mononuclear hydrolysis species of Pu(OH)³⁺, Pu(OH)₂²⁺ and Pu(OH)₃⁺ in equilibrium with Pu(OH)₄(am) while the observed solubility curve for Zr(OH)₄(am) may include not only mononuclear species but also polynuclear or colloidal species. A careful analysis is then needed to obtain the solubility product values.

SOLUBILITY PRODUCTS

The solubility product ($\log K_{sp}^0$) values at ionic strength $I=0$ were obtained from the solubility data by using the SIT corrections. Fig. 2 shows a comparison of the K_{sp}^0 values of tetravalent metal oxides, in which the values are plotted as a function of the inverse square of the M⁴⁺ ionic radii. Different trends of the K_{sp}^0 values are clearly observed for tetravalent actinides and for zirconium, which may be explained by considering non-electrostatic interactions of actinides.

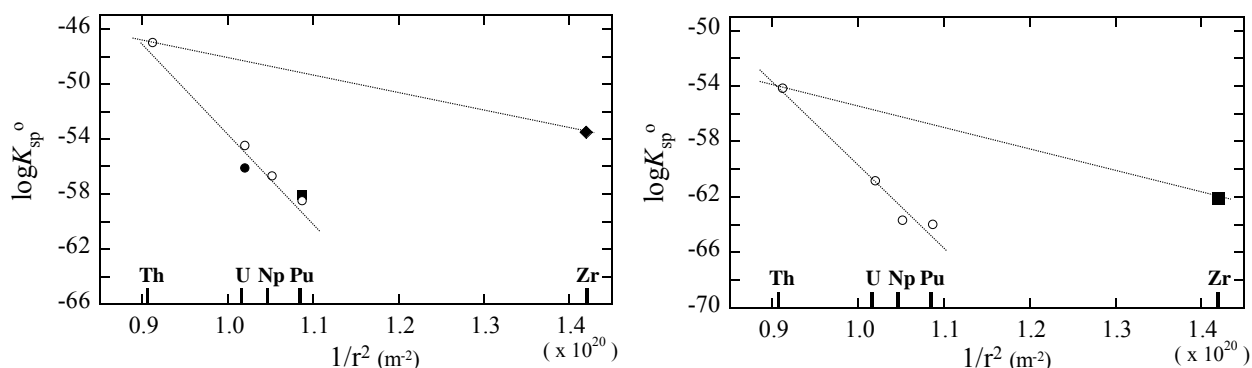


Fig 2. Variation of solubility product values for M(OH)₄(am) (left) and MO₂(cr) (right) of actinides^{1,2} and zirconium³.

- 1 V. Neck and J.I. Kim, Radiochim. Acta, **89** (2001) 1.
- 2 K. Fujiwara, H. Yamana, T. Fujii and H. Moriyama, Radiochim. Acta, **90** (2002) 857.
- 3 T. Kobayashi, *et al.*, submitted to: Radiochim. Acta., (2006).
- 4 H. Moriyama, T. Sasaki, T. Kobayashi and I. Takagi, J. Nucl. Sci. Technol., **42** (2005) 626.

Ternary Complex Formation of Eu(III) and Am(III) with Pyridine-2,6-dicarboxylate in Aquatic Solutions

K.K. Park, T.R. Kwon, Y.J. Park, E.C. Jung, W.H. Kim

Korea Atomic Energy Research Institute, 150 Deokjin-dong, Yuseong, Daejeon, Korea, 305-353

1. INTRODUCTION

Reliable estimates of radionuclide solubilities are needed for the safety assessment of nuclear fuel disposal in an underground vault. Solubility of radionuclides in an aquatic system is controlled mainly by solid-water equilibria and partially by complexation with ligands coexisting in the aquatic system. Many researches on the binary complex formation of radionuclides with carbonate and several organic ligands have been performed. More recently, studies on the ternary complex formation are of interest because organic matters react with binary hydrolyzed- or carbonate- complexes to form a ternary complex, thereby affecting the solubility of radionuclides.

In this work, the hydrolysis and the carbonate complexation of Eu(III) and Am(III) in the presence of pyridine-2,6-dicarboxylate are investigated.

2. EXPERIMENT

Ternary complex formation of M(III)-L-OH and M(III)-L-CO₃ (M=Eu or Eu with trace ²⁴¹Am, L= pyridine-2,6-dicarboxylate) was investigated in the pH range of 7 to 10 in 0.1 and 0.01 M NaClO₄ media at 25 °C. For the formation of M-L-OH, NaOH free of CO₂ was added to the metal-ligand solution (M=0.1 mM, L=0 to 0.15 mM) of pH 7 under Ar gas environment. For the formation of M-L-CO₃, HClO₄ was added to the solution containing Na₂CO₃ (0.2 to 10 mM) of pH 10 in air sealed vessel. The precipitate was separated by filtration or by centrifugation. The content of metal in aqueous phase was determined by ICP-AES or ICP-MS(Eu), LSC(²⁴¹Am) and that of ligand was determined by absorption spectrophotometry (in the presence of excess EDTA at pH 8). Finally, the composition of precipitate was calculated.

3. RESULTS AND DISCUSSION

An increase in pH of Eu-ligand solution ([L]/[Eu]=1) caused a precipitation at pH ≥ 7, while the precipitate was not observed in case of [L]/[Eu] ≥ 2. This suggests that another insoluble species is formed together with Eu(OH)₃ in the presence of L. From the measurement of fluorescence spectra for the solution containing dispersed precipitates ([L]/[Eu]=1, pH 8) by the excitation of 277 nm-line (absorption line of L), it was found that the emission peak of Eu at 615 nm due to 'hypersensitive' transition (⁷F₂ → ⁵D₀) was greater than that of Eu at 585 nm due to 'non-hypersensitive' transition (⁷F₀ → ⁵D₀). This spectral feature is found to be essentially the same as in the complexation between Eu³⁺ ion and ligands,¹ indicating that the precipitate has a Eu-L bond to exert intra-molecular energy transfer. These observations can be explained by the formation of ternary complex such as {EuL(OH)}⁰ through the reaction between {EuL}⁺ and OH⁻.

The removal of Eu and L from aqueous phase by precipitation depended on pH as well as the concentrations of L and carbonate. In absence of carbonate and L, the removal of Eu began at

about pH 7.2 and was completed at pH lower than 8. In the presence of L alone, the removal of Eu started at higher pHs, *i.e.* 7.6 when $[L]/[Eu]=1.0$ and 7.9 when $[L]/[Eu]=1.5$, and the removal was not completed even at pH 10. Simultaneously, the removal behavior of ligand with respect to pH was observed essentially the same as in that of Eu. This suggests that the formation of soluble species such as $\{EuL_n\}^{(3-2n)}$ ($n=2$ or 3) competes with the formation of $Eu(OH)_3$ and $EuL(OH)$, and that the formation of $EuL(OH)$ is favored over that of $Eu(OH)_3$ in this experiment.

The species distribution calculation based on the stability constants² shows that, with increasing pH, the $\{EuL\}^+$ species decreases but $\{EuL_n\}^{(3-2n)}$ ($n=2$ or 3) species increases, thereby expected that the removal of Eu decreases. In our experiment, however, the removal of Eu did not decrease with an increase in pH. Moreover, the concentration ratio of L to Eu removed by precipitation was calculated and found to be almost constant value of 0.65 at relatively high pH. These mean that $EuL(OH)$ and $\{EuL_n\}^{(3-2n)}$ are formed. It is proposed here that the formation of the former is favored over that of the latter at our experimental conditions. The solubility product of $EuL(OH)$ was calculated and the value of pK_{sp} was 14.

The presence of carbonate caused a decrease in the formation of precipitate, as expected by the formation of soluble carbonate species. The concentration ratio of L to Eu in precipitates was decreased. However, the solubility of Eu was higher than expected by stability of carbonate complex³, indicating that $\{EuL\}^+$ reacts with CO_3^{2-} to form a soluble species such as $\{EuL(CO_3)\}^-$.

The trace ^{241}Am showed exactly the same removal behavior as Eu, indicating that Am(III) also can form ternary complexes of insoluble $AmL(OH)$ and soluble $\{AmL(CO_3)\}^-$ species.

4. CONCLUSION

In the presence of ligand with two carbonate-functional groups, Eu(III) and Am(III) could form an insoluble hydrolyzed ternary complex, $ML(OH)$ and a soluble carbonate ternary complex, $\{ML(CO_3)\}^-$. The solubility product of $EuL(OH)$ ($L=$ pyridine-2,6-dicarboxylate) was determined ($pK_{sp}=14$) and could be considered similar to that for Am(III).

Acknowledgements-This study is supported by the Ministry of Science and Technology. We thank for help to Y.B. Kim in ^{241}Am measurement with LSC, and K.S. Choi and Dr. S.H. Han in Eu measurement with ICP-AES and ICP-MS.

REFERENCES

1. Richardson, F. S. Chem. Rev. **82**, 541(1982).
2. A.E. Maetell and R.M. Smith, Critical Stability Constants, Vol. 1, Plenum Press, New York, 1974.
3. A.E. Maetell and R.M. Smith, Critical Stability Constants, Vol. 5, Plenum Press, New York, 1982.

Determining the Electronic Structure of Pu using Unorthodox Spectroscopies

James G. Tobin

*Lawrence Livermore National Laboratory, Livermore CA 94552 USA
Email: Tobin1@LLNL.Gov

DISCUSSION

The standard method to determine the band structure of a condensed phase material is to (1) obtain a single crystal with a well defined surface and (2) map the bands with angle resolved photoelectron spectroscopy (occupied or valence bands) and inverse photoelectron spectroscopy (unoccupied or conduction bands). Unfortunately, in the case of Pu, the single crystals of Pu are either nonexistent, very small and/or having poorly defined surfaces. Furthermore, effects such as electron correlation and a large spin-orbit splitting in the 5f states have further complicated the situation. Thus, we have embarked upon the utilization of unorthodox electron spectroscopies, to circumvent the problems caused by the absence of large single crystals of Pu with well-defined surfaces. The talk will include a discussion of resonant photoelectron spectroscopy [1], x-ray absorption spectroscopy [1,2,3,4], electron energy loss spectroscopy [2,3,4], Fano Effect measurements [5], and bremsstrahlung isochromat spectroscopy [6], including the utilization of micro-focused beams to probe single-crystallite regions of polycrystalline Pu samples. [2,3,6]

This work was performed under the auspices of the U.S. DOE by Univ. of California, Lawrence Livermore National Laboratory under contract W-7405-Eng-48.

REFERENCES

1. J.G. Tobin, B.W. Chung, R. K. Schulze, J. Terry, J. D. Farr, D. K. Shuh, K. Heinzelman, E. Rotenberg, G.D. Waddill, and G. Van der Laan, "Resonant Photoemission in f-electron Systems: Pu and Gd", Phys. Rev. B **68**, 155109 (October 2003).
2. K.T. Moore, M.A. Wall, A.J. Schwartz, B.W. Chung, D.K. Shuh, R.K. Schulze, and J.G. Tobin, "The Failure of Russell-Saunders Coupling in the 5f States of Plutonium", Phys. Rev. Lett. **90**, 196404 (May 2003).
3. G. van der Laan, K.T. Moore, J.G. Tobin, B.W. Chung, M.A. Wall, and A.J. Schwartz, "Applicability of the spin-orbit sum rule for the actinide 5f states," Phys. Rev. Lett. **93**, 097401 (Aug 2004).
4. J.G. Tobin, K.T. Moore, B.W. Chung, M.A. Wall, A.J. Schwartz, G. van der Laan, and A.L. Kutepov, "Competition Between Delocalization and Spin-Orbit Splitting in the Actinide 5f States," Phys. Rev. B **72**, 085109 (2005).
5. J.G. Tobin, S.A. Morton, B.W. Chung, S.W. Yu and G.D. Waddill, "Spin-Resolved Electronic Structure Studies of Non-Magnetic Systems: Possible Observation of the Fano Effect in Polycrystal Ce," Physica B, Proceedings of SCES05, Vienna, Austria, Accepted 2005.
6. J.G. Tobin, M.T. Butterfield, N.E. Teslich Jr., R.A. Bliss, M.A. Wall, A.K. McMahan, B.W. Chung, A.J. Schwartz, "Using Nano-focussed Bremsstrahlung Isochromat Spectroscopy (nBIS) to Determine the Unoccupied Electronic Structure of Pu," Royal Society of Chemistry, Proceedings of the Actinides 2005 Meeting, Manchester, UK, Accepted 2005.

Symmetry reduction of δ -plutonium: an electronic-structure effect

K.T. Moore*, P. Söderlind†, A.J. Schwartz†, D.E. Laughlin†

*Lawrence Livermore National Laboratory, Livermore, CA 94550, USA.

†Materials Science and Engineering, Carnegie Mellon University, Pittsburgh, PA 15213 USA.

Classical crystallography does not incorporate anisotropy of atomic bonds within its framework [1]. Rather, it assumes a spherical atom at each lattice site. While this assumption is justifiable for some elements, it becomes less reliable for those with complicated electronic structures. Nowhere is this more the case than with plutonium, which is the most enigmatic metal in the Period Table [2-8]. Recently, the phonon dispersion curves for single-grain δ -plutonium were recorded using inelastic X-ray scattering [9], confirming other measurements [10,11] that it is the most anisotropic face-centered cubic (fcc) metal known. The shear moduli C_{44} and C' differ by a factor of ~ 7 , which is in strong contrast to aluminum exhibiting a factor of 1.2 [12]. In addition, δ -Pu has a negative coefficient of thermal expansion and has the most crystallographically expanded lattice of all six Pu allotropes (fcc is usually the most densely packed crystal structure). This is evidence that a simple hard-sphere assumption is inappropriate for Pu and that the bonding strengths between the 12 nearest neighbors of the fcc δ -Pu lattice are not equal. In turn, this means that the total symmetry of the metal may not be fcc, but rather a lower symmetry class.

We present a novel use of first-principles calculations, which yields the bond strengths of the 12 nearest neighbors within the δ -Pu crystal. Using these calculated bond strengths, we systematically progress through crystallographic arguments showing that δ -Pu belongs to the monoclinic space group Cm rather than the cubic $Fm\bar{3}m$ space group. Our results provide new insight into why plutonium is the only metal with a monoclinic ground state and why tetragonal, orthorhombic, or monoclinic distortions of δ -Pu are likely. These distortions have considerable ramifications for the behavior of the metal as it ages, accumulating damage via self-irradiation. Finally, we anticipate the use of these calculations and crystallographic arguments in tandem will expand crystallographic determination of complicated materials to incorporate electronic structure, consequently providing a unique way to explain complex properties.

Calculating the energy response (ΔE) of a small ($\sim 2\%$) displacement of an atom along each of the 12 nearest-neighbor directions and scaling this with the displacement magnitude ($u = 0.049\text{\AA}$), an approximate force or strength of the bonds is realized. This is the “bond strength.” These energies are obtained from first-principles electronic-structure calculations within the framework of density-functional theory (DFT). This approach has proven to be accurate for most metals in the Periodic Table, including Pu [13]. The computational details are similar to those in Ref. [13] with the major difference being that here we study a 27-atom supercell of fcc Pu to allow for the above-mentioned atomic displacements. To simplify the calculations, the effect of electron spin is only accounted for by a parallel arrangement and not coupled to the orbital degree of freedom.

We begin with the assumption that the lattice is fcc with $a = b = c$; the motif is the calculated bond strengths for the 12 nearest neighbors. The results of the calculations are shown

in Figure 1. where the change in energy normalized by the displacement length ($\Delta E/u$) are given. Notice how $\Delta E/u$ varies from ~ 3.3 to ~ 5.3 , showing the large degree of variation in bond strength between the 12 nearest neighbors. The twelve nearest neighbors can be separated into six pairs of two where the bond strengths are close in value: blue (3.3), black (3.5-3.7), red (3.7-3.9), pink (3.9-4.1), green (4.5-4.7), and brown (4.7-5.3). In the (001) plane, the $[110]$ bond is roughly equal to the $[\bar{1}\bar{1}0]$ bond (green), and the $[\bar{1}10]$ bond is roughly equal to the $[\bar{1}\bar{1}0]$ bond (black). In the $\{011\}$ planes, we see that $[01\bar{1}] \sim [\bar{1}0\bar{1}]$ (blue), $[0\bar{1}\bar{1}] \sim [\bar{1}0\bar{1}]$ (red), $[0\bar{1}\bar{1}] \sim [10\bar{1}]$ (pink), and $[011] \sim [\bar{1}0\bar{1}]$ (brown). It is important to note that not only the bond strength, but also the repeatability of groupings dictate the choice of sets. In other words, there is a clear separation between the brown and pink sets and the clear separation between the red and blue sets. It is interesting that the bonds in the (001) plane are almost equal directly across the central atom, whereas the bonds in the $\{011\}$ planes are not and have a more complicated arrangement.

When an fcc lattice is joined with the calculated bond strengths as a motif, the resultant structure is *c*-centered monoclinic with the space group *Cm*; there is one mirror plane along (110). In addition, the structure is not centrosymmetric (defined as: $x = -x$; $y = -y$; $z = -z$). The reduced space group for δ -plutonium enlightens why the ground state of the metal is monoclinic, why distortions of the metal are viable, and has considerable implications for the behavior of the material as it ages.

This work was performed under the auspices of U.S. Department of Energy by the University of California, Lawrence Livermore National Laboratory under contract No. W-7405-Eng-48.

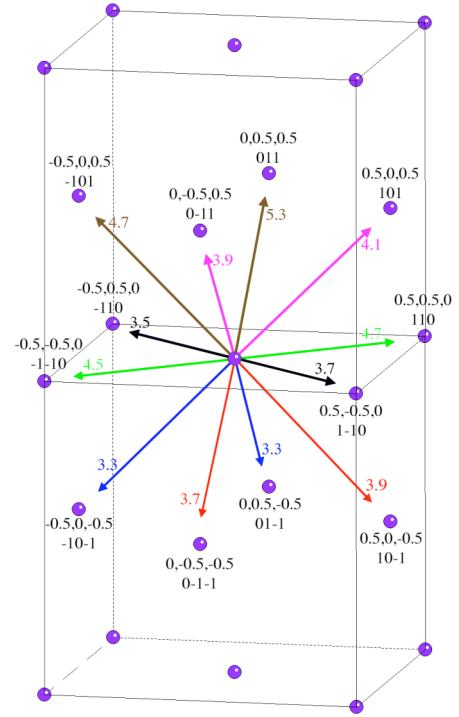


Figure 1. Calculated bond strengths for δ -Pu.

- [1] F.D. Bloss, *Crystallography and Crystal Chemistry* (Holt, Rinehart, and Winston Inc., 1971).
- [2] R.C. Albers, *Nature* **410**, 759 (2001).
- [3] S.S. Hecker, *Metall. Mat. Trans. A* **35**, 2207 (2004).
- [4] H.L. Skriver, O.K. Andersen, B. Johansson, *Phys. Rev. Lett.* **41**, 42 (1978).
- [5] J.L. Smith, E.A. Kmetko, *J Less Comm. Met.* **90**, 83 (1983).
- [6] S.Y. Savrasov, G. Kotliar, E. Abrahams, *Nature* **410**, 793 (2001).
- [7] K.T. Moore *et al.*, *Phys. Rev. Lett* **90**, 196404 (2003).
- [8] G. van der Laan *et al.*, *Phys. Rev. Lett* **93**, 097401 (2004).
- [9] J. Wong *et al.*, *Science* **301**, 1078-1080 (2003).
- [10] H.M. Ledbetter, R.L. Moment, *Acta Metall.* **24**, 891 (1976).
- [11] R. J. McQueeney *et al.*, *Phys. Rev. Lett.* **92**, 146401 (2004).
- [12] R. Stedman, G. Nilsson, *Phys. Rev.* **145**, 492 (1966).
- [13] P. Söderlind, B. Sadigh, *Phys. Rev. Lett* **92**, 185702 (2004).

Effect of Chemical and External Pressure on the Structure of Intermetallic Compound CeNi

A. Mirmelstein*, E. Clementyev*, V. Voronin†, D. Kozlenko§, A. Kutepov*, A. Petrovtsev*, Yu. Zuev*

*Russian Federal Nuclear Center – Institute of Technical Physics, Snezhinsk 456770, Russia

†Institute for Metal Physics, Russian Academy of Sciences, 620041 Ekaterinburg GSP-170, Russia

§Frank Laboratory of Neutron Physics, JINR, Dubna 141980, Russia

INTRODUCTION

The study of mechanisms of the transitions between different structural modifications for the materials with almost empty or almost filled $f_{5/2}$ -electronic configurations may provide a new insight into the origin of their ground-state properties, especially in the case if the structural transitions involve volume discontinuity driven by electron correlation effects. The intermediate-valence compound CeNi exhibits anomalous behavior of many physical properties including the first-order structural phase transition with volume discontinuity^{1,2} and well-defined ground-state coherent effects in the magnetic response function observed by the inelastic neutron scattering technique³. Thus, CeNi is an attractive model system to investigate the influence of the coherent effects on the mechanism of the volume-collapse phase transitions. However, the structure of the high pressure phase remains unknown and the P - T phase diagram is established only at relatively low pressures (< 0.8 GPa) in the limited temperature range below 150 K.

The aim of the present work is to determine the structure of the high-pressure phase of CeNi and to compare the results with the structural modifications resulting from the chemical pressure induced by either La (negative chemical pressure) or Lu (positive chemical pressure) substitutions for Ce in the CrB-type CeNi lattice.

RESULTS AND DISCUSSION

CeNi, $\text{Ce}_{1-x}\text{La}_x\text{Ni}$ ($0 \leq x \leq 1$) and $\text{Ce}_{1-x}\text{Lu}_x\text{Ni}$ ($0 \leq x \leq 0.4$) samples were prepared by arc melting of high purity elements (~ 99.98) in the argon atmosphere. Obtained compositions were then recrystallized in vacuum and founded in cylindrical ingots of a diameter ~ 10 mm. Ingots were then annealed in dynamical vacuum for 120 h. According to X-ray and neutron powder diffraction measurements, all samples were found to be of single phase with the CrB-type of crystal structure (the $Cmcm$ space group).

In order to study the effect of chemical pressure, neutron powder diffraction patterns for the samples under study were recorder at room temperature using D7A diffractometer (Institute for Metal Physics, Ekaterinburg) with $\lambda=1.5324$ Å. The results are summarized in Table 1 and Fig. 1. La substitutions for Ce expand the crystal lattice in all the main crystallographic directions, while substitutions with Lu lead to the lattice compression. The main structural elements of the CrB structure are the zig-zag chains of Ce and Ni ions propagating along the c crystallographic direction. Respectively, the lattice parameter c varies much less due to chemical pressure than a and b parameters.

While direct high-pressure structural data were absent, there is a strong argument that the topology of the Fermi surface of CeNi does not change across the transition⁴. It means that the primary external pressure effect is to rearrange the atomic coordinates within the primitive cell of CeNi. Such an effect is also essential for chemical doping. Figure 1 demonstrates the variation of

Table 1. The crystal lattice parameters of CeNi as a function of La and Lu substitutions for Ce.

Composition	a (Å)	b (Å)	c (Å)
Ce _{0.8} Lu _{0.2} Ni	3.7457(9)	10.4069(11)	4.3416(10)
CeNi	3.7860(8)	10.5489(10)	4.6335(9)
Ce _{0.9} La _{0.1} Ni	3.8014(9)	10.5716(10)	4.3683(10)
Ce _{0.8} La _{0.2} Ni	3.8191(10)	10.5869(10)	4.3697(10)
LaNi	3.9048(9)	10.7917(9)	4.3900(10)

the atomic coordinate y for Ce/La/Lu and Ni as a function of the unit cell volume ($x = 0$ and $z = 0.25$ for both the rare-earth and Ni positions).

The results of neutron powder diffraction study of structural modifications in CeNi induced by either chemical (negative for Ce_{1-x}La_xNi, $0 < x < 1$, and positive for Ce_{1-x}Lu_xNi, $0 < x < 0.4$) or external pressure up to 5 GPa are used for electronic structure calculations of CeNi in terms of the spin-polarized relativistic density functional theory in generalized gradient approximation.

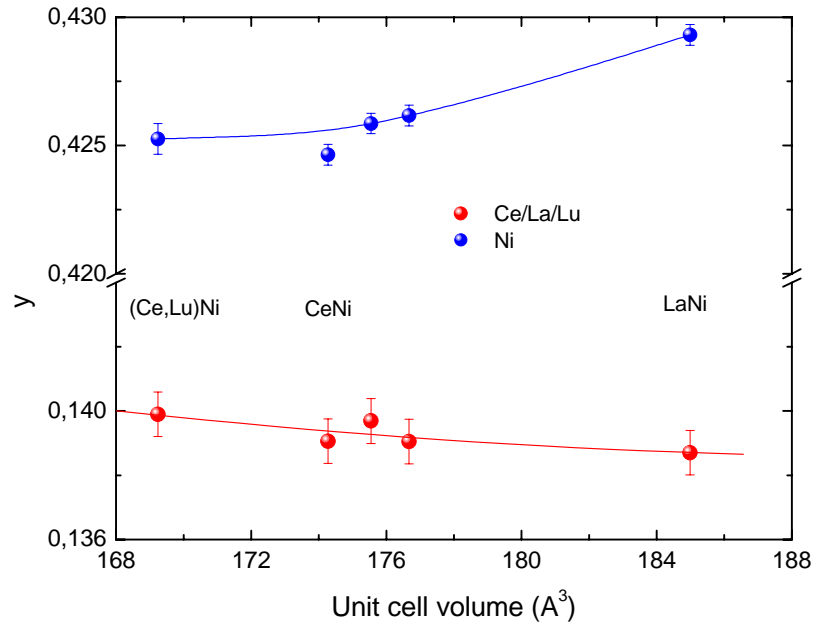


Fig. 1. Atomic coordinate y for Ce/La/Lu and Ni atoms in Ce_{1-x}Ln_xNi (Ln = La, Lu) as a function of the unit cell volume.

This work was performed under auspices of Russian Federal Agency for Atomic Energy (project "Actinides"). Financial support by RFBR (grant # 05-08-33456-a) is gratefully acknowledged.

- 1 D. Gignoux and J. Voiron, Phys. Rev. B **32**, 4822 (1985).
- 2 D. Gignoux *et al.*, JMMM **70**, 388 (1987).
- 3 E. Clementyev *et al.*, Phys. Rev. B **61**, 6189 (2000).
- 4 S. Araki, R. Settai, Y. Inada, Y. Onuki, Physica B **281&282**, 736 (2000).

Magnetic Dynamics in Correlated Electron Metals Poised Between Localization and Itinerancy

E. Clementyev^{*,†}, A. Mirmelstein^{*}, and P. Böni[†]

^{*}Russian Federal Nuclear Center - Institute of Technical Physics, 456770 Snezhinsk, Russia

[†]Physics Department E21, Technical University of Munich, 85747 Garching, Germany

INTRODUCTION

Excitation spectra are indispensable experimental data to the understanding of the ground state and the major interactions in plutonium. In particular inelastic neutron scattering (INS) experiments can yield valuable answers with respect to the puzzling question raised over the absence of any evidence of magnetic moments in plutonium¹. Despite of the impressive range of information which has been attained by measurements of physical properties and theoretical studies the investigation of the dynamic properties of plutonium is by no means complete². INS is very limited in the case of plutonium to say it soft and almost nothing is known on the magnetic spectral response in this metal. However a lot of INS data has been collected for other strongly correlated metals and intermetallics with electrons balanced between itinerant and

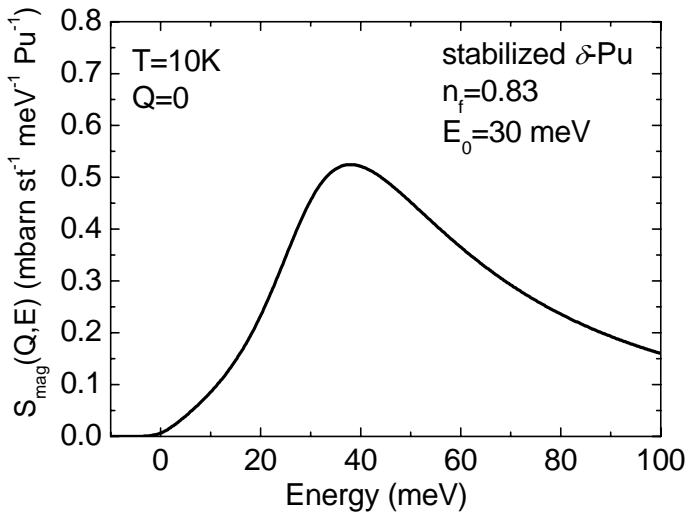


Fig 1: Calculated magnetic spectral response in fcc Pu at $T=10\text{K}$. Parameters of the KMH spectral function: Kondo energy $E_0=30$, fractional occupation of the 5f shell $n_f=0.83$.

RESULTS AND DISCUSSION

The magnetic spectra of Ce-based compounds contain various contributions. In addition to the main spectral feature, namely the broad single-ion-like magnetic response due to spin fluctuations, other peaks are clearly visible in the INS spectra⁴. We discuss coherent magnetic peaks in paramagnetic Ce-based systems, crystal field and intermultiplet transitions,

localized states. Pu is not unique among metallic systems regarding such phenomena as the unit cell volume collapse and the partial delocalization of the f-electrons. Cerium and Ce-based compounds demonstrate many peculiarities of the 4f electron shell similar to the 5f shell in Pu. The concept of shifted homology of Ce and Pu is known for about 30 years³. In the present study we discuss the magnetic spectral response observed in Kondo systems with different characteristic Kondo energy scales. The plausible magnetic excitation spectrum of fcc Pu is calculated on the basis of the INS data collected in Ce-based systems and the analysis of the thermodynamic properties of Pu.

contributions due to dynamic magnetic correlations and soft magnetic modes observed by INS on single crystals and powder samples.

A realistic description of the INS spectra in Kondo systems can be achieved on the basis of the non-crossing approximation solution of the non-interacting Kondo impurities model and using the spectral function derived by Kuramoto and Müller-Hartmann (KMH)⁵. INS spectra, specific heat, magnetic susceptibility in Ce systems are reasonably well described by the single energy scale. According to our analysis of the thermodynamic properties of δ -Pu (Pu fcc phase stabilized at low temperatures by Ga) the characteristic Kondo energy scale in fcc Pu is about 30 meV. This energy scale along with the fractional occupation of the 5f shell $n_f=0.83$ yields the value of the Sommerfeld coefficient $\gamma=64.5 \text{ mJ K}^{-2} \text{ mol}^{-1}$ and the low temperature magnetic susceptibility $\chi=0.4 \text{ memu mol}^{-1}$. The plausible INS spectrum of fcc Pu at $T=10\text{K}$ is shown in Fig. 1. Due to the single-ion model used in the calculation any possible coherent magnetic excitations are missing in the spectrum. Using the Kramers-Kronig relation of the dynamic and static magnetic susceptibilities and the KMH spectral function (see Ref.6 and references therein) the static bulk susceptibility has been calculated for fcc Pu $\chi(10\text{K})=0.38 \text{ memu mol}^{-1}$.

To illustrate the unusual dynamics of a pure itinerant system we present new results on the magnetic and electronic excitations in chromium single crystal⁷. Both Cr and α -Pu demonstrate characteristic features of itinerant electrons.

The most interesting energy transfer range to search for the magnetic excitations in fcc Pu is $20 \text{ meV} < E < 150 \text{ meV}$. Such a range implies relatively high incoming neutron energy, much higher than used in Ref. 1. As far as α -Pu is concerned the range of interest extends up to a few hundred meV. The most promising INS measurements must be done on ²⁴²Pu samples. On the basis of our positive experience with highly absorbing samples (like natural boron based MgB₂ with the neutron absorption cross section of about 1500 barn/f.u. and 10-boron rich TmB₁₂) we discuss the feasibility of the INS experiments using the most common ²³⁹Pu isotope ($\sigma_{\text{abs}}=1017 \text{ barn}$).

This work was performed under the auspices of the Russian Federal Agency of Atomic Energy (project "Actinides"). Financial support by the RFBR (grant 05-08—33456-a) is gratefully acknowledged.

- 1 J.C. Lashley, *et al.*, Phys. Rev. B **72**, 054416 (2005).
- 2 Los-Alamos Science, ed. By N. Cooper, v. **26** (2000).
- 3 B. Johansen and A. Rosengren, Phys. Rev. B **11**, 1367 (1975).
- 4 E. Clementyev, *et al.*, Phys. Rev. B **61**, 6189 (2000).
- 5 Y. Kuramoto and E. Müller-Hartmann, J. Magn. Magn. Mater. **52**, 122 (1985).
- 6 E. Holland-Moritz and G.H. Lander, in *Handbook on the Phys. and Chem. of Rare Earths*, v. **19**, ed. K.A. Gschneidner, *et al.*, Elsevier (1994).
- 7 E. Clementyev, *et al.*, Physica B **350** (1-3), 67 (2004).

Density-Functional Calculations of α -Pu-Ga (Al) Alloys

A. Landa^{*}, P. Söderlind^{*}, L. Vitos[†]

^{*}Lawrence Livermore National Laboratory, Livermore CA 94552, USA

[†]Royal Institute of Technology, Stockholm, SE-10044, Sweden

At atmospheric pressure plutonium metal exhibits six crystal structures upon heating from room temperature to the melting point. The least dense phase (δ -Pu, fcc) has a 25% larger volume than the ground-state (α -Pu, monoclinic) phase and is thermodynamically stable at temperatures between 593 and 736 K. In order to extend the stability of δ -Pu to ambient temperatures, plutonium is alloyed with a small amount of so-called ' δ -stabilizers', for example, Ga or Al. The α phase has no equilibrium solubility with any of these δ -stabilizers but upon cooling of the δ -Pu-Ga (Al) alloys, under certain conditions, Ga (Al) atoms can be trapped in the α lattice causing an expansion. An expanded monoclinic Pu-Ga (Al) phase is usually called "the α' phase". Hecker *et al.*¹ suggested that the enhanced volume of α' -Pu is solely due to the random distribution of Ga (Al) solutes in the monoclinic lattice and the unexpanded α lattice can be restored if the solute atoms are forced to move into preferred positions, e.g., during annealing. Recently, Sadigh and Wolfer confirmed this hypothesis by performing the plane-wave pseudopotential calculations for a variety of super-cell configurations². However, all these configurations reproduced specific ordering of the solute atoms (Ga) at the selected sites in the α -Pu monoclinic structure, and disordered Pu-Ga alloys could not be considered. This problem is solved in the present calculations.

We employed two complementary techniques: (i) the exact muffin-tin orbital method (EMTO)³ incorporated with the coherent potential approximation (CPA) to treat a compositional disorder and (ii) an all-electron full-potential linear muffin-tin orbital method (FPLMTO)⁴ that accounts for all relativistic effects in Pu. Both methods establish that a random distribution of Ga (Al) atoms in the monoclinic lattice of α -Pu results in a maximum expansion of this lattice. Any kind of ordering of Ga (Al) on the monoclinic lattice results in shrinking of the lattice constant in comparison with complete disorder of the solutes. The ordered α_8 -(Pu-Ga (Al)) configuration possesses the smallest lattice constant which is very close to that of pure α -Pu. In addition, energetics of the ordered and disordered configurations is discussed.

Acknowledgements: This work was performed under the auspices of the U.S. Department of Energy by the University of California Lawrence Livermore National Laboratory under Contract No. W-7405-Eng-48.

1 S.S. Hecker, D.R. Harbur, and T.G. Zocco, Prog. Mater. Sci. **49**, 429 (2004).

2 B. Sadigh and W. G. Wolfer, Phys. Rev. B **72**, 205122 (2005).

3 L. Vitos, in *Recent Research and Development in Physics* (Transworld Research Network Publisher, Trivandrum, 2004), Vol. 5, pp. 103-140.

4 J.M. Wills, O. Eriksson, M. Alouani, and D.L. Price, in *Electronic Structure and Physical Properties of Solids: The Uses of the LMTO Method*, edited by H. Dreyse, Lecture Notes in Physics Vol. 535 (Springer, Berlin, 2000), pp.148-167.

Electronic structure of Pu with ab-initio Gutzwiller method

J.P. Julien*, J. Bouchet†

*CNRS-LEPES, BP 166, 38042 Grenoble cedex 9, FRANCE

†CEA-DAM, DPTA, 91680 Bruyères-le-Châtel, FRANCE

ABSTRACT

We present an ab-initio, variational, multi-configurational method to study solids with strong local Coulomb interactions. First, we generalize a density matrix approach to multiband Gutzwiller ansatz. The variational (Rayleigh-Ritz) parameters are the probabilities of atomic configurations. As a result, an effective Hamiltonian includes renormalized hoppings as well as an analytic formula for optimized on-site levels. Secondly, this approach is coupled to a first principles DFT-LDA (density functional theory in the local density approximation) LMTO (Linearized Muffin Tin Orbitals) calculation that provides a band Hamiltonian. When the interaction term is added to get the full Hamiltonian we treat in this 'LDA+Gutzwiller' formalism, we avoid the double counting of the LDA interaction by subtracting it from the on-site energies. Our method conciliates the ab-initio, parameter free, realistic description of bands, as well as a strong correlation aspect of the coherent part of the spectrum. It can be considered as an improvement of the 'LDA+U' method having the same starting Hamiltonian but where interactions are calculated beyond a too crude mean field level. Application to Plutonium will be presented, with peculiar attention to the equilibrium volume, electronic specific heat and discrimination between localized and less localized states, giving some new insight in the still controversial electronic structure of this element.

This work was initialized under the auspices of the Commissariat à l'Energie Atomique under Contract No 9M 1898. The authors wish to thank R.C Albers of Los alamos National Laboratory for supporting of the present work and warmfull hospitality. We are also grateful to F. Jollet, A. Pasturel and A. Georges for stimulating discussions.

- 1 J.P. Julien and J. Bouchet, Physica B 359-361, 783 (2005).
- 2 J.P. Julien and J. Bouchet, *accepted to*: Prog. Theor. Chem. Phys. (2006) and arXiv:cond-mat/0509321(2005).

Magnetic state of *f* electrons in δ -phase of Pu-Ga alloys studied by Ga NMR

S. Verkhovskii*, V. Arkhipov*, Yu. Zouev†, Yu. Piskunov*, K. Mikhalev*, A. Korolev, S. Lekomtsev†, I. Svyatov†, A. Pogudin*, V. Ogloblichev*, and A. Buzlukov*.

*Institute of Metal Physics, Ural Branch of Russian Academy of Sciences, Ekaterinburg, Russian Federation (verkhovskii@imp.uran.ru)

†Russian Federal Nuclear Center - Institute of Technical Physics, Snezhinsk, Russian Federation

The rich phase diagram of plutonium¹ presents six polymorphous transitions. The unique structural, transport and magnetic properties are determined by the degree of itinerancy for 5*f* electrons in each of the Pu allotropes. Many efforts are undertaken, at present, to elucidate the ground state of the *f*-electron system in δ -Pu and in stabilized δ -phase alloys.

In the report on the basis of the ⁶⁹Ga NMR and static magnetic susceptibility data (Fig.1) the temperature dependence of spin susceptibility is discussed for the Pu_{0.95}Ga_{0.05} alloy, stabilized in δ -phase. The static magnetic susceptibility and the ⁶⁹Ga NMR spectra were measured in the temperature range (10 - 350) K and (10 - 650) K, respectively, at the sample, prepared as a set of electrochemically polished plates ~200 μ m in thickness. Magnetic shift (the Knight shift) of the ⁶⁹Ga NMR line is controlled by static local magnetic field arisen at nonmagnetic gallium due to the spin polarization transferred from the *f* electrons shell of the more magnetic neighboring Pu-ions². Thus the Knight shift *K*, dependent of electron spin, measures local spin susceptibility, $\chi_{s,loc}$, which can be composed by contributions being different in origin.

At $T > T^* = 235$ K the temperature dependent part of the Knight shift tracks the bulk susceptibility $\chi(T)$, following the Curie-Weiss law $K(T) \sim (T + \theta)^{-1}$ with $\theta = 280(40)$ K. The relation $K(T) \sim \chi(T)$ is violated with decreasing temperature below 200 K. A similar breakdown of the proportionality between $K(T)$ and $\chi(T)$ occurs at low temperature in many metallic compounds with the heavy fermion (HF) behavior, and this phenomenon is considered to occur at the expense of the *f* electron system.

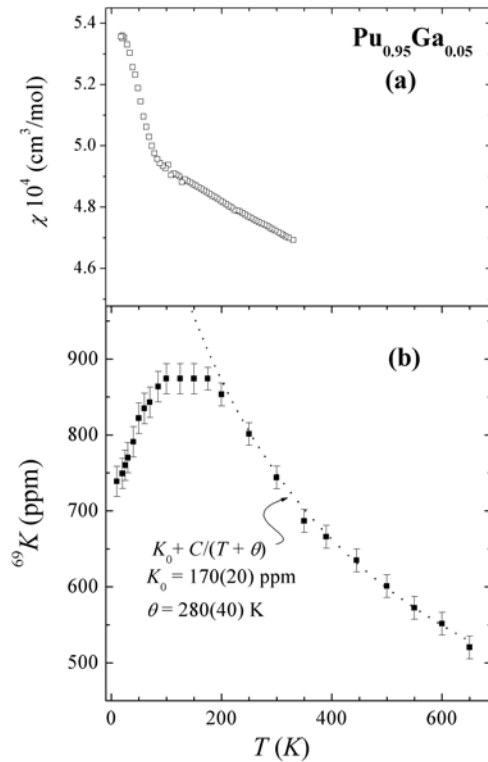


Fig.1. Magnetic susceptibility (a) and Ga NMR shift (b) vs *T* in Pu_{0.95}Ga_{0.05} alloy.

The subsequent joint analysis of the static magnetic susceptibility and the Knight shift data sets obtained in a wide range of temperature has allowed to find out the following peculiarities of the magnetic state of f electrons in the $\text{Pu}_{0.95}\text{Ga}_{0.05}$ alloy³:

- The temperature dependence of spin susceptibility at $T > T^*$ is typical for nonmagnetic Kondo lattice, where the localized electron spins fluctuate independently each other without any macroscopic coherence.
- The spin contribution of the f -electrons $\chi_{s,5f}$ to the total magnetic susceptibility is estimated as $\chi_{s,5f} \sim 0,08(1)\chi$. This estimate correspond to the localized f -electrons with very small value of magnetic moment $\mu_{\text{eff},5f}(g_e=2) = 0,15(5) \mu_B/\text{at.Pu}$. The corresponding filling of the $5f$ shell should resemble the $5f^6$ atomic configuration of Pu with $L = 0$, $S = 0$, as it was suggested for δ -Pu in Ref.4. This feature leads to suppression of the spin magnetism in δ -Pu. The T -independent orbital term determines the value of the f electron susceptibility of in δ -phase of the alloy.
- The different behavior of $K(T)$ and $\chi(T)$ occurred in alloy below 200K can be described rather well using two-spin fluid description of the HF materials developed in Ref. 5. As shown in Fig.2 the HF component of the Knight shift K_{cf} is increased with temperature decreasing. The tendency for K_{cf} to saturate below 300K can indicate, that, probably, the HF (coherent) spin-fluid component is formed completely. The final conclusion on the magnetic state of the Pu-ions occurred at low temperature can be done after the origin of additional excess in the local spin susceptibility revealed below 70K will be properly clarified.

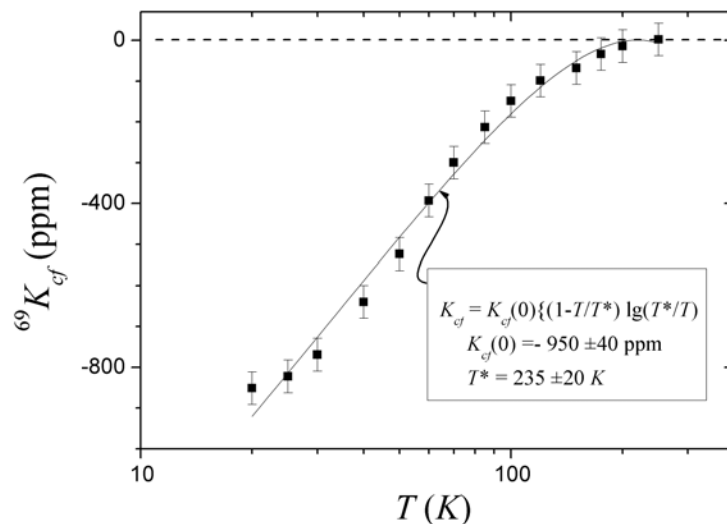


Fig.2. The coherent HF component of the Knight shift vs T in $\text{Pu}_{0.95}\text{Ga}_{0.05}$ alloy. The black curve is a fit with the expression $K_{\text{cf}}(T) = K_{\text{cf}}(0)\{(1 - T/T^*) \lg(T^*/T)\}$ according Ref. 5 at $K_{\text{cf}}(0) = -950(80)$ ppm и $T^* = 235(40)$ K

Acknowledgments

The work was supported by the Russian Grant (RFBR No 06-02-16130).

¹ S.S. Hecker and L.F. Timofeeva, *Los Alamos Sci.* **26**, 244 (2000)

² Yu. Piskunov, et al., *Phys. Rev. B* **71**, 174410 (2005).

³ S.V. Verkhovskii, et al., *JETP Lett.* **82**, 139 (2005).

⁴ A.O. Shorikov, A.V. Lukoyanov, M.A. Korotin, and V.I. Anisimov, *Phys. Rev. B* **82**, 024458 (2005).

⁵ N.J. Curro, B.-L. Young, J. Schmalian, D. Pines, *Phys. Rev. B* **70**, 235117 (2004).

The ground state and localization of $5f$ electrons in α - Pu

H. R. Gong and A. K. Ray

Department of Physics, the University of Texas at Arlington, Arlington, TX 76019

INTRODUCTION

Plutonium (Pu) is arguably the most complex metallic element known to mankind and has attracted extraordinary scientific and technological interests because of its unique properties. For instance, it has, at least, six stable allotropes between room temperature and melting at atmospheric pressure, and undergoes a 25 percent increase in volume when transformed from its α -phase to δ -phase, an effect which is crucial for issues of long-term storage and disposal. It is commonly believed that $5f$ electrons in Pu, which represent the boundary between the delocalized (itinerant) $5f$ electrons in the light actinides and the localized $5f$ electrons in the heavy actinides, are responsible for the unique properties of Pu, but the exact phase of the delocalization-localization transition has not been clearly identified so far. Among the six allotropes, the ambient ground-state α -Pu with a low-symmetry monoclinic structure has been studied by various groups over the years both experimentally and theoretically. It is commonly believed that α -Pu is relatively accurately described by standard density functional theory. However, the ground state of α -Pu continues to be a matter of significant controversy.¹ As a continuation of our research in actinide chemistry and physics,² we report here results on bulk α -Pu at NSP-NSO, NSP-SO, SP-NSO, SP-SO, AFM-NSO, and AFM-SO levels of theory, with two types of anti-ferromagnetic configurations.

COMPUTATIONAL METHOD AND RESULTS

Our computations have been carried out using the full-potential all-electron method with mixed basis APW+lo/LAPW method implemented in the WIEN2k suite of programs.³ The generalized-gradient-approximation to density functional theory (GGA-DFT) with a gradient corrected Perdew-Berke-Ernzerhof (PBE) exchange-correlation functional is used and the Brillouin-zone integrations are conducted by an improved tetrahedron method of Blöchl-Jepsen-Andersen. As far as relativistic effects are concerned, core states are treated fully relativistically in WIEN2k and for valence states, two levels of treatments are implemented: (1) a scalar relativistic scheme that describes the main contraction or expansion of various orbitals due to the mass-velocity correction and the Darwin s-shift and (2) a fully relativistic scheme with spin-orbit coupling included in a second-variational treatment using the scalar-relativistic eigenfunctions as basis. For all the calculations, a constant muffin-tin radius (R_{mt}) of 2.30 a.u. is used and the plane-wave cut-off K_{cut} is determined by $R_{\text{mt}} K_{\text{cut}} = 8.0$. The Brillouin zone is sampled on a uniform mesh with 24 irreducible K -points and the energy convergence criterion is set to be 0.01 mRy. In the present study, the unit cell of α -Pu is a simple monoclinic structure ($P2_1/m$) with sixteen atoms. To find the total energy minimum, the atomic volume of α -Pu is varied at each

theoretical level, respectively, while the following parameters are fixed according to experimental values: the atomic positions, the ratios of b/a and c/a , and the angles between the three axes.

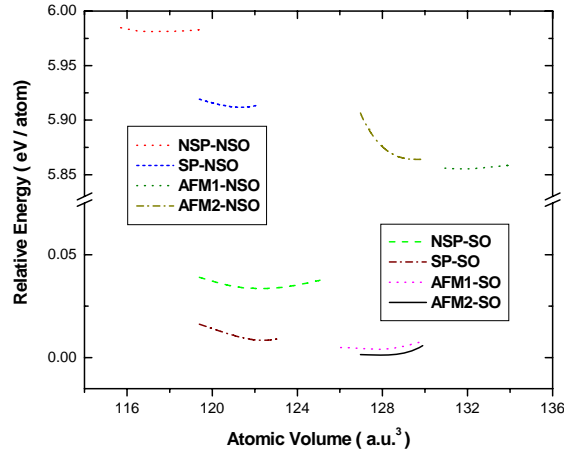


FIG. 1. Calculated total energies of α -Pu at various theoretical levels.

As Fig. 1 indicates, an anti-ferromagnetic state including spin-orbit coupling effects is found to be the ground state of α -Pu with an atomic volume of 128.9 a.u.³ and a bulk modulus of 58.8 GPa, in excellent agreement with experimental results. Density of states studies indicate that the 5f electrons of α -Pu are primarily delocalized as compared to our previous results of δ -Pu where the 5f electrons were found to be mainly localized. Thus the 5f electrons of α -Pu are on the delocalized side of the localization-delocalization transition, while 5f electrons of δ -Pu are on the localized side, signifying that the delocalization-to-localization transition from light actinides to heavy actinides should happen somewhere between α -Pu and δ -Pu. In addition, we find that specific anti-ferromagnetic settings have important roles on the properties of α -Pu and the spins of ferromagnetic α -Pu have a tendency to become anti-ferromagnetic.

This work is supported by the Chemical Sciences, Geosciences and Biosciences Division, Office of Basic Energy Sciences, Office of Science, U. S. Department of Energy (Grant No. DE-FG02-03ER15409) and the Welch Foundation, Houston, Texas (Grant No. Y-1525).

1. A. O. Shorikov, A. V. Lukoyanov, M. A. Korotin, and V. I. Anisimov, Phys. Rev. B **72**, 024458 (2005).
2. X. Wu and A. K. Ray, Phys. Rev. B **72**, 045115 (2005); A. K. Ray and J. C. Boettger, Phys. Rev. B **70**, 085418 (2004); J. C. Boettger and A. K. Ray, Int. J. Quant. Chem., **105**, 564 (2005); M. N. Huda and A. K. Ray, Eur. Phys. J. B **40**, 337 (2004); Physica B **352**, 5 (2004); Eur. Phys. J. B **43**, 131 (2005); Physica B **366**, 95 (2005); Phys. Rev. B **72**, 085101 (2005); Int. J. Quant. Chem. **105**, 280 (2005); H. R. Gong and A. K. Ray, Eur. Phys. J. B, **48**, 409 (2005); H. R. Gong and A. K. Ray, Proc. MRS Fall 2005 Symposium; accepted for publication; Surf. Sci. accepted for publication; D. Gao and A. K. Ray, Eur. Phys. J. B, in press; Proc. MRS Fall 2005 Symposium; accepted for publication; D. Gao and A. K. Ray, submitted for publication; P. Dholabhai and A. K. Ray, submitted for publication.
3. K. Schwarz, P. Blaha, and G. K. H. Madsen, Comp. Phys. Comm. **147**, 71 (2002).

Magnetic Properties of Pu-Ga Alloys

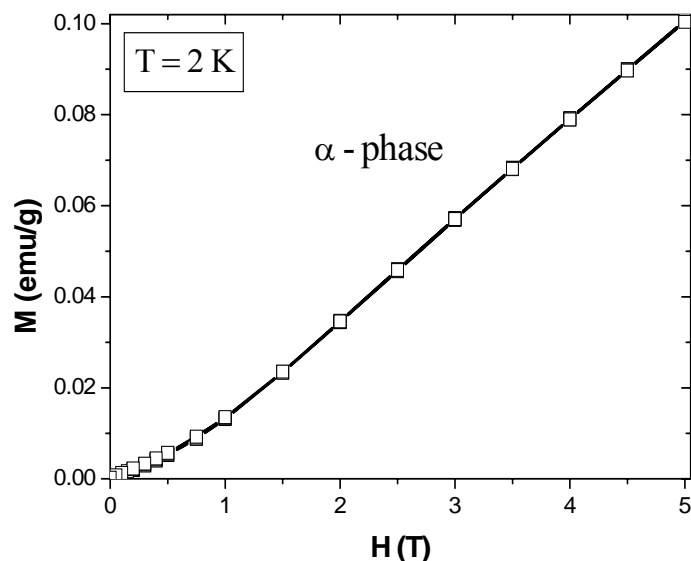
V. Arkhipov^{*}, Yu. Zuev[†], F. Kassan-Ogly^{*}, A. Korolev^{*}, I. Svyatov[†]

^{*}Institute of Metal Physics, Ural Branch of RAS, Ekaterinburg, Russia

[†]Russian Federal Nuclear Center — Institute of Technical Physics, Snezhinsk, Russia

The results of studies of temperature and field dependences of the magnetization and susceptibility of Pu-Ga alloys with 0.5 and 5.0 at % of Ga are presented. At room temperature the samples were in α and δ phases according to either U.S. or Russian Pu-Ga phase diagram¹. The measurements were performed on a SQUID magnetometer MPMS-5XL (Quantum Design) in the fields up to 5 T and in the temperature range from 2 to 400 K. The samples were put in a Pyrex ampoule filled with gaseous helium under the pressure of 0.5 atm. The figure shows anomalous magnetization dependence on an external magnetic field for a sample with 0.5 at.% Ga (α phase) at $T=2$ K.

As it is seen from the figure the behaviour of magnetization differs from that in pure paramagnet in which case it should be a straight line intersecting the origin. Moreover, as our



measurements showed, the magnetization curves over the cycle $+5\text{T} \rightarrow 0\text{T} \rightarrow -5\text{T} \rightarrow 0\text{T} \rightarrow +5\text{T}$ manifest a hysteresis with a residual magnetization of 0.002 emu/g and coercive force of $\sim 1800\text{--}2000$ Oe. Our further measurements showed that the anomaly, discovered at $T=2$ K, disappears at ~ 10 K. A similar anomalous behaviour of $M(T)$ at $T < 10$ K is also observed for the samples with 5 at.% Ga (δ phase). It may be supposed that the observed anomalies of magnetic properties (magnetization and magnetic susceptibility) of Pu-Ga alloys

are related to a possible appearance of the α' phase at low temperatures. To our knowledge such anomalies of $M(T)$ and $\chi(T)$ were not yet reported in available literature references.

This work was supported by the Russian Foundation for Basic Research, Project No. 06-02-16130

Electronic Structure Measurements and Photoemission Band Mapping of α -Uranium

R.K. Schulze, C.P. Opeil, B. Milhaila, M.E. Manley, R. Albers, K.B. Blagoev, and J.L. Smith

Los Alamos National Laboratory, Los Alamos, NM 87545

α -URANIUM SINGLE CRYSTAL

For the first time, relatively large, high quality single crystals of a pure actinide metal, in this case, α -uranium, have become available¹ through electrolytic growth from a molten salt, and we have begun a comprehensive investigation of the electronic structure of this material by photoemission and band mapping measurements. The platelet-like crystals of the orthorhombic α -uranium exhibit the (001) plane as the largest dimension, and it is upon this surface that these measurements have been performed. The surface exhibits sharp LEED patterns upon cleaning and annealing to 480 K, consistent with the bulk orthorhombic structure of the α -uranium and thus indicating that no dramatic surface reconstruction exists. XPS analysis indicates initial cleaned surfaces at the annealing temperature of less than 1% of a monolayer oxygen impurity.

α -URANIUM ELECTRONIC STRUCTURE

We have measured the α -uranium photoemission core level spectra and valence band energy distribution curves in both angle resolved and partially angle integrated modes. In addition, we have made these measurements on high purity polycrystalline α -uranium samples in an attempt to more closely have the measurement reflect a fully angle integrated density of states. These measurements have been done as a function of temperature from 173 to 873K, and yield not previously observed high-resolution features in the ultraviolet photoemission spectroscopy (UPS) data, particularly at low temperatures (figure 1). At higher temperatures the manifold at the Fermi edge is broadened and the peak top location appears to shift in energy. Comparison of the valence band at excitation photon energies of 21.21 and 40.81 eV at a sample temperature of 173K indicates a mix of U5f and U6d density in the initial manifold within 0.5 eV of the Fermi edge. These assignments will be discussed. In addition we have examined the shallow U6p states using soft X-ray photoemission. These states, and in particular the U6p_{3/2} spin-orbit state, show anomalous splitting. The indication here is that the 6p state is no longer core-like and is hybridized in the uranium metal. This is confirmed with comparison to a full Dirac calculation, which shows the correct value in the spin-orbit splitting and indicates the hybridization in the U6p_{3/2} band.

α -URANIUM BAND MAPPING

We have examined the band structure across the principal symmetry directions of the Brillouin zone $\Gamma \rightarrow \Sigma$, $\Gamma \rightarrow Y$, and $\Gamma \rightarrow S$, as well as an examination of the band structure and Fermi distribution as a function of temperature from 173 K to 373 K. First-principles electronic band-structure calculations have been performed using a generalized gradient approximation

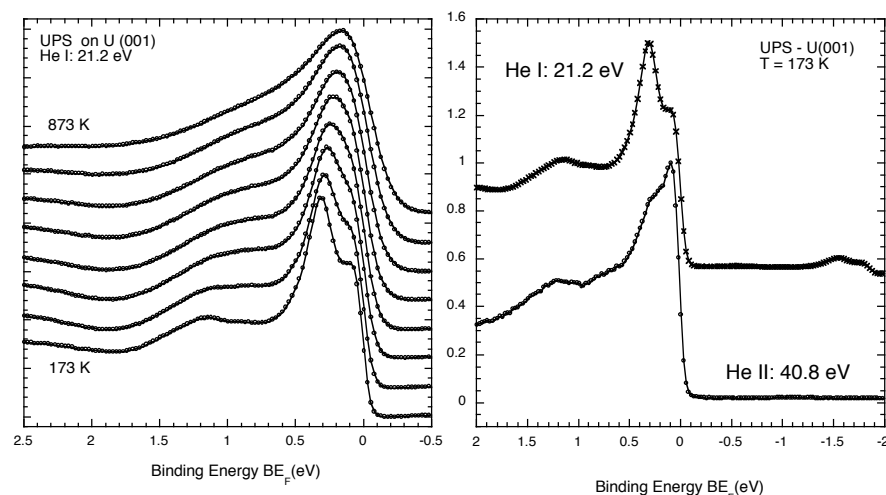


Figure 1. Temperature dependent valence band photoemission (left) of the near Fermi edge DOS of the U(001) surface from 173 to 873K in 100K steps. Comparison of the near Fermi edge photoemission with $h\nu=21.21$ and 40.81 eV at a sample temperature of 173K (right).

(GGA) method in the full-potential linearized-augmented-plane-wave (FLAPW) method, including 6p orbitals to accommodate the shallow U 6p states as interacting. These calculations show partial agreement with the experimental measurements (figure 2). The major differences have been justified by the presence of electronic surface states and the strong suggestion of electron-phonon coupling effects. We believe the electron-phonon

coupling in this system to be related to the unusual thermal allotropic phase transformations exhibited in uranium and other actinides including plutonium. The behaviour exhibited in uranium is believed to be a precursor for the full electronic state transition of plutonium in moving through the allotropic phases, and localization of the f-electrons. The details of these measurements and their implications for actinide electronic structure will be discussed.

1 H.F. McFarlane, K.M. Goff, F.S. Felicione, C.C. Dwight and D.B. Barber, *Journal of Metals* **49** (1997) 14.

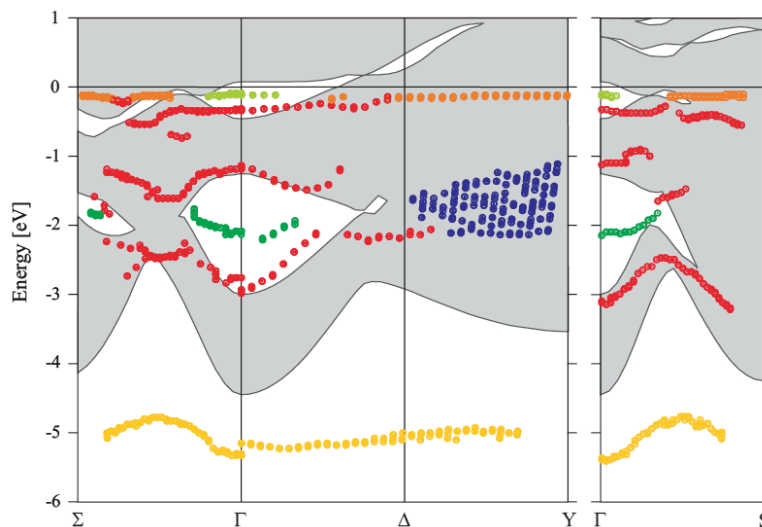


Figure 2. Electronic band map of α -uranium. The coloured data points are band locations in energy and momentum extracted from the experimental data, and the grey background fill the $\Gamma \rightarrow Z$ integrated calculation of the band structure.

Symmetry considerations on the ground state of NpO_2

S. Di Matteo ^{*}, R. Caciuffo[§]

^{*}European Synchrotron Radiation Facility, B P 220, F-38043 Grenoble CEDEX, France

[§]European Commission, Joint Research Centre, Institute for Transuranium Elements, Postfach 2340, Karlsruhe, D-76125 Germany

INTRODUCTION

The ground-state symmetries of Np ions in the low temperature phase of NpO_2 ($T < T_0 = 25$ K) are discussed with reference to the results of resonant x-ray scattering (RXS) experiments suggesting the occurrence of long-range magnetic octupolar order with an electric quadrupole secondary order parameter¹. Two models have been proposed in the literature: one based on a 4 doublet² (in D_{3d} point group), the other on a $5(6)$ singlet³. We show, through a theoretical group analysis, that the 4 doublet is not compatible with the available experimental data. Our analysis supports the hypothesis of a singlet ground state.

Experimental results indicate the absence of structural distortions, either internal or external, and an ordered magnetic dipole moment smaller than $0.01 \mu_B$ (see Ref. 3 for a brief review of the experimental results, and a complete list of references). Quadrupole magnetic moments being excluded, because Np positions are inversion centres, magnetic octupole moments can be considered as possible order parameters, as suggested by Santini and Amoretti². In particular, the components of the octupole moments transforming like 2 (singlet) and 5 (triplet) in octahedral fields can be considered, the 4 triplet being rejected because it would imply the presence of an induced magnetic dipole, as detailed in Ref. 2. The first possibility is maintained in Ref. 2 and appears compatible with a 4 doublet ground-state in D_{3d} . The second type of symmetry for the octupole has been advanced in Ref. 3 and assumes a $5(6)$ singlet ground-state.

Here, we analysis of the ground-state symmetry, from the perspective of the D_{3d} local symmetry at Np^{4+} -sites indicated by RXS, and we try to clarify some subtleties related to time-reversal symmetry. This also opens the way to a straightforward identification of the allowed order parameters and a direct classification of the possible ground states. The analysis supports the conclusions reported in Ref. 4, where a singlet ground state was proposed for NpO_2 on the basis of specific heat measurements.

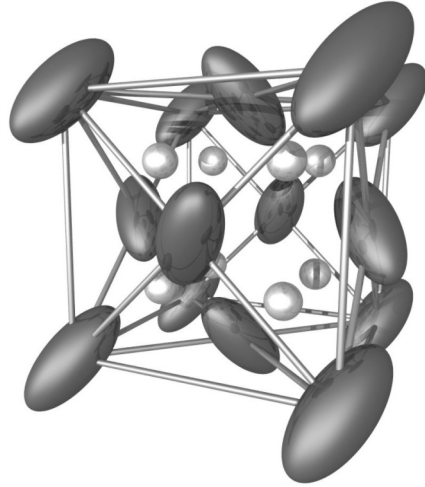


Fig 1: Schematic representation of the triple- k longitudinal ordering of Np electric-quadrupole moments in NpO_2 .

SYMMETRY CONSIDERATIONS

In the high-temperature phase, NpO_2 crystallises in the Fm-3m space group. The (003) reflection in such a group is forbidden by symmetry at all orders, even in resonant conditions. Therefore, its detection at Np M_4 edge in the low-temperature phase shows that the local symmetry of Np^{4+} ions below T_0 is a subgroup of the cubic group m-3m (O_h). The only maximal nonisomorphic subgroup of Fm-3m that is non-symmorphic and simple cubic is Pn-3m, which has the same diffraction pattern as Fm-3m for both Np and O atoms, thus explaining why usual diffraction is not sensitive to any symmetry-lowering below T_0 . The Np ions are accommodated at positions 4b, with reduced local symmetry -3m (D_{3d}). The character table of the D_{3d} (double) group can then be used to derive the ground state symmetry and the allowed octupolar components.

The seven degenerate components of the octupole magnetic moment in spherical symmetry $SO(3)$ split, in D_{3d} symmetry, into two doublets $_3$, two singlets $_2$ and one singlet $_1$, the latter corresponding to the totally symmetric irreducible representation of $L=3$ in D_{3d} . The experimental evidence of the absence of dipolar long-range order forces us to consider only those components of magnetic octupole not belonging to the same representations as the dipole, otherwise this latter would be induced as secondary order parameter. In D_{3d} symmetry only one octupolar component has the desired property, the one belonging to the totally symmetric representation $_1$. This latter can be written in terms of spherical harmonics with quantization axis along the trigonal [111] direction, and the corresponding expression in terms of equivalent angular momentum operators can be easily derived.

The $_8$ ground-state quartet of O_h splits, in D_{3d} , into a doublet $_4$ and a couple of Kramers-related singlets $_5$ and $_6$. Even though they belong to two different representations of the D_{3d} double group, the latter are degenerate in presence of time-reversal symmetry, and their degeneracy splits only when time-reversal is broken. The four states can be written in terms of the basis $||J=9/2, J_z\rangle$, assuming the quantization direction along the three-fold symmetry axis. In presence of a time-reversal symmetry breaking, the double degeneracy of the $_4$ doublet would be lifted giving a lowest-lying component with a net dipolar moment. This is against the experimental evidence. Therefore, we have to assume that the ground state of Np in the low-temperature phase is a $_5$ (or a $_6$) singlet. The structure of the singlet is such that the average value of any component of the magnetic moment J_a ($a=x, y, z$) is zero: only trilinear objects $J_a J_b J_c$, e. g. magnetic octupoles, have expectation values different from zero.

- 1 J.A. Paixao et al., Phys. Rev. Lett. **89**, 187202 (2002)
- 2 P. Santini and G. Amoretti, Phys. Rev. Lett. **85**, 2188 (2000)
- 3 R. Caciuffo et al., J. Phys. Cond. Matt., **15**, S2287 (2003)
- 4 N. Magnani et al., Physica B **359-361**, 1087 (2005)

^{69}Ga NMR in $\text{Pu}_{1-x}\text{Ga}_x$ ($x < 0.01$) alloy

Yu.V. Piskunov^{*}, K.N. Mikhalev^{*}, Yu.N. Zuev[†], S.V. Verkhovskii^{*}, V.E. Arkhipov^{*}, I.L. Svyatov[†], A.E. Shestakov[†], A.V. Pogudin^{*}, V.V. Ogloblichev^{*}, and A.L. Buzlukov^{*}

^{*}Institute of Metal Physics, Ural Branch of Russian Academy of Sciences, Ekaterinburg, Russia (piskunov@imp.uran.ru)

[†]Russian Federal Nuclear Center - Institute of Technical Physics, Snezhinsk, Russia

^{69}Ga NMR spectra measured in the monoclinic α -phase¹ of the $\text{Pu}_{0.995}\text{Ga}_{0.005}$ alloy are presented in this report. The investigated strips of alloy (20x3x0.2 mm) were single phase without detectable macroscopic impurity of other phases in accordance with the optical metallography and x-ray diffraction technique.

The ^{69}Ga NMR spectrum of this alloy in the external magnetic field of 9.4 T consists of central line (transition $-1/2 \leftrightarrow +1/2$) and a broad pedestal of the satellite lines (transitions $\pm 1/2 \leftrightarrow \pm 3/2$). Such a spectrum can be considered as typical for a powder of imperfect cubic crystals, where the local deviations of cubic symmetry of charge distribution around Ga-atom take place. The nucleus of Ga has electric quadrupole moment $eQ=0.17 \cdot 10^{-24} \text{ cm}^2$. Arising electric field gradient (eq_{ii}) causes essential broadening of satellite lines $\Delta\nu_Q \sim e^2Qq_{zz}$. At the same time, the shift (^{69}K) and the linewidth ($\Delta\nu$) of central transition are determined by local fields, which are caused by hyperfine coupling from the nearest surrounding of Pu-atoms.

In initial state of alloy (see Figure 1a), the linewidth of central transition essentially (in 2.5-3 times) larger than its magnitude for the stabilized δ -phase alloys^{2,3}. The growth of ($\Delta\nu$) is determined by the distribution width of the Ga-Pu interatomic distances, which is increased in the mechanically-pressed state of the α -phase of alloy under investigation.

Annealing of the sample at the temperature higher than α - β structural transformation (150° C during 8 h.) causes an essential change in the shape of central line (see Figure 1b). The fine structure of the central line can be represented as a superposition of two lines with different $\Delta\nu$ and ^{69}K . The broad line-2 of relative intensity 0.67(10) demonstrates a shift being approximately independent on temperature,

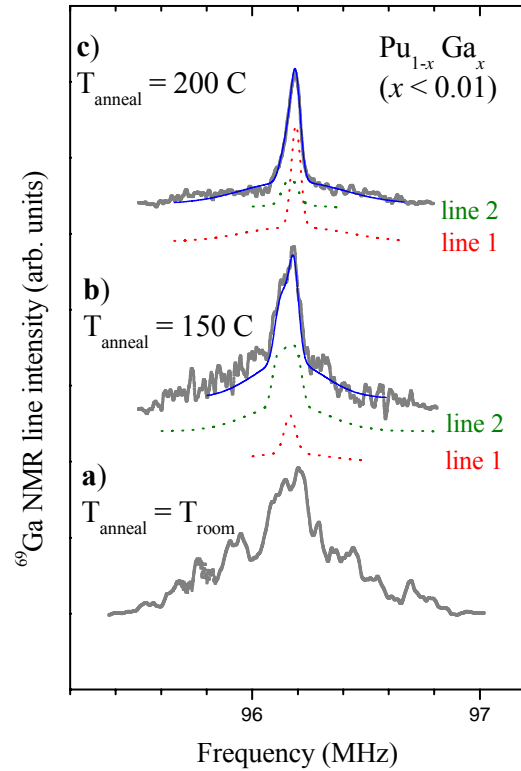


Fig 1: The ^{69}Ga NMR spectra measured at magnetic field of 9.4 T at 20 K in $\text{Pu}_{0.995}\text{Ga}_{0.005}$ alloy. a) the initial α -phase; b) after annealing at $T_{\text{anneal}}=150$ C during 8 h.; c) after annealing at $T_{\text{anneal}}=200$ C during 20 h. The dotted lines are the result of simulation of the experimental spectrum by two lines with different intensities.

as it takes place for static magnetic susceptibility of α -Pu (see Figure 2). While the shift of the more narrow line-1 having the less intensity changes with temperature like $^{69}\text{K}(T)$ -dependence in the stabilized δ -Pu alloy $\text{Pu}_{0.95}\text{Ga}_{0.05}$ ^{2,3}. An additional annealing of the alloy at $T = 200$ C during 20 h. leads to progressive narrowing of the central line at the expense of the line-1, dominating in intensity, as shown in Figure 1c.

It is reasonable to assume that the annealing performed above the α - β structural transformation, should take off only the mechanical strength, persisted in the initial α -phase¹. The x-ray examination of the annealed sample at room temperature results in the absence of any traces of macroscopic areas of δ - phase with characteristic size exceeding 100 nm.

In accordance with the ^{69}Ga NMR and x-ray data one can conclude that in the α -phase of $\text{Pu}_{0.995}\text{Ga}_{0.005}$ the microscopic areas with a size less than 100 nm exist. The local charge and magnetic environment of the solute Ga in these microscopic areas is similar to the observed in the stabilized δ -Pu alloy $\text{Pu}_{0.95}\text{Ga}_{0.05}$ ^{2,3}.

Acknowledgments

The work was supported by the Russian Foundation for Basic Researches (Project No. 06-02-16130). Yu.P. acknowledges the "Russian Science Support Foundation" for a financial support.

¹S.S. Hecker and L.F. Timofeeva. Los Alamos Sci. **26**, 244 (2000)

²Yu. Piskunov, K. Mikhalev, A. Gerashenko, et al., Phys. Rev. B **71**, 174410 (2005).

³S. Verkhovskii, et al., JETP Lett. **82**, 139 (2005).

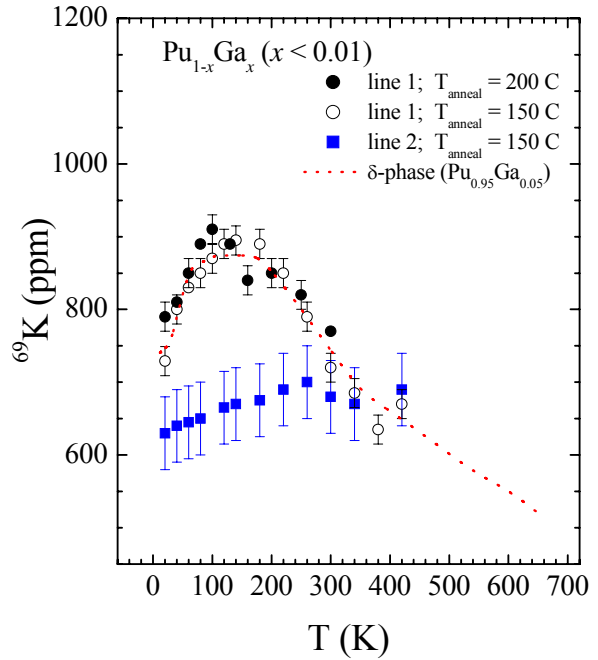


Fig 2: Temperature dependences of the ^{69}Ga NMR shift for the line-1 and line-2 in the $\text{Pu}_{0.995}\text{Ga}_{0.005}$ alloy.

Effect of Composition and Age on the Density of Delta Plutonium Metal

R. Mulford^{*}, W. Brown[†]

^{*}Los Alamos National Laboratory, Los Alamos, NM 87545 USA

DENSITY CHANGES AND AGING

Measurements on new and aged plutonium metal from a variety of sources indicate some factors which affect the density of the delta-phase metal. The density is observed to vary as a function of age. The rate of variation with age is not uniform, but exhibits three stages: an early stage of about three to ten years, an intermediate stage of up to 35 years, and a late stage. Behavior observed for samples of advanced age may be due to differences in composition as well as age.

Changes in density are due to several consequences of radioactive decay of the plutonium atoms. Possible causes include helium accretion in the metal lattice, accumulation of americium, ingrowth of uranium, and radiation damage. The relative rates of self-irradiation processes and decay processes in plutonium permit some separation of some of the physical and chemical aging effects in time, and may allow distinct rates for lattice damage and gas accumulation to be inferred.

The oldest plutonium samples available exhibit a wider range of compositions than newer material. Compositional variations may mask possible aging mechanisms, but do allow study of perturbations to density produced by compositional variations.

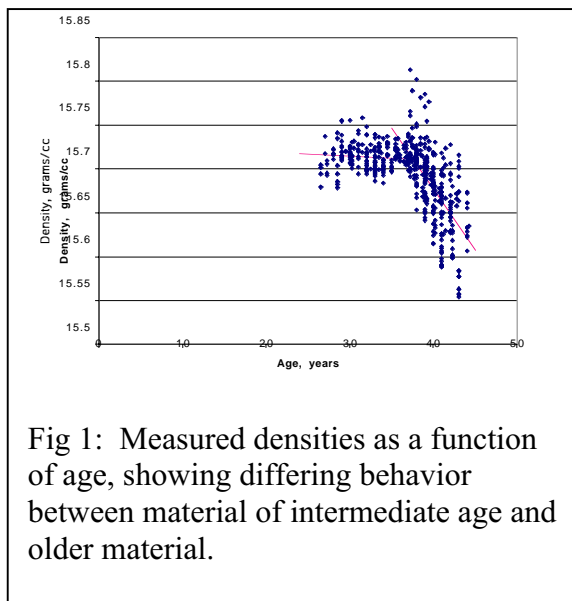


Fig 1: Measured densities as a function of age, showing differing behavior between material of intermediate age and older material.

MEASUREMENTS, ANALYSIS AND RESULTS

Measurements were made by the Archimedes method of immersion, and corrected for temperature expansion of the immersion fluid, FC-43. A posteriori uncertainty varied between 0.0003 and 0.001 g/cc. Daily calibrations yielded information on the behavior of the immersion fluid, and provided statistical information on variations in the measurements. We report the effect of sample mass on measured values of density and on observed a posteriori uncertainties in reported values. The influence of oxidation on measurements is examined. Limitations of the technique are discussed.

Rates are obtained by making linear fits to ensembles of similar samples, by tracking the changes in a single sample over several years, or both. Results indicate a decrease of about 0.003%/annum for samples of intermediate age, in agreements with results of TEM imaging and

measurement of helium bubbles.¹ New material exhibits rates of between 0.016% and 0.02%/annum, somewhat less than rates of 0.06%/annum reported for XRD studies.² Plutonium of advanced age exhibits a rate of 0.06%/annum, both in the behavior of the ensemble and in the change in individual samples.

Corrections for lattice expansion by americium have an effect on the reported rates of change in density. The behavior of americium in the lattice has been reported to depend on the location and thermal history of the americium. Corrections to density and assumptions are discussed.

The possibility of the formation of uranium plutonide as uranium accumulates within the lattice has been examined. In most cases, excess uranium present at casting has been observed in a second phase as U_6Fe . Cases examined here permit study of uranium introduced into the lattice without thermal equilibration with second phase regions, and present a case in which insufficient iron makes consumption of uranium by the formation of U_6Fe stoichiometrically impossible.

Early time behavior of castings has received some study^{2,3} as a case of lattice disorder, and also as a perturbation by chemical changes produced by decay.⁴ Changes in helium accommodation may also play a role.⁵ Density measurements on new and aged castings are compared with data obtained from a variety of sources⁶ in an effort to clarify some of the mechanisms that contribute to the density and structural changes.

SIGNIFICANCE AND RELEVANCE

Changes in the structure of plutonium metal as a function of age are of interest as an example of radiation damage at very low dose rates, relative to the majority of externally irradiated cases available for study. The effects of auto-irradiation have implications for engineering and lifetime prediction in nuclear weapons and devices such as sources.

Density changes must be factored into a wide variety of other physical measurements, such as compressibility, strength, elastic properties, and permittivities, particularly as they apply to samples that may be aging during the course of the study. A general study of density changes may simplify the interpretation of detailed measurements intended to quantify specific mechanisms.

- 1 A.J. Schwartz, M.A. Wall, T.G. Zocco, and W.G. Wolfer, *Phil. Mag.*, **85**(4-7) (2005)
- 2 N.T. Chebotarev and O.N. Utkina, in *Plutonium and Other Actinides*, Eds. JH. Blank and R. Lindner, North-Holland Publishing Company, Amsterdam p. 559-565 (1976)
- 3 R.N. Mulford, Los Alamos National Laboratory report, LA-UR-06-0771 (2006)
- 4 W. Wolfer, Lawrence Livermore National Laboratory, private communication.
- 5 M. Baskes, Los Alamos National Laboratory, unpublished work.
- 6 B. Chung, Lawrence Livermore National Laboratory and L. Morales, Los Alamos National Laboratory, private communications.

Analysis of Density Changes in Plutonium Observed from Accelerated Aging using Pu-238 Enrichment

B. W. Chung, C.K. Saw, S.R. Thompson, T.M. Quick, C.H. Woods, D.J. Hopkins, and B.B. Ebbinghaus

Lawrence Livermore National Laboratory, Livermore CA 94552 USA

INTRODUCTION

Plutonium, because of its radioactive nature, relentlessly undergoes self-irradiation damage through out its volume. Plutonium decays to uranium by α -particle emission. The α -particle takes away most of the energy and eventually comes to rest as a helium atom. While both particles produce displacement damage in the form of Frenkel-type defects, most of the damage results from the uranium recoil nucleus. The defects resulting from the residual lattice damage and helium in-growth results in microstructural and physical property changes. Because these self-irradiation effects would normally require decades to measure, with a fraction (7.5 wt%) of ^{238}Pu is added to the reference plutonium alloy thus accelerating the aging process by approximately 18 times the normal rate. By monitoring the properties of the ^{238}Pu -enriched alloy over a period of about 3.5 years, the properties of plutonium in storage can be projected for periods up to about 60 years. Previously, we reported the observation of density and volume changes due to self-irradiation in enriched alloys¹. In this paper, it will shown that the change in density is a result of the change in lattice parameters, which saturates within approximately three years of aging, and the continued build-up of helium in-growth. This analysis is founded upon microstructural measurements such as X-ray diffraction.

EXPERIMENTAL

The length change was primarily determined by dilatometry measurements. The length change was compared to immersion density measurements and lattice parameters measured from X-ray diffraction.

Dilatometers have been set up to monitor long-term growth resulting from the lattice damage and helium in-growth in (~ 7.5 wt%) ^{238}Pu -enriched alloys. Details of experiments are presented elsewhere¹. Two different lengths of ^{238}Pu -enriched alloy specimens (3 cm and 2 cm) are used to differentiate between surface oxidation and volumetric swelling in the materials. The dilatometer chamber atmosphere is helium backfilled after evacuation with an oil-less vacuum pump. Each dilatometer has three wells: one for a 3 cm long specimen, one for a 2 cm long specimen, and one for a zero-dur reference material.

The immersion densities on the enriched and reference alloys were obtained shortly after the initial fabrication and then subsequently at least every six months. Between measurements, the samples were stored in a helium-filled incubator at 50°C. The equipment closely matches a design used by Bowman *et al.*² and uses about 200 ml of Fluorinert Electronic Liquid FC-43 as the immersion fluid. Prior to a measurement, the system is calibrated using NIST glass (SRM 1827A) and a tantalum specimen as standards. This is generally followed by a measurement on

the plutonium reference alloy and the ^{238}Pu -enriched alloy. To obtain stable measurements and ensure that all surface oxide is removed, multiple measurements are performed.

RESULTS and DISCUSSION

The length change (ΔL) normalized with the initial length (L_0) of each spiked alloys at 35°C is shown in Figure 1. The time is represented as an equivalent time (in year) obtained by multiplying the measurement time by the accelerating factor of 18.59. Each dilatometer contains a pair of long (3cm) and short (2cm) length specimens. The $\Delta a/a_0$ of the sample is from X-ray diffraction where $\Delta a/a_0$ represents the measured lattice constant change (Δa) normalized with the initial lattice constant (a_0). As plotted in Figure 1, the spiked alloys have increased in length significantly. Based on microstructural characterizations, the initial changes in the volume and density are a result of the change in lattice parameters, which saturates within approximately three years of aging. Following the initial transient, the change is mainly caused by continued build-up of helium in-growth.

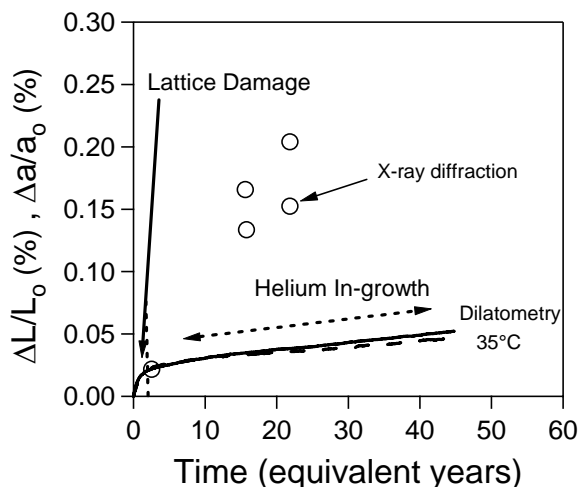


Figure 2. Dilatometry and X-ray diffraction measurements show dimensional expansion with aging.

SUMMARY

We found reasonable agreement in the density change behaviour between enriched and reference alloys from combined dilatometry and immersion density measurements. Based on microstructural analysis, the decrease in plutonium alloy density is a result of the dimensional expansion from the accumulation of residual lattice damage and helium in-growth.

This work was performed under the auspices of the U.S. Department of Energy by the University of California, Lawrence Livermore National Laboratory under Contract No. W-7405-Eng-48.

- 1 B.W. Chung, S.R. Thompson, C.H. Woods, D.J. Hopkins, W.H. Gourdin, and B.B. Ebbinghaus, submitted to: J. Nucl. Mater. (UCRL-JRNL-216611) (2005)
- 2 H.A. Bowman, R.M. Schoonover, and M.W. Jones, J. of Res. Nat. Bur. Stand., 71C, (1967) 179.

Modeling of plutonium alloy swelling by kinetic rate equation

N. Gras-Naulin, P. Julia

CEA – Centre de Valduc, F-21 120 IS-SUR-TILLE, FRANCE

INTRODUCTION

Understanding and predicting all the impact of plutonium alloys aging on the reliability and safety of nuclear stockpile is one of the most challenging aspects of plutonium metallurgy. One of the consequences of plutonium aging is swelling. This phenomenon has several origins: voids or bubbles formation due to vacancies clustering, alpha decay sub products (Am, Np, U, He ...). These defects are created by displacement cascades due to alpha decay of plutonium. Many experiments allow measurement of the total swelling but none of them permit a perfect identification and quantification of each contribution. So we try to use modeling as a tool to evaluate the contribution of the different phenomenon involved in swelling.

Kinetic rate equation modeling allows determination of the concentration in vacancies clusters versus time for each size of cluster¹. From these concentrations we can extract the total change in volume of the material due to void formation, $\Delta V/V$:

$$\Delta V/V = \sum 4/3 \pi r_n^3 C_n$$

with r_n : radius of a cluster containing n vacancies

C_n : concentration in cluster of size n.

The results obtained by this modeling are compared to those measured by optical-fiber Bragg grating sensors. This technique allows continuous measurement of the elongation of the sample². The total swelling of the material is then obtained versus time.

RESULTS

Kinetic rate equation physics is in the input data. Energetic data such as formation and migration energies of vacancy and interstitial, diffusion coefficient of interstitial and vacancy are needed. Molecular dynamic calculations were performed in order to obtain pertinent data in regard with the material we want to model³. Dose rate is an important parameter, but the key data is the freely migrating defects that escape their nascent cascade and are able to induce microstructure evolution. This fraction depends on mobility of defects and can be estimated by simulation using molecular dynamic and Kinetic Monte Carlo models. For the time being, we did not perform this simulation and we use results obtained on aluminium⁴. The production efficiency of freely migrating defect is 15% of the defect production value predicted by NRT model.

Simulation over several years was performed and results are presented on figure 1. Superposition of the curve calculated by kinetic rate equation with the one obtained by dilatometry exhibited a difference of behavior. Contribution of defects induces a saturation of swelling after about 6 months whereas no saturation is observed experimentally.

Contribution of chemical defects is quite important and can explain the continuous rise of swelling. So we add to the results obtained by kinetic rate equation, swelling due to the increase of americium concentration⁵ and helium contribution through out the increase of volume due to formation of helium bubbles⁶. Total swelling is reported on figure 2 and compared to experimental results. Calculated curve is a little bit more conform to the dilatometric measurement but there is still a difference between the two curves.

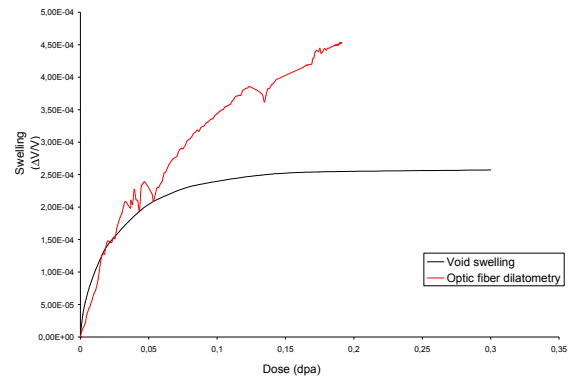


Figure 1: Void swelling versus dose

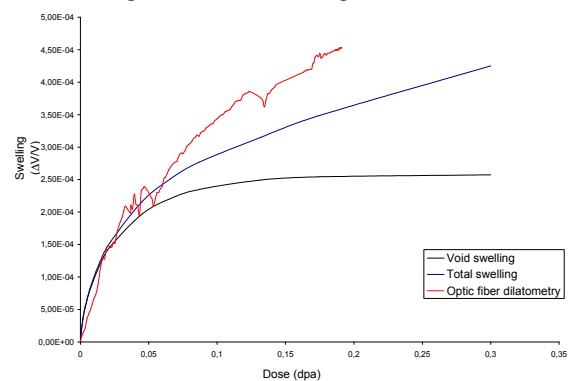


Figure 2: Total swelling versus dose

DISCUSSION

The difference of swelling is probably due to a complementary effect which is neglected in the previous simulation. This neglected phenomenon has an increasing importance and we can not predict long term swelling without understanding it and take it into account. Several guesses are explored; the most favorable is an interaction between vacancies clusters and helium which could exacerbate volume change. Modeling this interaction is a great challenge and is our current subject of interest.

References:

- 1: A. Hardouin Duparc *et al.*, J. Nucl. Mater. 302 (2002) 143
- 2: P. Julia, Plutonium Futures – The Science (2003) 109
- 3: L. Berlu, Technical report CEA/DRMN/SEMP (2006)
- 4: A. Almazouzi *et al.*, Nuclear Instruments and Methods in Physics Research B 153 (1999) 105-115
- 5: F.H. Ellinger *et al.*, J. of Nucl. Mater., 20 (1966) 83-86
- 6: W.G. Wolfer, Los Alamos Science 26 (2000), 277-285

The TTT-diagram of unalloyed plutonium $\alpha \rightarrow \beta$ -transformation.

A.V. Troshev, A.M. Lyasota, S.I. Abramenko, Yu.N. Zuyev, V.N. Kordyukov,
B.G. Levakov, B.V. Litvinov, E.P. Magda, A.A. Snopkov

*Academician E.I. Zababakhin All-Russia Research Institute of Technical Physics,
456770, Snezhinsk, Chelyabinsk region, PO Box 245
Fax: 351-323-51, E-mail: btk@five.ch70.chel.su*

The majority of investigations into kinetics of plutonium $\alpha \rightarrow \beta$ -transformation were performed under quasi- and isothermal conditions using oil baths to maintain constant temperature of the samples. The exception are experiments, performed by M.C. Faiers and R.G. Loasby, on studying kinetics of $\alpha \rightarrow \beta$ -transformation at pulse electric heating (Proceedings of the 3-rd and 5-th International Conferences – Plutonium-1965 and Plutonium-1975).

As a result of this work thermal-kinetic curves were obtained in temperature-time-degree of phase transformation coordinates, the so-called TTT-diagrams (Temperature-Time-Transformation). These diagrams represent one of fundamental properties of plutonium.

But until the present time due to inconsistency and spread in values of temperatures of transformation starting in some intervals of incubation period the known TTT-diagrams can not be combined into a uniform TTT-diagram of plutonium $\alpha \rightarrow \beta$ transformation starting.

The authors of this paper have supplemented the known data with the results of investigations into kinetics of phase transformation during pulse volumetric heating of plutonium samples on pulse nuclear reactors available at VNIITF. The authors propose the version of reasonably completed TTT-diagram of unalloyed plutonium $\alpha \rightarrow \beta$ -transformation, which covers a change in incubation period of starting of isothermal phase transformation within $10^{-5} \dots 10^5$ s (Fig.1).

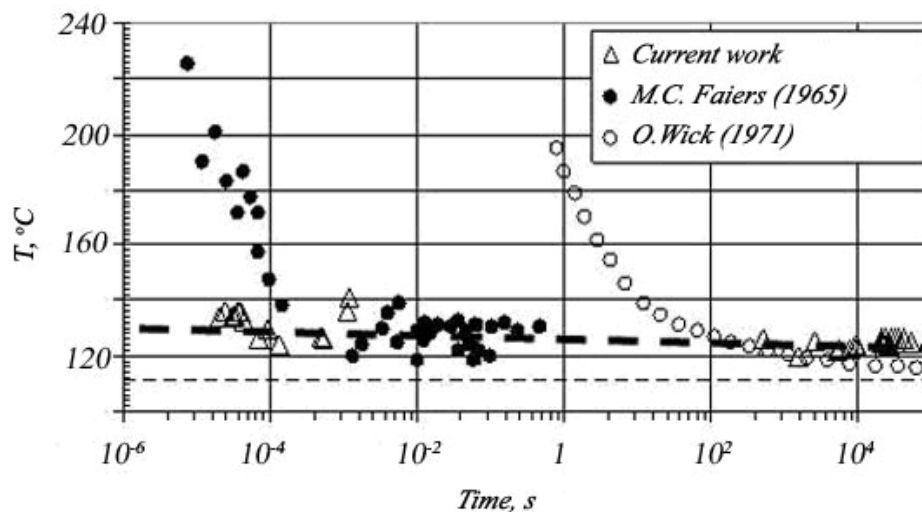


Fig. 1 – Generalized TTT-diagram of plutonium $\alpha \rightarrow \beta$ -transformation starting (dotted line), proposed by authors, and published data.

Helium Bubble Behavior in Plutonium Alloys at the Atomistic Level

S. Valone^{*}, M. Baskes^{*}, R. Hoagland^{*}

^{*}Los Alamos National Laboratory, Los Alamos NM 87545 USA

MODELING RADIATION DAMAGE IN PLUTONIUM

Self-irradiation damage in plutonium metal and alloys generates a series of defect structures that range from point defects to macroscopic density changes. One approach to modeling these defect structures is a reliable atomic level model, which at a minimum accounts for the Pu-Ga-He system. An atomistic model for this system has been previously developed based on the modified embedded atom method (MEAM) [1]. The model was applied to both alloys [2] and He bubbles in those alloys, under constant temperature and volume conditions [3]. Changes in the local structure of the bubbles at various temperatures, gallium concentrations, and helium concentration within a single bubble could be observed. In this study, we use constant hydrostatic pressure boundary conditions. The MEAM potential for the Pu-Ga-He system used here is substantially the same as before [3], except for small changes in the He-He and Pu-He interactions. The He-He interaction was reduced at high pressure by requiring that interaction to exactly reproduce the experimental cold curve at those pressures, as well as exactly matching the *ab initio* curve for the He₂ dimer. The Pu-He interaction was modified to reduce the solubility of the He in the metal. This was done by changing the scaling ratio between the He and Pu density contributions to 0.15 from 0.04. This value was chosen to obtain a 0.75 eV heat of solution for the He. This heat of solution was chosen because it is in the mid-range of accepted values for He in metals when the He is placed in a substitutional site in the metal. Changes in the constant volume results were inconsequential at the He bubble pressures considered, as a result of the small changes in the potential.

HELIUM BUBBLE BEHAVIOR AT CONSTANT HYDROSTATIC PRESSURE

The results of simulations of He bubbles in 5 at-% Ga-stabilized Pu at constant pressure show minimal changes relative to those at constant volume. The volume changes are less than 1 %. The interstitial cluster in the cell at 300 K and a 2:1 He-to-vacancy ratio, remains immobile on the timescale of the simulations (50 ps). The distribution of He in the bubble at these conditions is shown in Fig. 1 for both constant volume and pressure boundary conditions.

At both higher temperatures (1000 K) and higher He densities (2.5:1 and 3:1 He:vac), the local structure of the metal lattice in the neighborhood of the He bubble remains close to the structures observed under constant volume conditions. At temperatures close to the melting point, there are indications of greater solubility of He in the metal. At high He densities, the He disturbs the local structure of the metal and some He is injected into the metal (Figs. 2a and 2b).

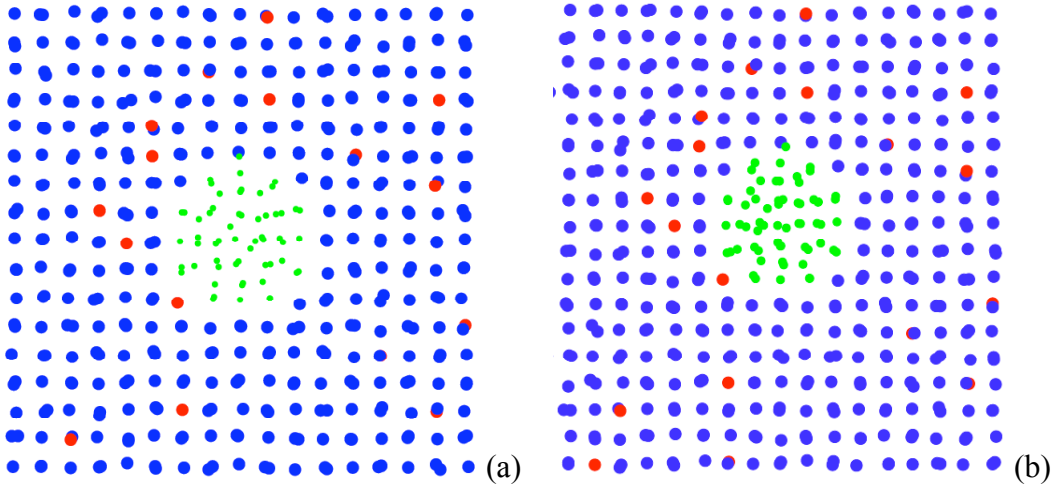


Fig. 1: Cross-sections of He Bubble at 300 K, 5 at-% Ga, 2:1 He:vac ratio, and (a) constant V and (b) constant P = 0.

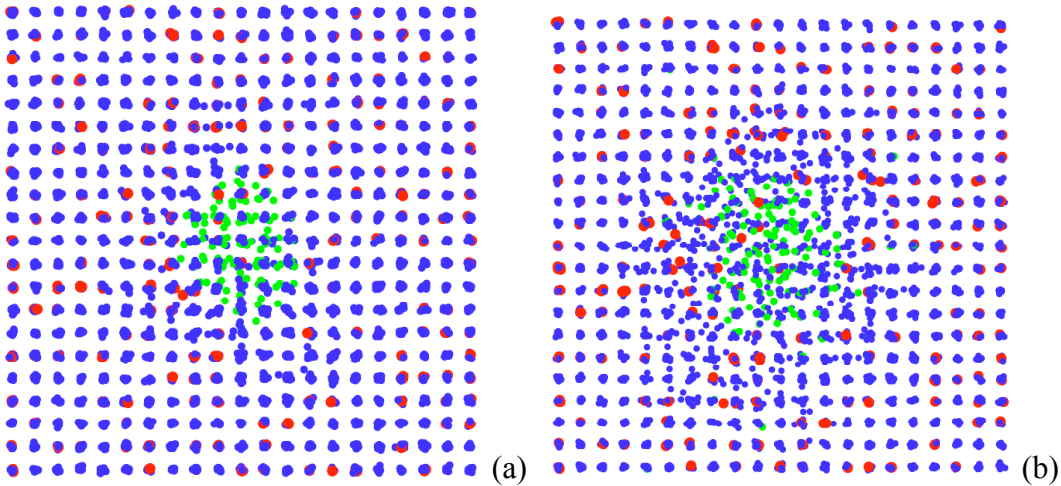


Fig. 2: He bubble at 300 K 5 at-% Ga, constant P, and (a) 2.5:1 and (b) 3:1 He:vac ratio.

This work was performed at Los Alamos National Laboratory under the auspices of the U. S. Department of Energy, under contract No. W-7405-ENG-36.

- [1] M. I. Baskes, Phys. Rev. B 46, 2727 (1992); M. I. Baskes, Phys. Rev. B 62, 15532 (2000); M. I. Baskes, S. P. Chen, and F. J. Cherne, Phys. Rev. B 66, 104 (2002).
- [2] M. I. Baskes, K. Muralidharan, M. Stan, S. M. Valone, and F. J. Cherne, JOM 55, 41 (2003).
- [3] S. M. Valone, M. I. Baskes, and R. L. Martin, Phys. Rev. B, accepted (2006).

Formation and Recovery of Irradiation and Mechanical Damage in Stabilized δ -Plutonium Alloys

F. J. Freibert, D. E. Dooley, D. A. Miller, and A. Migliori

Los Alamos National Laboratory, Los Alamos NM 87545 USA

HISTORICAL PERSPECTIVE

In 1958, Bochvar, et.al. authored a paper in which the binary phase diagram for the Pu-Al system exhibited a stabilized δ -phase field which extended to compositions no greater than 14 atomic percent and to temperatures no lower than 175 °C, at which point the alloy undergoes a eutectoid decomposition into β -Pu and Pu₃Al.¹ This behavior was cited in 1961 by Ellinger, Land and Miner when discussing X-ray diffraction data for stabilized δ -phase Pu-Al alloys, which had been aged at ambient temperatures for 10 years.² In this work, Ellinger, et.al. witnessed a slight lattice expansion (~0.1%) in Pu-Al alloys varying in composition from 11.5 to 12.8 atomic percent and attributed this swelling to lattice defects.² Following on this theme, in 1975 Chebotarev and Utkina reported observing lattice expansion (<0.2%) in δ -phase Pu-Al and Pu-Ga alloys, increasing linearly with alloy concentration, whether the materials had undergone shear or self-irradiation damage.³ Based on this experimental data, Chebotarev, et.al. attributed this lattice expansion to a crystallographic modification, a lattice distortion in the face-centered cubic (FCC) atomic positions. Later work by Inozemtsev, Panteleyev, and Chebotarev showed lattice swelling of similar magnitude in Pu-Al and Pu-Ga alloys exposed to neutron irradiation.⁴ In all reported cases of this behavior, the volumetric expansion was relieved by annealing the alloys at temperatures up to 250 °C.¹⁻⁴

EXPERIMENTAL RECOGNITION OF DAMAGE ACCUMULATION

Interstitial defects in crystalline structures have often been cited as explaining thermo-physical and mechanical changes which result from the accumulation radiation damage. The most stable interstitial atomic configuration of FCC metallic elements is that of the $\langle 100 \rangle$ split-interstitial or $\langle 100 \rangle$ dumbbell interstitial.⁵ These defect structures were first uniquely identified in electron-irradiated Al single crystals via diffuse X-ray scattering as inducing a lattice expansion and having a tetragonal symmetry.⁶ Many studies of radiation damage in FCC alloys has shown that these defect structures can form at substitutional impurity sites as a mixed $\langle 100 \rangle$ dumbbell interstitial consisting of an impurity atom and a host atom being stable to temperatures of 200K or higher.⁷ No matter what atoms combine to form the $\langle 100 \rangle$ dumbbell interstitials in FCC metals, these defect structures not only generate lattice swelling, but also induce unusual changes in the lattice properties such as decreased elastic moduli, large thermal atomic displacements, and decreased Debye-Waller factors.⁷

Based on the results of recent work conducted at Los Alamos National Laboratory^{8,9} it is proposed that Pu-Ga mixed $\langle 100 \rangle$ dumbbell interstitials, caused by self-irradiation processes in naturally and accelerated aged Pu-Ga alloys, induce volumetric swelling and elastic modulus alterations in these alloys as a function of time and Ga concentration. This volumetric swelling, which is in agreement with the historic mechanical and self-irradiation damage data¹⁻⁴, is

similarly removed at temperatures greater than 250 °C and returns on further room temperature aging (see Figure 1). The explanation for the extreme thermal stability of these defect structures can be found in the altered local bonding environment for the interstitial pair and first-nearest neighbors in which the Pu atom, when trapped adjacent to a Ga atom, reduces its size through the on-site localization of a *5f* electron in response to its reduced coordination number. Recent magnetic susceptibility experiments conducted by McCall, indicate that *5f* electron localization accompanies self-irradiation damage.¹⁰ Data from X-ray diffraction¹¹, EXAFS¹², and neutron diffraction¹³ experiments in naturally and accelerated aged Pu-Ga alloys have shown tetragonal lattice distortions, altered Pu-Ga and Pu-Pu bond lengths, lattice micro-strain, and large thermal atomic displacements correlating with similar radiological and thermal histories. The existence of these defect structures in Pu-Ga alloys would also explain the absence of void swelling, which is typical for other FCC metals in similar irradiation environments.

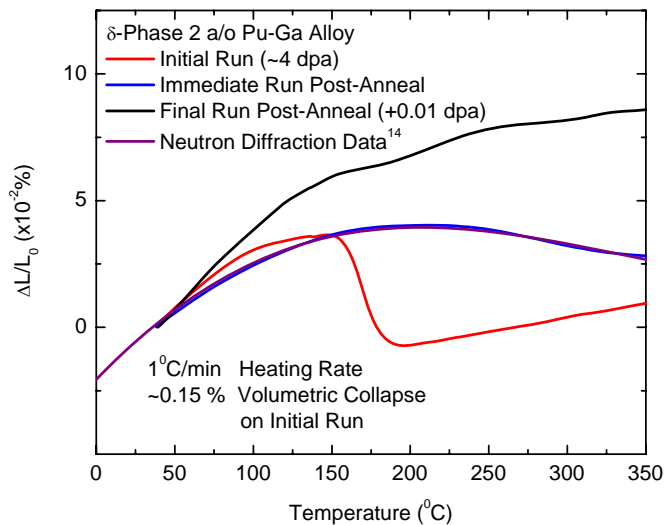


Fig 1: Thermal expansion data for self-irradiated δ -phase Pu-Ga alloy before and after high temperature annealing (>450 °C). Crystallographic data¹⁴ is included to show that annealing removes bulk defects.

This work was conducted under the auspices of the Department of Energy.

- 1 A.A. Bochvar, S.T. Konobeevsky, V.I. Kutaitsev, I.S. Menshikova, and N.T. Chebotarev, Proceedings of the Second United Nations International Conference on the Peaceful Uses of Atomic Energy, **6** 184 (1958).
- 2 F.H. Ellinger, C.C. Land, and W.N. Miner, J. Nucl. Mater. **5**, 165 (1962).
- 3 N.T. Chebotarev and O.N. Utkina, Proceedings of the 5th International Conference on Plutonium and Other Actinides, edited by H. Blank and R. Linder, 559 (1975).
- 4 V.V. Inozemtsev, L.D. Panteleyev, and N.T. Chebotarev, International Conference on Radiation Material Science (22-25 May 1990: Alushta (USSR)).
- 5 R.A. Johnson and E. Brown, Phys Rev **127**, 446 (1962).
- 6 P. Ehrhart and W. Schilling, Phys Rev B **8**, 2604 (1973).
- 7 P.H. Dedrichs, C. Lehmann, H.R. Schober, A. Scholz and R. Zeller, J. Nucl. Mater. **69&70**, 176 (1978).
- 8 F. Freibert, unpublished data (2006).
- 9 A. Migliori, private communication (2006).
- 10 S. McCall, private communication (2006).
- 11 L. A. Morales, A. C. Lawson, S. Conradson, D. P. Moore, E. N. Butler, M. Ramos, and T. Lee, Actinide Workshop, Los Alamos National Laboratory, LAUR-04-3104 (2004).
- 12 S.D. Conradson, L.A. Morales, D.P. Moore, M. Ramos, J. D. Olivas, C. Valot, and A. Ignatov, Los Alamos National Laboratory Report, LAUR-02-6246 (2002).
- 13 A.C. Lawson, et.al., Philosophical Magazine **85**, 2007 (2005).
- 14 A.C. Lawson, et.al., Los Alamos Science **26**, LAUR-00-4100 (2000).

Atomistic Study of Vacancy Clustering and Cluster Dynamics in Pu

BP Uberuaga, RG Hoagland, AF Voter, and SM Valone

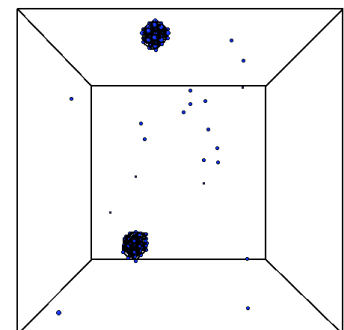
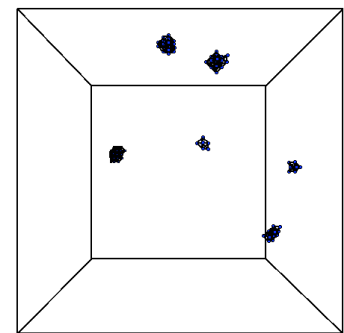
*Los Alamos National Laboratory, Los Alamos NM 87545 USA

Understanding defect mobility and defect-defect interactions is crucial for predicting the long time behaviour of materials. This is especially important for Pu, in which aging phenomena lead to void swelling, the physics of which are determined by interstitial and vacancy point defects. Vacancy clustering will lead to void growth, which will, in turn, give rise to macroscopic swelling. Voids also act as a trap for He gas, giving rise to bubbles that also impact the properties of the material. Thus, understanding the mechanisms by which vacancy voids form and their properties once formed is a key component to understanding Pu aging. While we are generally interested in the full problem of void growth and He incorporation, in this talk we will focus on the properties of the voids themselves.

Using atomistic models, we investigate the clustering behaviour of vacancies in delta-Pu. We study the stability and dynamical properties of clusters containing between 1 and 20 vacancies using the modified embedded atom method¹ (MEAM) to describe the Pu-Pu interaction. The dynamics of these clusters are examined using accelerated molecular dynamics methods², in particular parallel-replica dynamics³.

We find that very small clusters, from size 1 to 5, are mobile, diffusing as objects with identifiable diffusion rates. In particular, di-vacancy clusters diffuse more rapidly than do mono-vacancies. The ramifications of this are explored in a simple kinetic Monte Carlo (KMC) model which ignores higher cluster mobility and which compares the predicted cluster behaviour for two MEAM parameterizations of Pu. These two parameterizations give different relative mobilities of the mono-vacancy versus the di-vacancy. In Pu4, an older parameter set, mono-vacancies diffuse faster than di-vacancies. For this model, many small clusters form and diffuse. In PuX, a new model, di-vacancies diffuse faster and the result is that larger, mobile clusters form which sweep up mono-vacancies as they diffuse. See Figure.

For larger clusters, we find surprising behaviour. In simulations of voids containing 20 vacancies using parallel-replica dynamics, we find that, at 400K, the void is essentially very stable on the microsecond timescale. However, after a microsecond has passed, the void spontaneously transforms into a stacking fault tetrahedron (SFT), at which point, the defect exhibits more vacancy motion on its surface than before the transformation. To our knowledge, this is the first time a direct transformation from void to SFT has been observed. In PuX, the SFT is actually significantly higher in energy than the original void, suggesting that this



KMC simulation of vacancy clustering with two MEAM models: Pu4 (top) and PuX (bottom)

transformation is entropically driven. This also illustrates the limitations of the previous KMC model, which assumed that vacancy clusters remain spherical even for large sizes.

We thus examine the stability of larger clusters, containing up to 20 vacancies. We first compare different cluster geometries to determine which is the most stable, energetically, for the various sizes. We compare planar arrangements versus spherical void geometries. We also examine stacking fault tetrahedra. This gives an idea of what structure will be the most stable as a function of size and temperature.

We also performed a similar study in Cu, to both understand the generality of the results obtained for Pu as well as to more thoroughly study a simpler model system. We find very similar behaviour for Cu. In particular, the 20 vacancy void also transforms into an SFT at temperatures of 400K and timescales of microseconds. In the case of Cu, we are better able to examine the details of the transformation from void to SFT and find that it is “catalyzed” by the motion of an extra vacancy on the surface of the void.

Acknowledgements should be placed at the end of the text in italics.

1 *M. I. Baskes Physical Review B* **46**, 2727 (1992).

2 *A. F. Voter, F. Montalenti, and T. C. Germann, Annual Review of Materials Research* **32**, 321 (2002).

3 *A. F. Voter, Physical Review B* **57**, R13985 (1998).

Mesoscale Structure and Collective and Cooperative Phenomena in Delta-Stabilized PuGa

Dylan R. Conradson, Nicolas Bock, Erik K. Holmstrom, Rafael Howell, Steven D. Conradson
Los Alamos National Laboratory, Los Alamos NM 87544 USA

Local structure measurements have demonstrated that below the 3.5 at-% Ga limit where delta-stabilized PuGa is susceptible to the temperature and pressure-induced martensitic transformation to the alpha phase it exhibits nanoscale heterogeneity. Embedded in the delta host, up to 20% of the Pu atoms reside in domains that are depleted of Ga and form a second type of structure called “sigma” that cannot relax to the alpha phase because of the tensile and epitaxial forces exerted on it by its intimate contact with the delta lattice. Although averaging to another cubic structure, sigma Pu is expanded by 6–7% relative to delta so that it must contain interstitial Pu atoms to retain the delta density and it is modulated so that the nearest neighbor shell is actually split around its average distance. It therefore does not resemble any of the known phases of Pu, posing the question of whether it is natural phase analogous to cubic Fe that would be stable under negative pressure or whether its structural properties are dominated by minimizing the strain at the delta-sigma interfaces. The answer is critical in understanding aging mechanisms in this material because defects are most likely stabilized in delta-stabilized PuGa at very high concentrations to form additional types of ordered structures and releasing internal epitaxial strain might explain this observation.

We have addressed this question by 1) using the information available to devise models of the structure of heterogeneous PuGa that duplicate certain aspects of its properties and 2) using band structure calculations to determine their stability. Within the first part of this work we have devised two structures that capture different features of sigma Pu. One of them duplicates both the local and long range average structures by multiplying the fcc unit cell into a 2x2x2 supercell and expanding and contracting the two cubes along one of its diagonals. Inserting interstitials is, however, not possible without creating some physically unrealistic short Pu-Pu distances so the density is too low. An alternative uses a different modulation of the same supercell to match the density, but in doing not all of the 3.5 Å Pu-Pu bonds are split so it fails to meet all of the structural criteria. Band structure calculations on this second structure show that minimizing the energy involves atoms displacements that do not render the structure closer to the experimental results, indicating that the epitaxial energy may be the dominant parameter determining the overall sigma structure. Additional calculations provide further insights into this process as well as helping to identify the preferred locations and structures of defect sites.

This work was supported by the Heavy Element Chemistry Program, Chemical Sciences, Biosciences, and Geosciences Division, Office of Basic Energy Sciences, and the Enhanced Surveillance Campaign, National Nuclear Security Administration, U.S. Department of Energy under contract W-7405. XAFS and XRD were performed at SSRL (Stanford Linear Accelerator Center) and APS (Argonne National Laboratory), which are operated by the US Department of Energy, Office of Basic Energy Sciences. Health Physics operations at SSRL and APS were supported by the Seaborg Institute for Transactinium Science at LANL.

Computation of Irradiation Damage in Alpha-Decay Actinides

I.I. Konovalov

All-Russia Scientific and Research Institute of Inorganic Materials (VNIINM), Rogov st. 5a
Moscow 123060 Russia

INTRODUCTION

Code VACS «Vacancy Activated Condense System» has been developed for calculation of microstructure parameters and properties change in metal nuclear fuel and structural materials producing inert gas atoms under neutron irradiation^{1,2}.

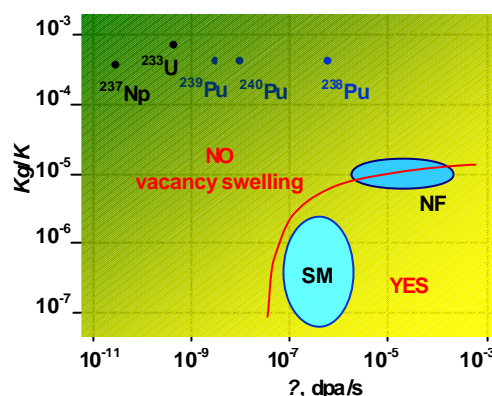
Use of code VACS for self-irradiated metal ^{239}Pu has shown certain conformity of calculated results and experimental data³. The code also has been used for calculation of structure change of alloys in hypothetical system $^{238}\text{Pu} - ^{239}\text{Pu}$ ⁴.

PHISICAL MODEL AND COMPUTAITION RESULTS

Basic thesis of calculation model used in code VACS are given. The kinetics of microstructure irradiation damage: concentration of point defects, density of loop and line dislocations, helium bubble morphology are calculated. The evaluation of influence of microstructure changes on macroproperties of some isotopes U, Np, Pu in metal form under long-life self-irradiation are discussed.

CONCLUSION

In studied field of isotopes physical parameters there are no areas of instable irradiation processes leading to accelerated vacancy swelling. Calculation results of structural changes in self-irradiating metals correspond to basic features of irradiation damage in metal nuclear fuels generating inert gas Xe, Kr and structural materials generating He in reactor core conditions.



The area of vacancy swelling in dependence of damage rate K and rate of inert atoms production K_g .
SM – Structural Materials, NF – Nuclear Fuel.

1. I.I. Konovalov "Code VACS. Theory and Swelling Computation of Nuclear Fuel", Moscow, VNIINM, 2001-3.
2. I.I. Konovalov, Proc. 23 RERTR Int. Meet., ANL/TD/TMDI-12, **135** (2001).
3. V.?. Orlov, I.I. Konovalov, S.A. Kisilev, et al. in Proc. V Int. Workshop "Fundamental Plutonium Properties", Snezhinsk, Russia, Sept. 12-16 2005, **52** (2005).
4. I.I. Konovalov and V.?. Orlov in Proc. V Int. Workshop "Fundamental Plutonium Properties", Snezhinsk, Russia, Sept. 12-16 2005, **54** (2005).

Atomistic study of small helium bubbles in plutonium

Bingyun Ao, Xiaolin Wang, Wangyu Hu, Jianyu Yang, Jixing Xia.

China Academy of Engineering Physics, P.O. Box919-71, Mianyang 621900, Sichuan, China

Department of Applied Physics, Hunan University, Changsha 410082, China

Abstract

We have performed a molecular dynamics (MD) technique to calculate the formation energies of small He_nV_m clusters in Pu using the embedded atom method (EAM), the Mores potential and the Lennard-Jones potential for describing the interactions of Pu-Pu, Pu-He and He-He, respectively. The binding energies of an interstitial He atom, an isolated vacancy and a self-interstitial Pu atom to a He_nV_m cluster are also obtained from the calculated formation energies of the clusters. All the binding energies mainly depend on the He-vacancy ratio (n/m) of clusters rather than the clusters size. The binding energies of a He atom and a Pu atom to a He_nV_m cluster decrease with the ratio, but the binding energy of a vacancy to a He_nV_m cluster increases with the ratio. The results indeed show that He atoms can increase the binding energy of a vacancy to a He_nV_m cluster, and decrease the binding energies of a He atom and a Pu atom to the cluster, namely, He atom acts as a catalyst for the formation of He_nV_m cluster

Keywords Plutonium; Helium; Radiation effects; Molecular dynamics

A multi-scale modelling of self-irradiation effects in plutonium

G. Jomard^{*}, L. Berlu[†], B. Oudot^{*}, G. Rosa[†], P. Faure[†], L. Jolly[†], N. Gras Naulin[†], J. Nadal[†], N. Baclet[†] and F. Jollet^{*}

^{*}CEA – Centre de Bruyères le Châtel, F-91680 Bruyères le Châtel, France

[†]CEA – Centre de Valduc, F-21120 Is-sur-Tille, France

^{*}LLNL

INTRODUCTION

Predicting the long term effects of self-irradiation in plutonium based materials is a real challenge for simulation since that imposes to couple models which span a large domain of length and time scales. Indeed, the fundamental process, the α -decay of plutonium nuclei, creates displacement cascades developing in few nanoseconds over few nanometers. But the tracked effects are macroscopic properties changes occurring after many months or years. Among others, the swelling of plutonium based materials which has been experimentally observed might be crucial for the reliability and safety of nuclear stockpile [1-2]. In order to link the emergence of such phenomenon to the radioactive character of plutonium, we must understand all the stages of aging involved : creation of point and/or clustered defects by collision cascades, long-term evolution of these elementary defects (diffusion, eventually aggregation,...). That is why we have initiated a multi-scale modelling approach of self-irradiation effects in plutonium which is presented in the following.

RESULTS AND DISCUSSION

The basic idea of our approach is to couple modelling methods ranging from ab initio and classical molecular dynamics simulation methods to more macroscopic ones such as Mesoscopic Monte Carlo (MMC) and Rate Equations (RE). Obviously, there is a strong interplay between experiments and the theoretical approach in order to parametrize and validate these various models [2].

Classical molecular dynamics has proven to be a powerful technique to simulate the development of collision cascades in materials [3]. But the pertinence of such simulations is hardly dependent on the interatomic potential used. Comparing two widely used models for metals, the EAM and the MEAM ones, we found that the former is too limited to correctly describe the physics of plutonium [4]. So all the simulations reported below have been carried out within the MEAM potential published by M.I. Baskes [5]. Our aim is to obtain the spatial configuration of defects created by cascades in order to use them as input data in the MMC and RE models. This implies to have defect populations that are statistically representative of the self-irradiation phenomena. We have thus achieved a parametric study to quantify the impact of input parameters as PKA (primary Knock-on Atom) direction, PKA energy or temperature on configuration of defects [6]. For the moment we have achieved simulations of various cascades of 2 and 10 keV at T=300K, that is in a temperature range where δ -Pu can only be metastabilized by imposing a volume constraint on the simulation box with the MEAM potential of Baskes. All these computer simulations show the formation of an amorphous zone that is stable for up to many nanoseconds. The complete annealing of the 2 keV cascades thus occurs after 15 ns (cf. Figure 1). It leads mainly isolated vacancies and small interstitial clusters. This result is quite different from what is observed for more classical FCC metals such as copper, lead or gold where the recombination stage of the cascades is achieved after only 15-20 ps and the major part of the vacancies forms big clusters. Like Valone and coworkers, we have attributed this particularity to the multi-phases character of the Baskes's plutonium potential [7]. In order to check the relevance of what we observed, we plan to repeat such a

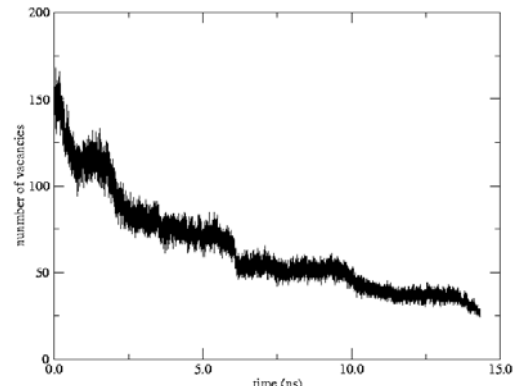


Fig 1: Computed evolution of the number of vacancies for a 2keV cascade in δ -Pu with the MEAM potential [4].

study with MEAM models for both Pu and Ga which will allow us to perform cascades simulations in a more realistic δ -stabilized plutonium crystal.

We have however started to use our predicted defects populations as source term in MMC and RE codes. The various parameters which drive these two models have been either calculated by first-principles or MD methods or set to their experimental values when available (these parameters are mainly the formation and migration energies of various point defects and their clusters). Owing to the limitations of these approaches, this preliminary study does not reach to reproduce the experimentally observed swelling. In particular, for the moment we are not able to take into account the effect of helium or decay elements such as americium. But developments of models are in progress in order to overcome these limitations (cf. communication of N. Gras Naulin et al.).

Concerning the role of helium in the swelling, we have initiated a coupled experimental and theoretical approach based on Positron Annihilation Spectroscopy. The idea is to use first-principles simulations to get a relation between a given defect and the associated positron lifetime in order to help the interpretation of the experiments. We have then implemented the TC-DFT (Two Component Density Functional Theory [8]) in the Abinit code [9].

The lifetimes calculated for bulk δ -Pu, for an isolated vacancy, and for an isolated vacancy containing a helium atom

	τ bulk (ps)	τ vacancy (ps)	τ He filled vacancy (ps)
current work	142	251	197
Sterne and Pask [10]	143	255	170-195

Tab 1 : Calculated positron lifetimes for bulk δ -Pu, in the presence of a vacancy and for a vacancy filled with a helium atom. Our results are compared to those of Sterne and Pask [10].

are in good agreement with previous results presented by Sterne and Pask [10] (cf. Table 1). The comparison between these preliminary results and the experiments seems to indicate that the major part of the vacancies-based defects present in aged plutonium-based materials contains helium. We are currently performing calculations for larger open defects with various helium concentrations to confirm this observation.

- 1 B. Oudot, PhD Thesis, Université de Franche-Comté, Besançon, France (2005).
- 2 N. Baclet, P. Faure, G. Rosa, B. Ravat, L. Jolly, B. Oudot, L. berlu, V. Klosek, J.L. Flament and G. Jomard, Actinides 2005 publishers (Royal Society of Chemistry- 'Advances in Actinide Science')
- 3 K. Nordlund et al., Phys. Rev. B **57**, 7556 (1998).
- 4 G. Jomard and P.M. Anglade, Proceedings of the 3rd International Conference on "Computational Modeling and Simulation of Materials", Part A, 489 (2004).
- 5 M.I. Baskes, Phys. Rev. B **29**, 6643 (2000).
- 6 L. Berlu, G. Rosa, P. Faure, N. Baclet and G. Jomard, MRS Fall Meeting, Boston (2005).
- 7 S. Valone et al., J. Nucl. Mater. **324**, 41 (2004).
- 8 M.J. Puska and R.M. Nieminen, Rev. Mod. Phys. **66**, 841 (1994).
- 9 X. Gonze et al. Comp. Mater. Sci. **25**, 478 (2002).
- 10 P.A. Sterne and J.E. Pask, Plutonium Futures-The science (2003).

Surface Analysis and Reactivity of Plutonium Metal/Oxide Layers

D. Moore^{*}, M. Butterfield[†], T. Durakiewicz^{*}, J. Farr^{*}, J. Joyce^{*}, R. Martin^{*}

^{*}Los Alamos National Laboratory, Los Alamos NM 87545 USA

[†]Lawrence Livermore National Laboratory, Livermore CA 94552 USA

The reactivity of plutonium surfaces is governed by the chemical and physical nature type of surface layers present at the gas-surface interface. These surface layers, under normal conditions, will likely be of a plutonium oxide character and the exact composition of these layers can dramatically influence the ultimate reactivity of the surface to its environment. Therefore, an understanding of the nature of the oxide layer and its formation processes on plutonium metal is important in ultimately understanding its reactivity. In order to more fully understand this complicated situation, we will present surface studies on the plutonium metal/oxide system using a variety of surface analytical techniques including photoemission spectroscopy (PES), x-ray photoelectron spectroscopy (XPS), and Auger electron spectroscopy (AES). In addition to these experimental studies, we will present theoretical calculations of the electronic structure of plutonium oxide layers by means of density functional theory (DFT) methods. Subsequent to the studies on oxide layer formation we will present results on the reactivity of the surfaces to small molecules, e.g. hydrogen. By utilizing a variety of techniques, in connection with theoretical calculations, we will be able to exploit their relative strengths and be able to more fully understand the formation of oxide layers on plutonium metal and their subsequent reactivity to their environment.

PES is an ideal tool for studying the electronic structure of surface oxides. We have performed PES studies of clean plutonium metal surfaces dosed with O₂ under a variety of conditions¹. These studies have revealed clear pictures of the electronic structure of oxide layers formed on clean plutonium metal surfaces under controlled conditions. In Figure 1 we show an example of the PES results for oxide layer formation on plutonium metal via Langmuir (L) level O₂ dosing at 77K. The presence of the Pu sesquioxide (Pu₂O₃) and Pu dioxide (PuO₂) are indicated by the labelled spectral peaks, as is that for Pu metal. We will present complete studies on O₂ dosing of plutonium metal surfaces and the subsequent oxide formation. Additionally, we will discuss the subsequent reactivity of these various surfaces at the gas-surface interface to e.g. H₂.

Recent hybrid DFT calculations have yielded promising results when compared to experimental studies². These calculations predict both actinide oxides to be insulators, with gaps of 2.4 and 2.5 eV for PuO₂ and Pu₂O₃, respectively. The hybrid calculations favorably reproduce the photoemission spectra with peak positions in good agreement with the experiment. For example, for PuO₂ the hybrid calculations show a strong peak at about 2.5 eV with a weaker one near 4.5

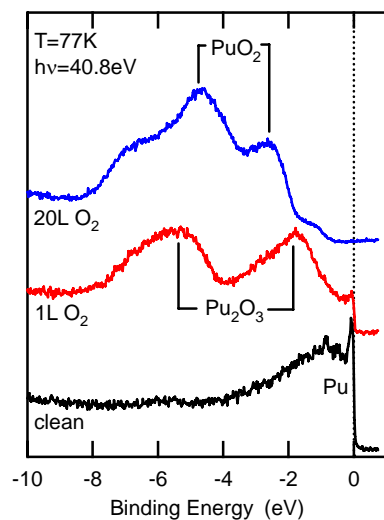


Fig 1: PES data of O₂ dosing on Pu metal showing spectral features of PuO₂, Pu₂O₃, and Pu metal.

eV, in good agreement with the positions from the PES studies shown in Figure 1. We will present results from these recent calculations of Pu oxides as well as recent theoretical results on the reactivity of these surfaces, in particular at the gas-surface interface.

XPS and AES studies will be presented that are complementary to the PES studies of oxide formation and reactivity. Extensive AES studies have been performed on plutonium surfaces and the AES spectra will be used to show the differences between oxide covered surfaces and the underlying plutonium metal. Shown in Figure 2 is an example of AES spectra for a plutonium oxide layer in comparison to the underlying plutonium metal for Pu metal dosed with O₂. Here we show the differentiated spectra for the Pu(OVV) and Pu(OPP) transitions in the left and right panels, respectively. The distinct differences are clearly evident in the differentiated Auger spectra for the oxide and metal surfaces in both cases. For the NOV transition, the peaks for the metal surface are at higher kinetic energies and are sharper than those for the oxide surface. The spectral differences observed between these surfaces are even more dramatic for the (OVV) and (OPP) transitions since these transitions involve the outer valence electrons and are quite sensitive to any changes in the chemical environment. We will in particular present analyses of these lower energy transitions in relation to oxide layer growth and gas-surface reactivity. Finally, similar to the PES studies, subsequent to investigation of the formation or character of the oxide surface we can study its reactivity towards its environment.

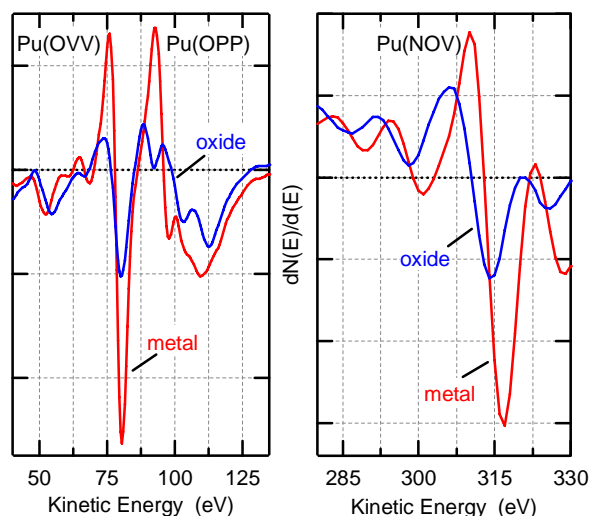


Fig 2: Differentiated AES spectra for O₂ dosing on Pu metal showing the Pu(OVV) and Pu(OPP), left, and Pu(NOV), right, Auger transitions for Pu metal and oxide.

Through the use of a variety of surface analytical techniques we will present results from studies of oxide formation on plutonium surfaces. We will discuss how character and formation of the oxide layers may have subsequent effects on the reactivity of the surface to small molecules, e.g. hydrogen. The experimental results will be complemented by theoretical calculations of the electronic structure of plutonium oxides as well as the reactivity of the gas-surface interface.

LA-UR-06-1267

- 1 M.T. Butterfield, T. Durakiewicz, E. Guzewicz, J.J. Joyce, A.J. Arko, K.S. Graham, D.P. Moore, L.A. Morales, *Surf. Sci.* **571** (2004).
- 2 M. Butterfield, T. Durakiewicz, R. Martin, in "The Actinide Research Quarterly (3rd Quarter 2004), Los Alamos National Laboratory document LALP-04-060, p. 22.

Plutonium oxide transformation kinetics and diffusion coefficient measurement

P Morrall^{*}, S Tull^{*}, J Glascott^{*}, P Roussel^{*}

^{*} AWE, Aldermaston, Reading, Berkshire RG7 4PR, UK

The highly oxophilic nature of plutonium has the consequence that, under ambient conditions, its surface readily develops a tetravalent, PuO_2 , oxide layer. In the absence of O_2 , PuO_2 is thermodynamically unstable on plutonium metal, although the dioxide layer still persists even under the stringent conditions of a high quality inert atmosphere dry box ($\text{O}_2 \sim 1\%$, $\text{H}_2\text{O} < 1$ ppm). However, when plutonium metal samples covered with surface dioxide layers are subjected to ultra high vacuum (UHV) conditions, the dioxide layer undergoes a spontaneous, thermodynamically driven, reduction to the trivalent sesqui-oxide, Pu_2O_3 . Kinetic information about this surface transformation, from PuO_2 to Pu_2O_3 , is gained by following the changing depths of the two oxide layers, using X-ray photoelectron spectroscopy (XPS) as a probe.

A model is proposed for this auto-reaction reaction based on a simple 2D layered structure, where initially a layer of Pu_2O_3 lies between the outer PuO_2 layer, and the Pu metal substrate. When left under UHV conditions the PuO_2 converts, at its interface with the Pu_2O_3 , so that the boundary between the two oxide layers slowly approaches the vacuum interface, and the oxide overlayer is converted to the sesqui-oxide. The rate of this plutonium oxide inter-conversion is controlled by diffusion of oxygen across the steadily expanding Pu_2O_3 layer. Therefore, through investigation of this auto-reduction process, values are obtained for the diffusion coefficient of oxygen through Pu_2O_3 .

© British Crown Copyright 2006/MOD.

PuO₂ Particle Size from Oxidation of Pu Metal in Air at Room Temperature

D. Spearing, B. Bluhm, W. Crooks, D.K. Veirs

Los Alamos National Laboratory, Los Alamos NM 87544 USA

BACKGROUND

Previous studies^{1,2} of PuO₂ particle size and surface area have focused on these properties as a function of sintering temperature. However, little has been done to characterize PuO₂ powder formed from the direct oxidation of Pu metal in air at room temperature. This sort of powder forms on Pu metal parts left exposed to air in non-inert atmosphere gloveboxes, and has been observed on α -Pu buttons shipped to LANL from the Savannah River Site. Of particular concern is the particle size distribution of such powder, and whether or not a significant fraction of the oxide would be at 0.3 μm in diameter, which is the size at which HEPA filter efficiency is at a minimum. According to DOE standard (DOE-STD-3020-97), HEPA filters "...shall exhibit a minimum efficiency of 99.97% when tested at an aerosol of 0.3 micrometers diameter."

EXPERIMENTAL METHOD

A 3.5 kg ingot of high purity α -phase plutonium metal from a previous experiment³ was allowed to oxidize at room temperature in a glovebox with an air atmosphere. Surface area measurements of the oxide were performed using the BET method, and particle size analysis was done using a Beckman Coulter Multisizer in the 2 – 60 μm range.

RESULTS

The surface area was measured to be 7.84 m²/g, which compares well with the value of 6.5 m²/g from a previous experiment⁴. This value also corresponds with the trend observed¹ in PuO₂ of relatively low surface area (≤ 12 m²/g) for oxides calcined at temperatures below 300°C, higher surface areas (30-35 m²/g) for oxides calcined between 300-600°C, and then a drop of in surface area² again at temperatures above 500°C.

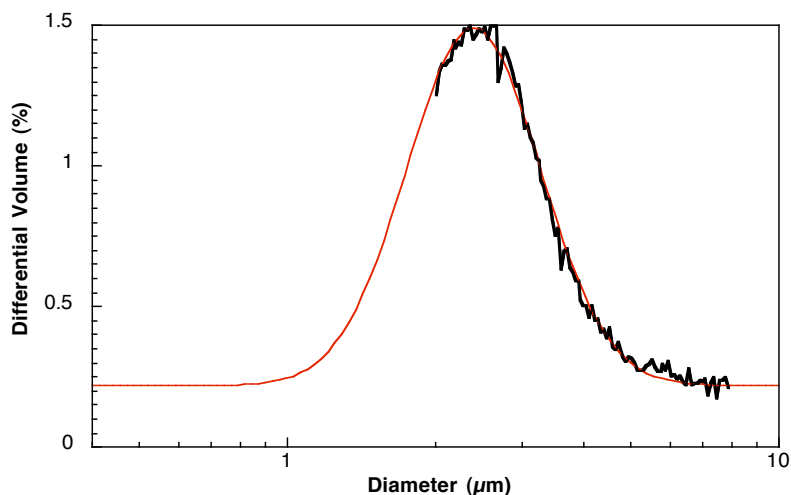


Figure 1 – Differential Volume (%) vs Particle Size (μm). Data are in black, log-normal curve fit is in red.

As mentioned above, particle sizes were measured between 2 – 60 μm . The particle size distribution from 2 – 8 μm is shown in Figure 1. As is evident from Figure 1, there is a significant fraction of particle sizes below 2 μm that we were unable to measure. In order to extrapolate below 2 μm , the observed particle size data were fit to a log-normal distribution⁵, which has been used previously to describe particle size distributions². Based on this fit, the mean particle size diameter was determined to be 2.4 μm with a standard deviation of 1.4 μm .

DISCUSSION

A plot of mean particle size as a function of calcination temperature from a previous study² along with the data point from the current study is shown in Figure 2. Data from the previous study indicate a slight *decrease* in mean particle size as a function of calcination temperature. The mean particle diameter of the plutonium oxide in this study is about one fifth that of the calcined material from previous studies. However, the powder for the calcination studies was synthesized via an oxalate precipitation method in contrast with direct oxidation of metal in air for this study, and thus may not be directly comparable.

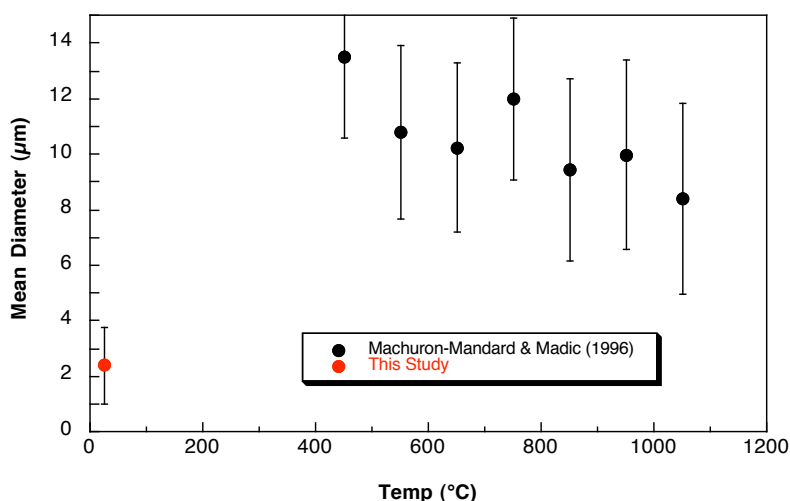


Figure 2 – Mean Particle Size (μm) vs Calcination Temperature ($^{\circ}\text{C}$).

The log-normal fit of the particle size distribution shown in Figure 1 suggests that there is little or no fraction of material below about 0.8 μm . As mentioned above, the HEPA filters are rated to remove 99.97% of all particles at 0.3 μm in diameter. However, a previous study on the gas generation from water adsorbed onto PuO_2 powder⁶ has shown that the particle size distribution of fine powders is not always well fit by a log-normal distribution. In particular, a “tail” was observed on the fine size of the distribution beyond what would be predicted by a log-normal fit. This suggests that there may be a significant fraction of particles at or below the 0.3 μm size. Future studies will focus on determining the particle size distribution below 2 μm and what impact it may have on HEPA filter efficiency.

- 1 O.R.H. Rasmussen, ARH-1153, Atlantic Richfield Hanford Company (1969).
- 2 X. Machuron-Mandard and C. Madic, J. Alloys and Compds. **235**, 216 (1996).
- 3 D. Spearing, D.K. Veirs, and F.C. Prenger, J Nucl Mater. **299**, 111 (2001).
- 4 J.L. Stakebake and L.M. Steward, J Colloid Interface Science, **42**, 328 (1972).
- 5 D.B. Siano, J Chemical Education, **49**, 755 (1972).
- 6 D.K. Veirs, LA-UR-05-8853, Los Alamos National Laboratory (2005)

Some physical chemical and radiation properties of plutonium-238 metal prepared from amalgam

V.F. Peretrukhin¹, S.I. Rovny², A.G. Maslennikov¹, V.V. Erchov², V.I. Kapitonov²,
P.P. Chinenov², V.L. Kuvaev²

1-Institute of Physical Chemistry and Electrochemistry, Russian Academy of Sciences, 31
Leninski prospect, Moscow, 119991, Russia

2-Production Association "Mayak", Ozersk, Chelyabinsk region, Russia.

²³⁸Pu metal was prepared from Pu(III) aqueous acetate solution by electrolysis with mercury cathode and by subsequent thermal destruction of plutonium amalgam [1]. This method of ²³⁸Pu metal preparation permits to avoid the neutron irradiation arising from (α, n) reactions with light nuclei, for instance with ¹⁸O. ²³⁸Pu(III) (20 g/l) was reduced to Pu⁰(Hg)_n (n=1-4) and transfer from aqueous solution to amalgam, where (α, n) reaction with mercury is impossible. The mercury was removed from amalgam and from compounds Pu⁰(Hg)_n with argon stream at 300-600°C, plutonium metal was melted in vacuum at 1100°C and cooled. Obtained plutonium ingots were pressed in air atmosphere to prepare the pellets with diameter 6 and height 6-8 mm.

The following properties of ²³⁸Pu metal pellets were measured: density, γ -spectra, specific heat power, specific neutron flux and kinetics of pellets corrosion in air atmosphere at ambient temperature. The pellets density at room temperature depended weakly on the pressure in studied interval 0.45-0.75 kbars and was equal to 16.1-17.1 g·cm⁻³ (81-85% of α -²³⁹Pu X-ray density at the same conditions). Specific heat power was determined by calorimetric measurement as 0.45 Wt/g for all prepared tablets. Gamma spectra of the pellets were registered in energy range from 100 to 3000 KeV to identify the possible impurities of stable light nuclei, which can enter in nuclear reactions ($\alpha, \alpha'\gamma$), ($\alpha, p\gamma$), ($\alpha, n\gamma$). Besides ²³⁸Pu γ -peaks, two γ -peaks with E $_{\gamma}$ 1395 and 1982 KeV were observed and associated with the presence of ¹⁸O, entering in the reactions ($\alpha, \alpha'\gamma$) and ($\alpha, n\gamma$). Analogous γ -measurements of biomedical ²³⁸PuO₂ have shown the number of γ -peaks caused by the presence of light nucleus impurities ¹⁰B, ¹⁸O, ¹⁹F, ²⁸Si. The comparison of ²³⁸Pu metal γ -spectra and that of biomedical ²³⁸PuO₂ demonstrates that electrochemical preparation of ²³⁸Pu metal via amalgam provides more high decontamination from light impurities than the biomedical ²³⁸PuO₂ preparation does.

Rapid neutron flux, emitted by ²³⁸Pu metal pellets, was measured using neutrons coincidence 4 π -counter and compared with calculated value, took into account the number of spontaneous fission neutrons of present Pu isotopes and the number of fissions induced in pellet by spontaneous neutrons. Measured specific neutron flux of the tablets (3.4·10³ ns⁻¹g⁻¹) was shown to be higher than calculated one on 300-600 ns⁻¹g⁻¹. This exceeding of experimental neutron flux value to calculated one is explained by the oxidation of ²³⁸Pu metal pellet and by the neutron contribution of the reaction ¹⁸O($\alpha, n\gamma$) ²¹Ne.

The kinetics of ²³⁸Pu metal corrosion was studied in air atmosphere at ambient temperature. Two techniques, sample weight gain and continuous neutron flux measurement were used for the determination of corrosion rate and gave the same results. The increase of the ²³⁸Pu mass sample $\Delta m_i/m_0$ in time was shown to be proportional to the increase of neutron flux

from the sample $\Delta I_t/I_0$. Three steps of corrosion kinetics have been observed at air atmosphere at ambient temperature: (1) slow latent step (so called “germination period”), (2) high rate corrosion step, ^{238}Pu metal corrosion rate achieved its maximum value $3.1 \cdot 10^{-3} \text{ mg} \cdot \text{cm}^{-2} \cdot \text{h}^{-1}$ and (3) some deceleration of corrosion rate because of PuO_2 layer growth on the metal surface. ^{238}Pu metal corrosion rate maximum value obtained in air atmosphere was the order of magnitude higher than that published for ^{239}Pu in the same experiment conditions. More high temperature and more strong radiation dose rate on the surface of the ^{238}Pu metal than those of ^{239}Pu are the reasons of the increased corrosion rate of ^{238}Pu metal. The mechanism of $^{238}, ^{239}\text{Pu}$ corrosion process is discussed in details in the report.

REFERENCES

- 1 V.F. Peretroukhin, P.P. Chinenov, V.I. Kapitonov, A.G. Maslennikov, V.L. Kuvaev, V.I. Silin. Preparation of plutonium-238 metal and its intermetallic compounds emitting low flux of (α ,n) neutrons. International conference GLOBAL-1995, Versailles, France, Sept. 1995. Proceed., vol.2, pp.1716-1724.

CORROSION OF URANIUM ALLOY FUEL IN WATER

V.F. Peretrukhin, A.G. Maslennikov, A.Yu. Tsivadze, C.H. Delegard*,
A.M. Fedosseev, V.P. Shilov, A.B. Yousov, N.Yu. Boudanova, A.A. Bessonov,
K.N. Gedgovd, G.S. Bulatov.

*A.N. Frumkin Institute of Physical Chemistry and Electrochemistry,
Russian Academy of Sciences, 31, Leninsky Prospect, Moscow, 119991, Russia*
* -Pacific Northwest National Laboratory, P.O. Box999, Richland, WA, 99342 USA

Though published data on the corrosion of uranium metal and its alloys are numerous, they are insufficient to accurately predict the corrosion behavior of irradiated uranium during long-term underwater storage. The goals of the present work are to study:

- the corrosion of uranium and its 0.5 and 5 wt% Zr, Nb, Tc, and Ru alloys in water,
- the primary corrosion process,
- the further oxidation of U(IV) hydroxide by dissolved oxygen, and
- U and U-alloys dissolution in water and nitric acid under hydrothermal conditions.

The uranium alloys were prepared from U-Me mixtures by 4-fold repeated arc melting under Ar followed by 24 hours of vacuum annealing at 1230 K. Alloy characterization included electron microscopy, elemental analysis, XRD, microstructure, grain size, and microhardness. The electrochemical corrosion tests were carried out with a rotating disk uranium electrode in anaerobic 0.1 M NaClO₄ (pH 4-9) and 0.1 M Na₂CO₃. Open circuit potentials (OCP) for pure and alloyed uranium at pH 4-9 ranged from -250 to -450 mV vs. the Ag/AgCl electrode and shifted by -100 to -150 mV in 0.1 M Na₂CO₃. The observed OCPs are similar to the standard oxidation potentials of the half reaction



at the studied pH. Closed circuit corrosion potentials (E_{corr}) determined at zero current differed by 20-60 mV from the corresponding OCP. Uranium corrosion rates, determined by chronocoulometry (CC), potential controlled electrolysis (PCE), and chemical element analysis, ranged from 0.00121 to 0.00222 mg cm⁻² h⁻¹ in pH 4-9 0.1 M NaClO₄ at 25°C.

The corrosion mechanism was studied by determining the number of electrons participating in the electrochemical process ($n \sim 1$), the transfer factor ($\alpha \sim 0.5$), and the exchange current density (i_0 from 0.53 to 1.1 $\mu\text{A cm}^{-2}$ at pH 4-9). To clarify the role of intermediary U(III) in the corrosion process, the stability of electrochemically prepared U(III) was investigated in neutral solution. Addition of Na₂B₄O₇ or NH₄OH solution to 0.002 M U(III) in 0.05 M HCl to attain pH 7-8 precipitated U(III) hydroxide. The broad UV-Vis bands characteristic of U(III) decreased with time in the U(III) hydroxide suspensions. Spectral analysis of the solution obtained by dissolving 15-min old precipitate in 1.5 M HCl showed that only ~40% of the original U(III) still remained. The rate of U(III) formation during U corrosion in pH 7-8 water and in 0.1 M NaHCO₃ thus is lower than the rate of U(III) hydroxide oxidation by anaerobic pH 7-9 water.

The corrosion rates for uranium alloys with 0.5-5 % Zr or Nb differ by factors of 0.2-5 from that of pure uranium. The addition of 0.5-5% Ru had a greater effect on decreasing the corrosion rate. Determinations of the effect of Tc alloying on the corrosion rate of U in water are in progress.

The oxidation of U(IV) by oxygen in NaHCO₃ solutions proceeds with a rate constant of 5 to 20 liters mol⁻¹ s⁻¹ in 0.01-0.15 M NaHCO₃ at 25°C. This process in pH 3-7 aqueous solution is complicated by the formation of mixed U(IV)-U(VI) colloid suspensions.

The dissolution of U metal in water and in HNO₃ solution has been studied in hydrothermal conditions at 120-160°C. These tests showed that oxidizers (H₂O₂, K₂S₂O₈, I₂) in presence of Pt catalyst dissolved uranium at controllable rates without increased pressurization under sealed tube conditions.

Electrochemical Corrosion Single Crystal Uranium

M.T. Paffett and R. Scott Lillard

Los Alamos National Laboratory, Los Alamos, NM 87545

The long-term stability and electrochemical corrosion characteristics of actinides have historically been examined using techniques and approaches that are macroscopic in nature. Furthermore, the published literature of actinide surface has, to date, been performed exclusively on polycrystalline monolithic samples. Prime examples of these approaches include potentiodynamic polarization of uranium solid samples in aqueous media [1,2]. In this work we approach the localized corrosion of uranium using an in-situ technique, electrochemical scanning tunneling microscopy (ECSTM). This approach has demonstrated great promise in our understanding of localized corrosion at other technologically important metals and alloys. In this presentation we will also compare global electrochemical corrosion characteristics of single crystal uranium to those previously observed for polycrystalline uranium and U-Nb alloys. Results of localized corrosion of single crystal uranium monitored using ECSTM will also be presented and compared with these prior studies. We will attempt to address the role of localized corrosion in observed electrochemical behavior of single and polycrystalline uranium.

1. J.A. Lillard, D.N. Kelly, M.T. Paffett, and R.J. Hanrahan, “**Electrochemically-grown oxides on U-Nb alloys,**” Proceedings - Electrochemical Society (2000), 2000-4(Oxide Films), 100-111.
2. J.W. McWirtter and J.E. Draley, “Aqueous Corrosion of Uranium and Alloys: Survey of Project Literature”, Argonne National Laboratory Report, ANL-4862, May 1952.

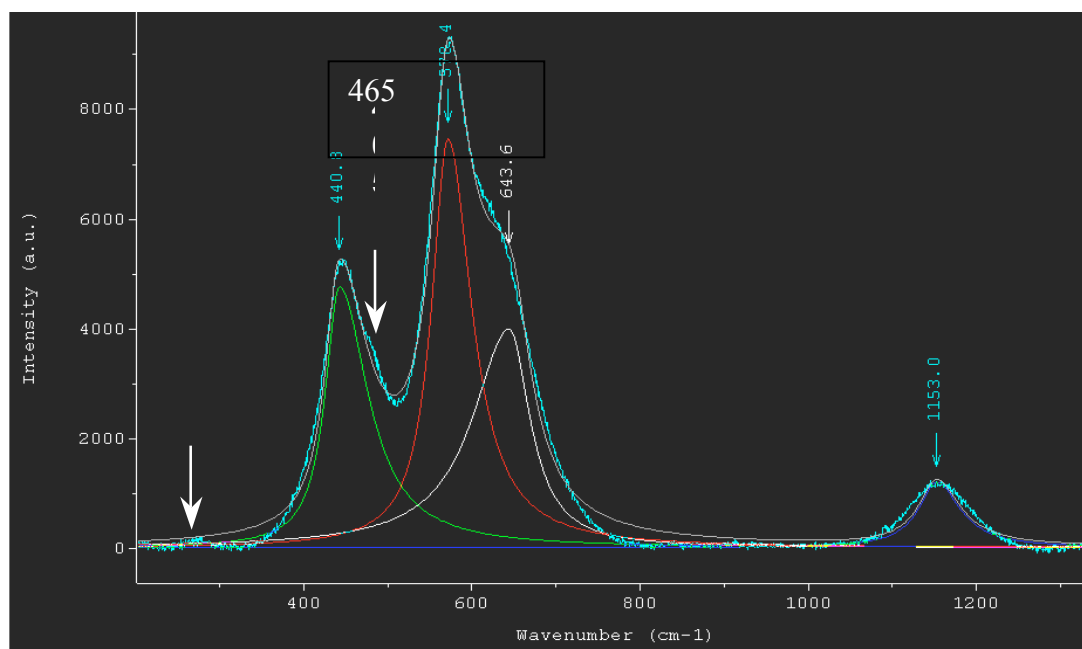
Optical Properties of Actinide Surface Oxides by Ellipsometry and μ -Raman Spectroscopy

W. Siekhaus, T. Trelenberg, M. Wall

Lawrence Livermore National Laboratory, Livermore CA 94552 USA

Uranium

The Raman spectra of epitaxial uranium oxide have recently been observed by μ -Raman spectroscopy¹.



Species	Literature values, cm ⁻¹											
α U ₃ O ₈		235	340	410			475	640	750	805		
U ₄ O ₉	210					465						
UO ₂					446							1150
UO ₂ Kr ion bomb.					446		575					1150
β -U ₃ O ₇	210					465						

Figure 1. Raman spectrum of epitaxial uranium oxide grown in air and comparison with literature values (see literature cited in reference 1).

¹ N. Caculitan, W. Siekhaus, MRS 2005 Fall Symposium Proceedings, in press.

Figure 1 demonstrates that air-grown uranium surface oxide consists of several moieties. The most prominent peak at $\sim 575\text{ cm}^{-1}$ has been seen in the literature only in UO_2 bombarded with Krypton ions, suggesting that the epitaxial oxide has a highly disordered lattice. Changes in the oxide composition induced by vacuum and exposure to hydrogen were observed in situ by placing the oxidized uranium sample into a small vacuum chamber and monitoring the surface through a fused silica window.

Ellipsometry and Reflectometry have been used to determine the optical constants n and k of the uranium substrate and of the surface oxide grown in air² over a wavelength range from 200 to 1000 nm.

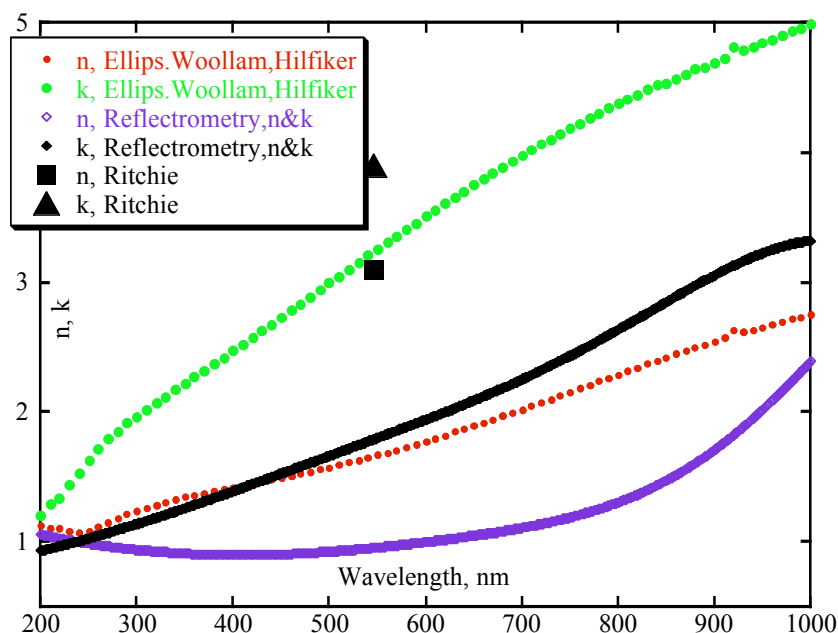


Figure 2. The optical constants n and k of bare uranium as a function of wavelength deduced from ellipsometry and reflectometry, and literature values (Ritchie) of n and k at 546 nm (see literature references in reference 2).

Figure 2 shows that for bare uranium there are substantial disagreements between literature values and values measured by ellipsometry or reflectometry. In both techniques all measurements were done in air while Ritchie's measurements were done on sputtered cleaned

² W. Siekhaus, A. Nelson, MRS 2005 Fall Symposium Proceedings, in press.

Uranium held in an ultrahigh vacuum system. The disagreement is not as pronounced in figure 3, where the n and k values of the oxide measured by ellipsometry and reflectrometry are compared with literature values. Both ellipsometry and reflectrometry were used to determine the oxide thickness as a function of exposure time to air, and the oxide thickness measurements agree with each other, despite the fact that the optical constants disagree.

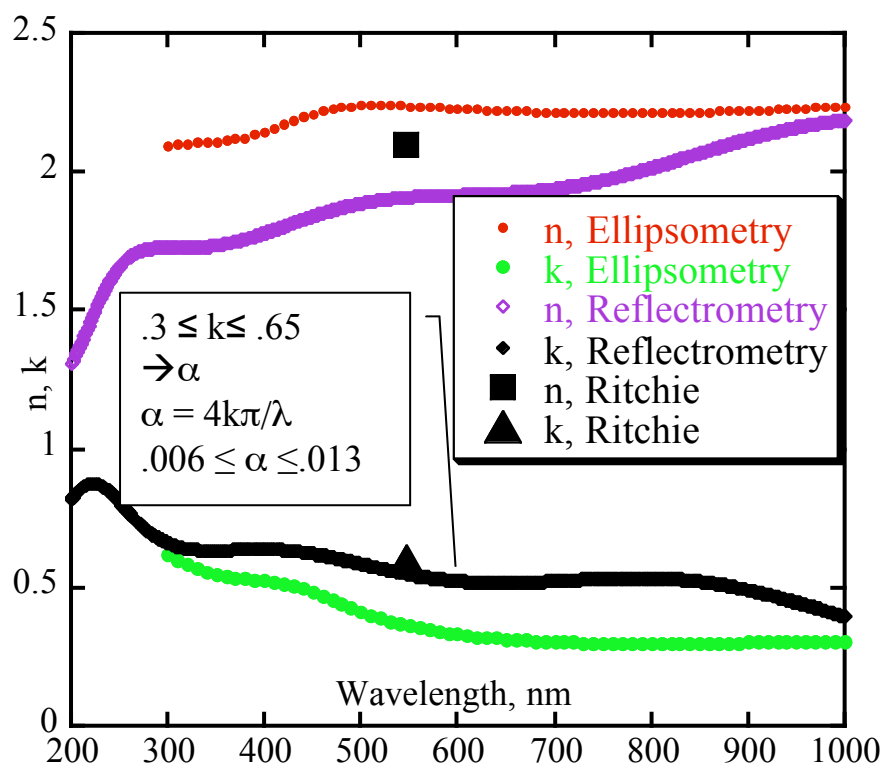


Figure 3. The optical constants n and k of epitaxial uranium oxide as a function of wavelength deduced from ellipsometry and reflectrometry, and literature values of n and k at 546 nm.

Plutonium

To perform the same measurements on plutonium a containment cell was designed that holds the small circular plutonium sample (3 mm diameter and .1 mm thick) behind two separated windows. This work is in progress and expected to be completed at the time of the conference.

This work was performed under the auspices of the U. S. Department of Energy by the University of California, Lawrence Livermore National Laboratory under Contract No. W-7405-Eng-48.

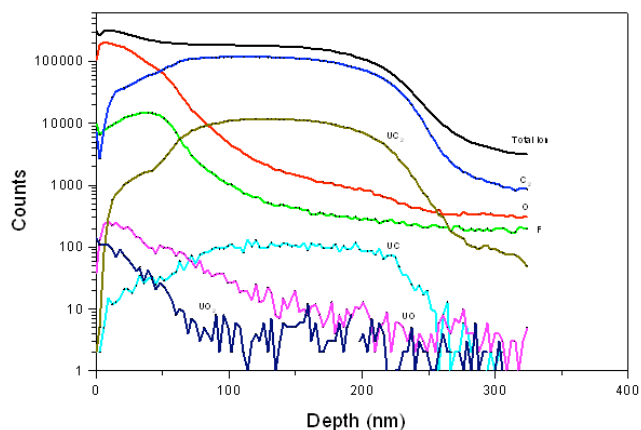
Surface Chemistry of C^+ Implanted Uranium Surfaces for Passivation

A. J. Nelson, T. E. Felter, K. J. Wu, C. Evans, J. L. Ferreira, W. J. Siekhaus, W. McLean

Lawrence Livermore National Laboratory, Livermore CA 94550 USA

ABSTRACT

Preventing the corrosion and oxidation of uranium is important to the continued development of advanced nuclear fuel technologies. Researchers have used N_2^+ and C^+ ion implantation to modify the surface chemistry and structure of uranium to affect the nucleation and growth kinetics of corrosion and to passivate the surface.¹⁻³ These researchers used Auger electron spectroscopy (AES) in conjunction with sputter depth profiling to show that the implanted surfaces had compositional gradients containing nitrides and carbides. Oxygen and molybdenum ion implantation has also been used to affect the hydriding properties and oxidation resistance of uranium.^{4,5} In addition to chemical modification, ion implantation can create special reactive surface species that include defect structures that affect the initial adsorption and dissociation of molecules on the surface. Overall the modified surface layers provide mechanical stability and protection against further air corrosion.



This paper presents the results from an investigation of the surface chemistry, surface morphology and electronic structure of air-exposed C^+ implanted U. Implantation of 33 keV C^+ ions into polycrystalline U^{238} with a dose of $4.3 \times 10^{17} \text{ cm}^{-2}$ produces a physically and chemically modified surface layer that prevents further air oxidation and corrosion. X-ray photoelectron spectroscopy and secondary ion mass spectrometry were used to investigate the surface chemistry and electronic structure of this C^+ ion implanted polycrystalline uranium and a non-implanted region of the sample, both regions exposed to air for more than a year. In addition, scanning electron microscopy was used to examine and compare the surface morphology of the two regions. The U 4f, O 1s and C 1s core-level and valence band spectra clearly indicate carbide formation in the modified surface layer. The time-of-flight secondary ion mass spectrometry depth profiling results shown in the figure reveal an oxy-carbide surface layer over an approximately 200 nm thick UC layer with little or no residual oxidation at the carbide layer/U metal transitional interface.

This work was performed under the auspices of the U.S. Department of Energy by the University of California Lawrence Livermore National Laboratory under Contract No. W-7405-Eng-48.

1. R. Arkush, M.H. Mintz and N. Shamir, J. Nucl. Mater. **281**, 182 (2000).
2. R. Arkush, M. Brill, S. Zalkind, M.H. Mintz and N. Shamir, J. Alloys Comp. **330-332**, 472 (2002).
3. R.G. Musket, Materials Research Society Conference Proceedings No. **93**, 49 (1987).
4. E.N. Kaufmann, R.G. Musket, C.A. Colmenares and B.R. Appleton, Materials Research Society Conference Proceedings No. **27**, 747 (1984).
5. R.G. Musket, G. Robinson-Weis and R.G. Patterson, Materials Research Society Conference Proceedings No. **27**, 753 (1984).

Surface Chemistry of Plutonium: Properties and Reactivity of the Oxide Carbide Solid Solution

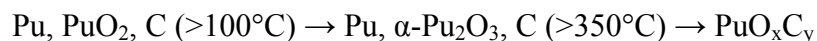
J. M. Haschke*, W. McLean[†]

*Actinide Science Consulting, Harwood TX 78632 USA

[†]Lawrence Livermore National Laboratory, Livermore CA 94551 USA

INTRODUCTION

Safe handling and storage of plutonium metal and alloys is contingent on adequate knowledge of surface chemistry and catalytic properties. Recent studies show that violent reaction of metal with air ensues if the surface becomes coated with a catalytically active compound during processing or inter-atmosphere storage.¹ In air at room temperature, Pu is covered by a passive PuO₂ layer that is inherently contaminated with C. When PuO₂-coated metal is heated in the absence of air, the surface layer reacts in a step-wise sequence to form α -Pu₂O₃ and oxide carbide²



The variable-composition oxide carbide solid solution³ is misidentified in early studies⁴ as the monoxide (PuO) and its properties remain largely undefined.

The violent Pu-air reaction cited above is initiated by an α -Pu₂O₃ surface layer that forms during heating or extended storage of the metal in the absence of air.¹ Unlike PuO₂, this oxide is reactive and promotes formation of hydride (PuH₂) by reaction of hydrogen from water, radiolysis or organic materials, and other sources in storage. The resulting Pu₂O₃-PuH₂ double layer initiates reaction of Pu with O₂ and N₂ upon exposure to air at room temperature. High temperatures are generated and metal is transformed into dispersible/respirable products at a rate of 6 cm Pu per hour.

The potential hazard created by formation of α -Pu₂O₃ during storage might be eliminated if the PuO_xC_y product formed above 350°C is passive. In that case, heating of oxide-coated metal in vacuum might be used in preparing Pu for extended storage. Relevant properties of the PuO_xC_y layer formed on the metal have been investigated in order to determine if thermal alteration holds potential for storage applications.

RESULTS

XRD characterization of the surface layer formed by heating PuO₂-coated δ -phase Ga alloy in vacuum at 520°C are consistent with results reported for NaCl-related oxide carbide in equilibrium with Pu.³ The phase formed by a relatively thick (~0.5 μm) PuO₂ layer has a unique composition (PuO_{0.54}C_{0.40}) that coexists only with Pu and Pu₂O₃ and has $a_0=5.956\text{\AA}$. Products obtained with relatively thin (~0.05 μm) PuO₂ layers have larger lattice parameters, but stoichiometry is not defined because a_0 increases as composition changes from PuC_{0.85} ($a_0=4.956\text{\AA}$) to (PuO_{0.30}C_{0.60}) ($a_0=4.969\text{\AA}$) and decreases with increasing x. All compositions are substoichiometric ($x+y<1$) and density data show anion vacancies.

Crystal chemistry of PuO_xC_y is consistent with hydrolysis studies showing that PuC_y forms CH_4 and lesser amounts of C_2H_6 .⁵ Since XPS data for PuO_xC_y results show that Pu is trivalent and O is present as O^{2-} , charge balance is achieved only if C is intervalent and present in a variable ratio of C^{4+} and C_2^{2-} . The maximum in a_0 coincides with the composition at which the C_2^{2-} concentration goes to zero. Charge balance is attained at high oxygen contents by occupancy of conduction bands with excess electrons. Metallic properties promote catalytic activity and anion vacancies facilitate transport of reactant species through the product layer.

Tests to determine the reactivity of the PuO_xC_y layer show divergent behavior upon exposure to air and to H_2 . XRD analyses are consistent with XPS results² showing that air forms a thin PuO_2 layer. Exposure to H_2 results in rapid reaction at the same rate as observed with a PuH_2 surface¹ and leads to spallation of PuO_xC_y as a hydride forms at the product-metal interface. Therefore, rapid reaction of PuO_xC_y -coated metal with H_2 forms a hydride surface that initiates violent reaction of air.¹

CONCLUSIONS

PuO_xC_y solid-solution layer formed by heating the metal has properties consistent with catalytic behavior. Reactivity studies demonstrate that thermal treatment of Pu does not passivate the surface. Rapid reaction of PuO_xC_y -coated Pu upon exposure to air is not expected. However, if H_2 sources exist in the storage environment, formation of a hydride surface that catalyzes violent reaction upon exposure to air is likely. Therefore caution should be exercised during handling of PuO_xC_y -coated metal.

- 1 J.M. Haschke and T. H. Allen, J. Alloys Compds. **320** (2001) 58.
- 2 D.T. Larson and J.M. Haschke, Inorg. Chem. **20** (1981) 1945.
- 3 R.N.R. Mulford, E.H. Ellinger and K.A. Johnson, J. Inorg. Nucl.Mater. **17** (1965) 327.
- 4 J.M. Cleveland, The Chemistry of Plutonium, Gordon and Breach, New York, 1970, p.305-06.
- 5 J.L. Drummond, B.J. McDonald, H.M. Ockenden and G.A. Welch, J. Chem. Soc. **1957** (1957) 4785.

Calculations of thermodynamic properties of PuO₂ from first principles

S. MINAMOTO^{*}, K. KONASHI[†], M. KATO[†], A. KUWABARA[†], K. MATSUNAGA[†], I. TANAKA[†]

^{*}Energy & Industrial Systems Dept., CRC Solutions Corp, Tokyo Japan

[†] Institute for Materials Research, Tohoku University, Sendai Japan

[†] Japan Atomic Energy Agency, Ibaraki Japan

[†] Department of Materials Science and Engineering, Kyoto University, Kyoto Japan

Abstract

Plutonium dioxide is non-stoichiometry compound and its thermal property would highly depend on the non-stoichiometry. And due to the lack of experimental data for plutonium dioxide, thermodynamical data were not established.

In recently, the coupling of first-principle calculation and lattice dynamics theory, thermodynamical data could be obtained numerically. In this study, we applied first principle plane-wave calculation to get total energy of plutonium dioxide and applied lattice dynamics theory to get phonon dispersion for both perfect crystal and crystal which contains oxygen defect.

Total energy calculation for perfect crystal reproduced experimental lattice parameter well. And after phonon density calculation for both types of crystal structures of plutonium dioxide, contribution of vibration to thermodynamical data was investigated.

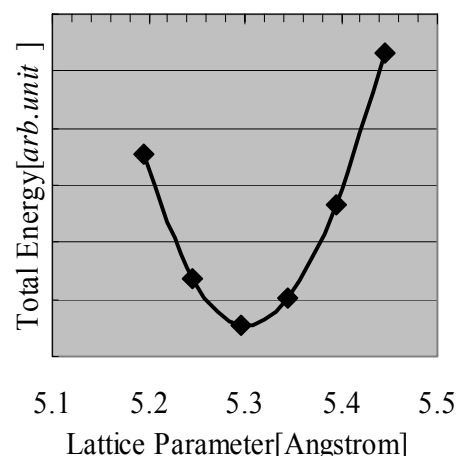


Fig.1 Total energy for perfect crystal

Reference.

1. M. Stan and P. Cristea, "Thermochemistry of Defects and Oxygen Diffusion in PuO₂-x", Trans. Am. Nucl. Soc. 91 (2004)491.
2. G. Kresse and J. Furthmüller, "Efficient iterative schemes for ab initio total-energy calculations using a plane-wave basis set", Phys. Rev. B 54(1996)11169.
3. M. Nolan, S. Grigoleit, D.C. Sayle, S.C. Parker, G.W. Watson, "Density functional theory studies of the structure and electronic structure of pure and defective low index surfaces of ceria", Surface Science 576 (2005)217-29.

A First-Principles Electronic Structure Study of the Adsorption of Carbon Monoxide on (100) Surface of γ -Uranium

Pratik P. Dholabhai and Asok K. Ray

Department of Physics, the University of Texas at Arlington, Arlington, TX 76019

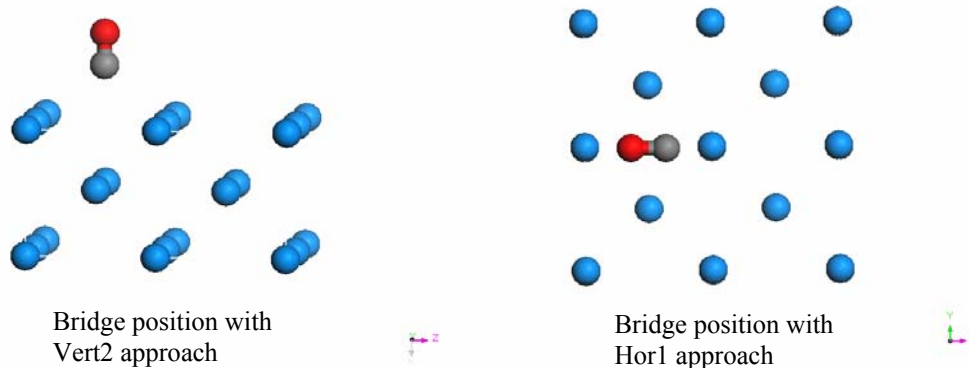
INTRODUCTION

The electronic structures of the actinides are of major scientific and technological interests, partly because of the fascinating and remarkable properties of the $5f$ electrons and partly because of the enormous potentials of the actinides in nuclear applications. Uranium (U), the heaviest naturally occurring actinide element, is largely known due to its use as a nuclear reactor fuel. U occupies a central position in the early actinide series, with only three $5f$ electrons hybridizing with the $6d$ and $7s$ electrons showing itinerant behavior. The uranium-oxygen system is one of the most complex metal oxide systems due to the high reactivity of uranium with oxygen and towards oxygen and carbon containing systems such as H_2O , CO_2 , and CO .¹ Uranium crystallizes in to a rather open structure, the orthorhombic α -phase with four molecules per unit cell at ambient conditions, followed by the body-centered tetragonal β (bct) phase at 940°K and then the γ (bcc) phase at 1050°K at ambient pressure.² As a continuation of our research in actinide surface chemistry and physics,³ this work has focused on the adsorption of CO on the (100) surface of γ - U.

COMPUTATIONAL METHOD AND RESULTS

Carbon monoxide adsorption on (100) surface of γ -uranium have been studied at the non-spin-polarized level of theory using the generalized gradient approximation of density functional theory (GGA-DFT) with Perdew and Wang (PW) functionals and the DMol3 suite of programs.⁴ Double numerical basis sets with polarization functions (DNP) are used for carbon and oxygen and a real space cut-off of 5.0 Å was used.. For uranium, the outer 14 electrons ($6s^2 6p^6 5f^3 6d^1 7s^2$) are treated as valence electrons and the remaining 78 electrons are treated as core by a hardness conserving semilocal pseudopotential. To simulate periodic boundary conditions, a vacuum layer of 30 Å was added to the unit cell of the layers. To study carbon monoxide adsorption, the (100) surface was modelled with three layers of uranium at the experimental lattice constant and the unit cell per layer was chosen to contain four uranium atoms. To simulate periodic boundary conditions, a vacuum layer of 30 Å was added to the unit cell of the layers. Carbon monoxide molecule, one per unit cell, was allowed to approach the uranium surface along three different symmetrical approaches: i) directly on top of a U atom (*top* position); ii) on the middle of two nearest neighbor U atoms (*bridge* position); iii) in the center of the smallest unit structures of the surfaces (*center* position). The interstitial positions were found not to be bound. For each of these positions, several approaches of chemisorption were considered: 1) CO molecule approaches vertically to the surface with oxygen atom facing the surface (Vert1 approach); 2) CO molecule approaches vertically to the surface with carbon atom facing the surface (Vert2 approach); 3) CO molecule parallel to the surface and parallel to the bcc lattice vectors (Hor1 approach); 4) CO molecule parallel to the surface having an angle of 45° with the

bcc lattice vectors, i.e., parallel to the diagonal of the square lattice (Hor2 approach). Some approach positions are shown below.



For CO adsorption, the bridge position of (100) surface with vert2 approach is found to be most favorable site with a chemisorption energy of 2.932eV for the non-spin-polarized case. The distance of the lower carbon atom from the uranium surface is found to be 1.589Å for non-spin-polarized case. The distance between the carbon and oxygen for this most favorable position is found to be 1.134Å for the non-spin-polarized case. A significant charge transfer from the first layer of the uranium surface to the carbon and oxygen atoms is found to occur, implying that the bonding is partly ionic. A comparison of the density of states (DOS) for the most favorable chemisorbed site with the DOS for bare uranium indicates that the CO 2*p* orbitals hybridize with U 5*f* bands, and a part of the U 5*f* electrons become more localized. Overall pattern of the density of states does not change significantly after the adsorption of CO on uranium layers.

This work is supported by the Chemical Sciences, Geosciences and Biosciences Division, Office of Basic Energy Sciences, Office of Science, U. S. Department of Energy (Grant No. DE-FG02-03ER15409) and the Welch Foundation, Houston, Texas (Grant No. Y-1525).

¹ E. Swissa, J. Bloch, U. Atzmony, and M. H. Mintz. Surf. Sci. **214**, 323 (1989).

² D. A. Young. Phase Diagrams of the Elements (University of California Press, Berkeley, CA, 1991).

³ X. Wu and A. K. Ray, Phys. Rev. B **72**, 045115 (2005); A. K. Ray and J. C. Boettger, Phys. Rev. B **70**, 085418 (2004); J. C. Boettger and A. K. Ray, Int. J. Quant. Chem., **105**, 564 (2005); M. N. Huda and A. K. Ray, Eur. Phys. J. B **40**, 337 (2004); Physica B **352**, 5 (2004); Eur. Phys. J. B **43**, 131 (2005); Physica B **366**, 95 (2005); Phys. Rev. B **72**, 085101 (2005); Int. J. Quant. Chem. **105**, 280 (2005); H. R. Gong and A. K. Ray, Eur. Phys. J. B, **48**, 409 (2005); H. R. Gong and A. K. Ray, Proc. MRS Fall 2005 Symposium; accepted for publication; Surf. Sci. accepted for publication; D. Gao and A. K. Ray, Eur. Phys. J. B, in press; Proc. MRS Fall 2005 Symposium; accepted for publication; D. Gao and A. K. Ray, submitted for publication; P. Dholabhai and A. K. Ray, submitted for publication.

⁴ B. Delley, J. Chem. Phys. **92**, 508 (1990); J. Chem. Phys. **113**, 7756 (2002).